UNIVERSITY OF NAPOLI FEDERICO II

Doctorate School in Molecular Medicine

Doctorate Program in

Genetics and Molecular Medicine

Coordinator: Prof. Lucio Nitsch

XXVI Cycle

"Identification and characterization of a novel potential transcription factor involved in osteogenic differentiation of mesenchymal stem cells"

Dr.ssa Francesca Querques

Napoli 2014

“Identification and characterization of a novel potential transcription factor involved in osteogenic differentiation of mesenchymal stem cells”

Table of contents

List of publications

Di Fiore R, Marcatti M, Drago-Ferrante R, D'Anneo A, Giuliano M, Carlisi D, De Blasio A, **Querques F**, Pastore L, Tesoriere G, Vento R. Mutant p53 gain of function can be at the root of dedifferentiation of human osteosarcoma MG63 cells into 3AB-OS cancer stem cells. Bone 2014;60C:198-212. doi:10.1016/j.bone.2013.12.021. Epub 2013 Dec 27. ISSN: 8756-3282.

Abstract

Osteogenesis is a complex and still poorly understood biological process regulated by intrinsic cellular signals and extrinsic micro-environmental stimuli from the surrounding stem cell-niche. Some regulators of osteogenesis, including growth factors and transcriptional factors, have been already identified, although further studies to better elucidate the molecular basis of this biological process are required in order to develop new and more effective therapeutic strategies for the treatment of osteogenic diseases, such as osteoporosis, bone fractures and osteosarcoma.

Osteoblasts arise from mesenchymal stem cells (MSCs), which are adult multipotent stem cells that can be successfully isolated from several adult and neonatal tissues, are able to generate, following appropriate stimuli, several differentiated mesoderm-derived cell lineages, including adipocytes, osteoblasts, chondrocytes and myoblasts and, therefore, represent a promising cell source for regenerative medicine.

In order to identify genes involved in the commitment of MSCs to osteoblasts, we performed a screening with an RNA interference-based approach and silenced a large number of genes during osteoblast differentiation of a murine MSC-derived cell line (W20-17). With this procedure we identified several candidate genes potentially involved in osteogenesis; in fact, their silencing caused a reduction of mineralized deposits, as assessed by Alizarin Red staining. We then analyzed the Gene Ontology classification of candidate genes and we found a significant fraction (30%) of genes with unknown function at the time of the screening. Hence, we focused our attention on one of these genes that we named *Osteoblasts Inducer* (ObI-1), predicted to be a transcription factor. Indeed, Ensembl analysis showed that ObI-1 encodes for a protein containing several zinc-finger domains and a Kruppel-associated box (KRAB) domain, usually involved in transcriptional repression.

We were able to observe a significant impairment in osteoblast differentiation, resulting in reduction of both alkaline phosphatase expression and mineralization, as a result of ObI-1 silencing. In addition, we evaluated ObI-1 expression in our cell system as well as in several mouse tissues and organs. Interestingly, ObI1 expression increases during osteogenic differentiation of both W20-17 cell line and primary murine MSCs from bone marrow. We demonstrated also the nuclear localization of ObI-1 through immunofluorescence analysis, corroborating the hypothesis that this gene may encode for a transcription factor. Finally, we analyzed the effect of ObI-1 silencing on the expression of osteogenic markers during the differentiation process.

1 – Background

1.1 - Bone Tissue

Bone tissue is a connective tissue specialized for support and trophic functions. Bones serve as a rigid structure to the body and as shields to protect delicate internal organs. Besides its structural function, bone significantly contributes to metabolism like a reservoir of calcium and phosphate, regulating homeostasis in the blood. Furthermore, bones provide a point of attachment for skeletal muscles and housing for the bone marrow, where the blood cells are formed. Intriguingly, in the last few years it has been demonstrated that bone could function also as an endocrine organ (Lee et al. 2007).

Bone is composed for only 5% of cells whereas the largest part is constituted by the extracellular organic and inorganic matrix. The organic matrix is mainly composed of type I collagen forming fibrils, glycosaminoglycans, osteocalcin, bone sialo-proteins, osteopontin and osteonectin. The inorganic mineral matrix is constituted by hydroxyapatite, that is largely responsible for the strength and density of the bone, composed mainly of calcium and other minerals. Therefore, in order to maintain bone density and strength, the body requires an adequate supply of calcium, other minerals and vitamin D.

All bones of the body have essentially the same structure. They present a compact hard outer part, called cortical bone, and a softer and less dense inner part, the trabecular bone; the spaces in the trabecular bone are filled by the bone marrow. Bones are covered by a thin membrane, the periosteum, in which nerves are located; blood vessels supplying blood to the bone enter through the periosteum.

Bone is a dynamic and constantly changing tissue that undergoes a continuous process of remodeling characterized by bone resorption and deposition of new bone tissue (bone neoformation); indeed, every bone of the body is completely reformed about every 10 years.

A characteristic of all connective tissues, including bone and cartilage, is that they contain a large amount of intercellular substance surrounding cells. There are four important types of cells associated with bone tissue: osteogenic cells, osteoblasts, osteocytes, and osteoclasts (Fig.1).

- Osteogenic cells are pre-osteoblast cells derived from mesenchyme, which is the precursor of all forms of connective tissue. When osteogenic cells undergo mitosis, the resulting daughter cells can differentiate into osteoblasts in relation to local or systemic needs.
- Osteoblasts are mononucleate bone-forming cells descending from osteoprogenitor cells. They are fully differentiated cells that cannot reproduced and are responsible for bone formation, secreting the organic matrix and mineral salts of the inorganic matrix. Osteoblasts express receptors for hormones regulating bone growth.

- Osteocytes are typical mature bone cells. They are osteoblasts that have become isolated in the intercellular substance they have deposited around themselves during bone neosynthesis. The spaces they occupy are known as lacunae. They are cells that have stopped laying down new bone, but they play an important role in maintaining the cellular activities of bone tissue in their immediate area by secreting enzymes and controlling the bone mineral content and the calcium release from the bone into the blood. Furthermore, osteocytes have been shown to act as mechano-sensory receptors, regulating the bone's response to stress and mechanical load.
- Osteoclasts are the cells responsible for bone resorption and play an important role in bone growth, healing and remodeling. They belong to the monocyte/macrophage cell lineage and are giant multinucleated cells (up to 50 nuclei per cell depending on the species) located in contact with calcified bone surfaces in Howship's lacunae. Osteoclasts produce enzymes, such as the tartrate resistant acid phosphatase secreted against the mineral substrate and express receptors for various hormones that regulate their activity.

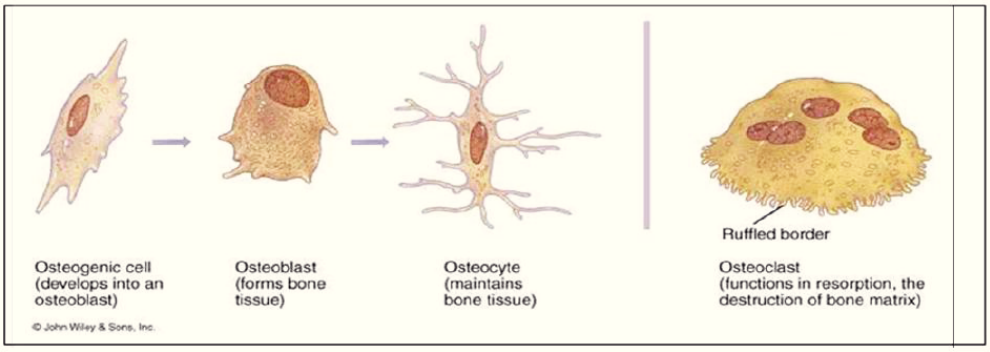

Fig.1: Bone cell types.

1.2 – Ossification

The skeleton is a complex organ consisting of more than 200 skeletal elements, different for shape, size and location, composed by two distinct tissues, cartilage and bone.

In mammals, bone development is the last event of skeleton development. During the first phase of skeletogenesis, mesenchymal cells aggregate at the sites where skeletal elements will develop (skeletal patterning); these mesenchymal condensations, prefiguring the future skeletal elements, are evident between 10.5 and 12.5 days postcoitum (dpc) in mouse.

Bone formation (or ossification) can occur through two different mechanisms. In the skeletal elements prefiguring the clavicles and some bones of the skull, cells of the mesenchymal condensations differentiate directly into osteoblasts, that appear at 15.5 dpc of mouse development, without a cartilage template through a process known as intramembranous ossification (Huang et

al. 1997). Development of the majority of skeletal elements, instead, contemplate the formation of a hyaline cartilagine intermediate model of the bone that is eventually replaced and ossified (Fig.2). In this process, called endochondral ossification, cells of the mesenchymal condensations differentiate into chondrocytes whereas cells at the periphery differentiate into osteoblasts and form the perichondrium. Chondrocytes located in the center of mesenchymal condensations stop proliferating, become hypertrophic and start producing a mineral matrix rich in type X collagen. Aferwards, while hypertrophic chondrocytes die through apoptosis, the vascular invasion from the perichondrium brings in cells of the osteoblastic lineage, at about 14.5-15.5 dpc in mouse, that differentiate into osteblasts and produce an extracellular matrix rich in type I collagen (Erlebacher et al. 1995). Endochondral ossification is the process associated with fetal bone development of long bones, such as the femur and humerus, day-to-day bone growth, and fracture repair.

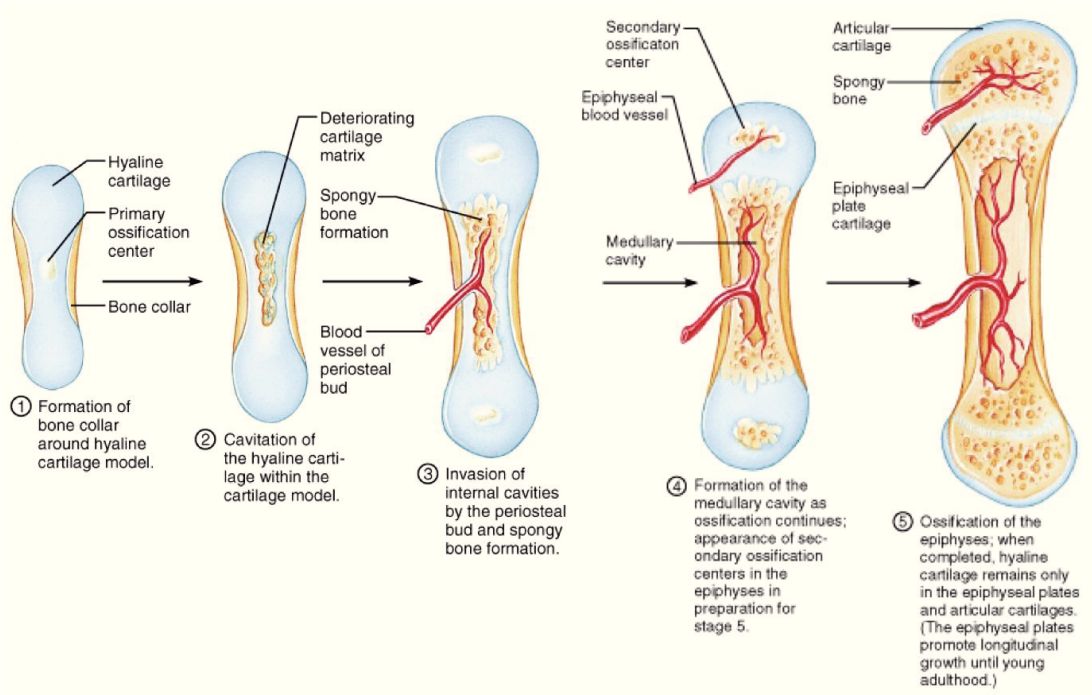

Fig. 2: Endochondral ossification.
Endochondral ossification begins in points in the cartilage called primary ossification centers. They mostly appear during fetal development, although a few short bones begin their primary ossification after birth. They are responsible for the formation of the diaphyses of long bones, short bones and certain parts of irregular bones. Secondary ossification occurs after birth, and forms the epiphyses of long bones and the extremities of irregular and flat bones. The diaphysis and both epiphyses of a long bone are separated by a growing zone of cartilage.

1.3 – Bone-related pathologies

1.3.1 - Bone fractures

A fracture is defined as a partial or complete loss of continuity of the bone that occurs under mechanical pressure. Most fractures are caused by traumatic injury, however bone cancer or metabolic disorders can cause fractures by weakening the bone. Different bones in the body have different tolerance levels and capacity to endure stress. Whichever is the cause, a bone fracture leads to a disruption of bone architecture, laceration of the periosteum and breakage of bone blood vessels.

Fractures may result in loss of function in the affected limb, guarded movements, pain, soft tissues swelling (edema) and deformity. They can be classified according to the anatomic location, the extent of the injury or the angle of the fracture.

1.3.1.2 - Fracture repair

Fracture repair is required to restore the normal alignment and function of a broken bone. Throughout the stages of fracture healing, the bone must be held firmly in the correct position. In the event that a fracture is not properly repaired, misalignment of the bone may occur, resulting in possible physical dysfunction of the bone. There are four phases in fracture healing:

1. Hematoma formation: this stage is characterized by inflammation and the formation of a granulation tissue. When a bone breaks it causes also the rupture of the blood vessels in the bone, periosteoum and surrounding tissues. This results, within a few hours after fracture, in the formation of a mass of clotted blood, or hematoma, at the fracture site.
2. Fibrocartilagineous callus formation: this phase is characterized by the formation of a soft tissue called cartilagineous callus, necessary to keep the broken bones together. Capillaries grow into hematoma and phagocytic cells digest the cellular debris.
3. Bone callus formation: blood vessels bring in osteoblasts that gradually replace the hyaline cartilage with the formation of a spongy bone callus.
4. Remodeling phase: In the following weeks or months, depending on the location and extent of the injury, osteoblasts and osteoclasts continue to migrate into the site of the fracture remodeling the existing callus.

1.3.2 - Osteoporosis

Osteoporosis is a chronic, systemic, metabolic disease characterized by loss of bone mass and disruption of the micro-architectural structure of bone tissue that leads to an increased risk of fracture. Osteoporosis has a multifactorial etiology and it can be primary, postmenopausal and senile, or

secondary; the underlying mechanism in all cases is an imbalance between bone resorption by osteoclasts and bone formation by osteoblasts during physiological bone remodeling. As bone resorption overwhelms bone formation, bones become weaker, fragile and more susceptible to fracture. The pathology usually affects the spongy bone of the spine, leading to compression fractures between vertebrae and the head of the femur.

Estrogen has been found to play a major role in osteoporosis pathogenesis, since it maintains bone homeostasis by slowing the rate of bone erosion. Indeed, it inhibits osteoclasts activity, and when estrogen levels decrease, osteoclasts activity increases to erode the bone matrix. Other factors contributing to osteoporosis can include an inactive lifestyle, a diet low in calcium an protein, or as a consequence of other diseases such as hyperthyroidism.

1.3.3 – Osteoarthritis

Osteoarthritis, or degenerative joint disease, refers to a set of diseases causing degradation of joints and represents the most common form of chronic arthritis. It is characterized by the degeneration of articular cartilage and the growth of bone tissue into the joint space; as the joint space decreases, movements become more difficult and painful. Osteoarthritis may occur as a consequence of aging and "wear and tear" on a joint over the years.

1.4 – Stem cells

Stem cells are undifferentiated cells that have the ability to self-renew and the potential to differentiate into several different cell lineages in response to appropriate stimuli .

Stem cells can be classified according to their origin, in embryonic (ESCs) and adult stem cells (ASCs), and their differentiation potential, in totipotent, pluripotent, multipotent, oligopotent and unipotent stem cells. Totipotent stem cells, i.e. the zygote, are the most versatile stem cells in that they can differentiate into embryonic and extra-embryonic tissues, giving rise to a complete and viable organism. Cells isolated from the inner cell mass of embryos at the blastocyst stage (ESCs) are pluripotent stem cells; they can differentiate into nearly all cell types, namely cells derived from any of the three germ layers, mesoderm, endoderm and ectoderm, but they are not able to differentiate into extra-embryonic tissues. Multipotent stem cells are stem cells that have the potential to differentiate into a quite large number of cell types but usually deriving from a unique germ layer. Finally, oligopotent stem cells can differentiate into only a few cell types, while unipotent stem cells give rise to one specific cell lineage.

More recently, an exciting new source of stem cells has been developed by Takahashi and Yamanaka (2006), the induced pluripotent stem (iPS) cells [4]. iPS cells are derived by genetic reprogramming of differentiated somatic cells using a cocktail of factors, originally Oct4, Sox2, Klf4 and c-Myc. They are regarded as a promising stem cell source for regenerative medicine, to

repair damaged tissues or organs, since iPS cells are pluripotent but, unlike ESCs, they do not pose ethical issues. Furthermore, iPSs can be established from the somatic cells of the patient, thereby avoiding issues of histhocompatibility. However, like ESCs, iPS can easily form teratomas *in vivo* and great efforts have been made in order to develop protocols that allow a complete and reproducible differentiation to appropriate cell lineages.

1.5 - Mesenchymal stem cells

Mesenchymal stem cells (MSCs) are adult, multipotent stem cells able to self-renew and generate, after appropriate stimuli, several mesodermal cell lineages, including adipocytes, osteoblasts, chondrocytes, myoblasts, tenocytes and haematopoiesis-supporting stroma. MSCs were identified by Alexander Friedenstein and coworkers in the 1960s. The investigators plated bone marrow cells at low density and identified a population of fibroblastoid, clonogenic plastic-adherent cells they named colony-forming unit-fibroblasts (CFU-f). Each colony, seeded under the kidney capsule of mice, was able to give rise in few weeks to fibrous tissue, bone and bone marrow; bone cells were of donor origin, whereas the hematopoietic tissue was of recipient origin, probably due to the homing of host circulating blood hematopoietic stem cells (HSCs) (Friedenstein et al. 1966). These data showed that in the bone marrow there is a population of cells distinct from hematopoietic precursors, able to generate bone tissue and to provide an appropriate microenvironment for HSCs homing and hematopoiesis. In the following years, further studies demonstrated that the inherently osteogenic cells discovered by Friedenstein and named osteogenic stem cells were actually multipotent and capable of generating not only osteoblasts, but also adipocytes, condrocytes and myoblasts (Prockop 1997).

In the last few years, several studies have shown that MSCs could exhibit a broad degree of plasticity, since they seem to be able to differentiate into non-mesodermal cell types, including neural cell lineages, endothelial cells, hepatocytes and pancreatic progenitor cells (Phinney et al. 2005; Oswald et al. 2004; Moriscot et al. 2005) (Fig.3). However, there are still controversies regarding the true plasticity of MSCs; in fact, differentiations observed *in vivo* could be due to the fusion of MSCs with endogenous cells, whereas *in vitro* non-standardized culture conditions may lead to the selection of rare cell populations with greater differentiation potential. Furthermore, recent reports have shown that, at least in some circumstances, the ability of MSCs to promote *in vivo* tissue regeneration in response to disease or injury is unlikely due to their ability to differentiate, since they exhibit very low or transient levels of engraftment (Iso et al. 2007). These observations suggest that MSCs could promote tissue repair through the secretion of molecules that modify tissue microenvironment and stimulate the regeneration.

Although MSCs were originally isolated from bone marrow, these cells are widely distributed throughout tissues, including adipose tissue, peripheral blood, skeletal muscle, tendon and several fetal tissues. However, several studies have reported that MSCs isolated from different sources are not

equivalent and, indeed, they show differences in many aspects, including the proliferation rate, the differentiation potential and the expression of some specific markers (Barlow et al. 2008). Therefore, further studies are required to better characterize MSCs populations from different sources in order to be able to select the most suitable ones for the specific purpose of the study as well as for clinical applications.

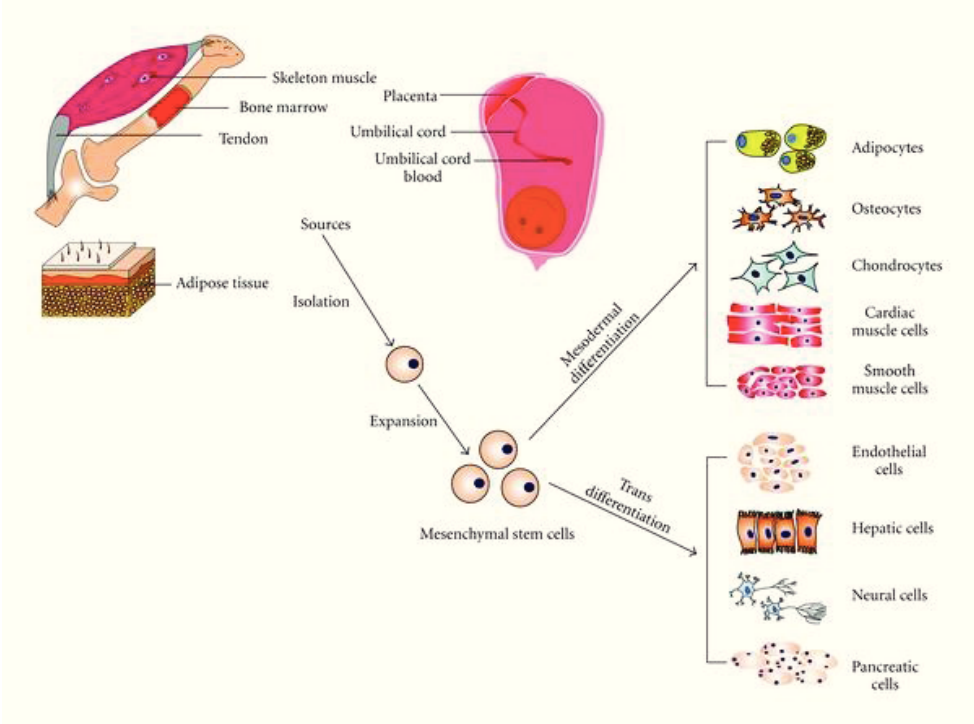

Fig. 3: Sources and multilineage differentiation of MSCs.

During the last years several techniques for MSCs isolation and culture-expansion have been developed and MSCs have been successfully harvested from several tissues of multiple species; so far, bone marrow-derived MSCs (BM-MSCs) are the most intensely studied. The conventional isolation protocol, widely used for the purification of BM-MSCs, is based on the ability of these cells to adhere to tissue culture plates (Esposito et al. 2009). However, in the last years, great efforts have been made to characterize MSCs immunophenotype in order to identify a surface antigen panel that could be useful for the isolation and purification of MSCs.

The definition of MSCs is extremely complicated as such cells represent a morphologically, phenotypically and functionally heterogeneous population of cells. For this reason, minimal criteria for the definition of human MSCs have been established: MSC have to be plastic-adherent, express CD105, CD73 and CD90, and lack expression of CD45, CD34, CD14 or CD11b, CD79alpha or CD19 and HLA-DR surface molecules and, finally, they

have to be able to differentiate at least into osteoblasts, adipocytes and chondroblasts *in vitro* (Dominici et al. 2006).

1.5.1 – Osteogenic differentiation of MSCs

Osteogenesis is a complex and not entirely elucidated biological process regulated by intrinsic cellular signals and extrinsic micro-environmental stimuli from the surrounding stem cell-niche. Cells differentiate in a multi-step process in which the progression from one stage to the following is regulated by a complex network of growth factors, signaling molecules and hormones, and it is characterized by the activation and subsequent inactivation of transcription factors and the expression of bone specific marker genes (Fig.4).

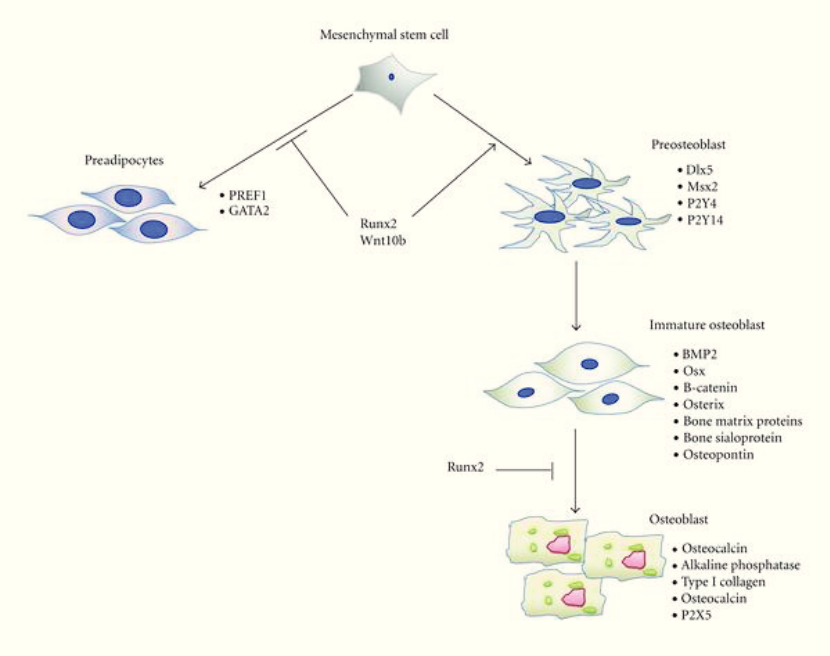

Fig. 4: **Differentiation of MSCs towards osteoblasts.**
Regulators and markers of the different stages of osteogenic differentiation

In vitro experiments have shown that osteogenesis proceeds through three different steps:

- a proliferation phase, characterized by the proliferation of MSCs and pre-osteoblasts
- a differentiation phase, characterized by the differentiation of osteoprogenitors into osteoblasts, mature cells able to produce new bone matrix. During this stage the cells gain the expression of bone specific markers, as alkaline phosphatase (ALP)
- A final mineralization phase that represents the last step of osteogenesis. The osteoblasts start to produce calcium and phosphate

mineralized deposits and to synthesize late-phase proteins, like osteocalcin

Although some determinants of osteogenesis have been already identified, further studies are require to better elucidate this biological process. Some of the most important regulators of osteogenesis, including growth factors and transcriptional factors, are described in this section (Fig.5).

Transcription factors: the earliest and most specific marker of osteoblast differentiation is Runt-related transcription factor (Runx)-2 or Corebinding factor (Cbfa)-1, member of the RUNX family of transcription factors, that stimulates MSCs commitment towards the osteogenic lineage and inhibits adipogenic differentiation. Indeed, Runx2 deletion in mice results in a skeleton constituted only by chondrocytes and in a complete lack of bone formation due to absence of osteoblasts (Ducy et al. 1997; Komori et al. 1997). Runx2 also plays an important role in mature osteoblasts and in matrix formation and mineralization, regulating the expression of osteoblast-specific genes, such as ALP, type I collagen, osteopontin and osteocalcin. However, its function in later stages of differentiation is less clear since Runx2 over-expression under the control of type I collagen promoter results in osteopenia due to the lack of terminal maturation of osteoblasts (Liu W et al. 2001).

Osterix is a zinc finger transcription factor expressed by osteoblast and required for endochondral and intramembranous bone formation. Osterix null mice show normal cartilage development but fail to develop mineralized bone (Nakashima et al. 2002). Osteoblast differentiation is arrested, and histological analysis reveals absence of trabecular bone. Furthermore, Osterix-null mice have reduced or absent expression of several bone matrix proteins, such as osteocalcin, ALP, type I collagen and osteopontin, confirming a key role of this transcription regulator in the induction of osteoblast differentiation. In contrast to Runx2 null mice that do not form osteoblasts, osterix null mice form cells of the osteoblastic lineage expressing Runx2, but these cells fail to mature.

The Msh family of homeobox genes includes three transcription factors: Msx 1, 2, and 3. Msx 3 is expressed in the central nervous system while Msx 1 and 2 are expressed in skeletal tissue and modulate osteogenesis. Msx 2 null mice show defects in skull ossification, enhanced in double Msx1/Msx2 mutants, and impaired chondrogenesis and osteogenesis due to a decreased number of osteoprogenitor cells (Satokata et al. 2000). The skeletal abnormalities are associated with a decreased expression of Runx2 indicating that Msx 2 is necessary for osteogenesis and acts upstream of Runx2. Furthermore, Msx2 could play a role also in late differentiation events since it is able to repress the transcription of osteocalcin, a marker expressed late in osteoblast differentiation, binding directly its promoter (Dodig et al. 1999).

The mammalian homolog of *Drosophila* Distalless (Dlx)-5 is an homeobox gene essential for craniofacial and skeletal development. Indeed, targeted gene inactivation of Dlx5 results in severe skeletal abnormalities, whereas Runx2 expression is unaltered (Robledo et al. 2002). Dlx5 mRNA is expressed in osteoblasts after differentiation, concomitant with a decline in

Msx2 mRNA and with the apperance of osteocalcin transcript, and it is able to induce the expression of ALP and osteocalcin and thereby the mineralization of the extracellular matrix (Miyama et al. 1999).

Growth Factors: Bone morphogenetic proteins (BMPs) are members of the Transforming Growth Factor (TGF) family of polypeptides (Wozney et al. 1988) and were originally identified for their ability to induce endochondral bone formation.

To date, around 20 BMP family members have been identified and characterized. BMPs signal explicates through serine/threonine kinase receptors, composed of type I and type II subtypes. After ligand binding they form a heterotetrameric-activated receptor complex and interact with SMAD proteins, that play a key role in the signal transduction from the receptor to target genes in the nucleus. Furthermore, BMPs can activate SMAD-independent pathways, such as Ras/MAPK pathway (Fig.5). BMPs are able to increase commitment of bone marrow mesenchymal stem cells to osteoblasts phenotype by increasing Runx2 mRNA expression (Lee et al. 2002).

Wnt proteins are signalling proteins that act on target cells by binding to Frizzleds (Fzs), sevenspan transmembrane receptor proteins, and LRP-5/6, single span transmembrane co-receptor proteins. Wnt pathway is involved in BMPs-mediated osteogenesis (Chen et al. 2007), and is able to induce the osteoblastic transcription factors Runx2, Dlx-5, and Osterix, indicating that this pathway is intimately associated with bone regenerative process.

1.5.2 - MSCs: advantages and applications

MSCs are considered a promising source for cell-based therapy and regenerative medicine, since they can be extensively expanded *in vitro* retaining their undifferentiated phenotype and differentiation potential, they do not cause teratoma formation *in vivo* and are well-tolerated in clinical trials. Moreover, they show unique features that largely contribute to their attractiveness: MSCs are immune-privileged, have the ability to migrate to injured tissues after systemic administration, produce several trophic factors and are able to regulate inflammatory and immune responses. For these reasons MSCs were largely employed in preclinical and clinical studies to treat a broad spectrum of diseases, including auto-immune and inflammatory diseases, graft versus host disease, myocardial infarction and spinal cord injuries (Ren et al. 2012).

The MSCs potential to differentiate into several cell types has opened a variety of tissue engineering applications. In fact, undifferentiated or differentiated MSCs seeded into a variety of natural or synthetic biomaterial scaffolds have been successfully applied in repair of cartilage and bone defects (Ren et al. 2012; Savarino et al. 2007).

Most interestingly, MSCs and their derived cell lines represent a valid *in vitro* differentiation system and a valuable tool for the identification of the molecular mechanisms underlying cellular differentiation; the identification of genes that regulate osteoblast differentiation, for instance, can directly provide

new pharmacological targets for the induction of bone neosynthesis and, therefore, the treatment of bone-related pathologies, such as osteoporosis and bone fractures.

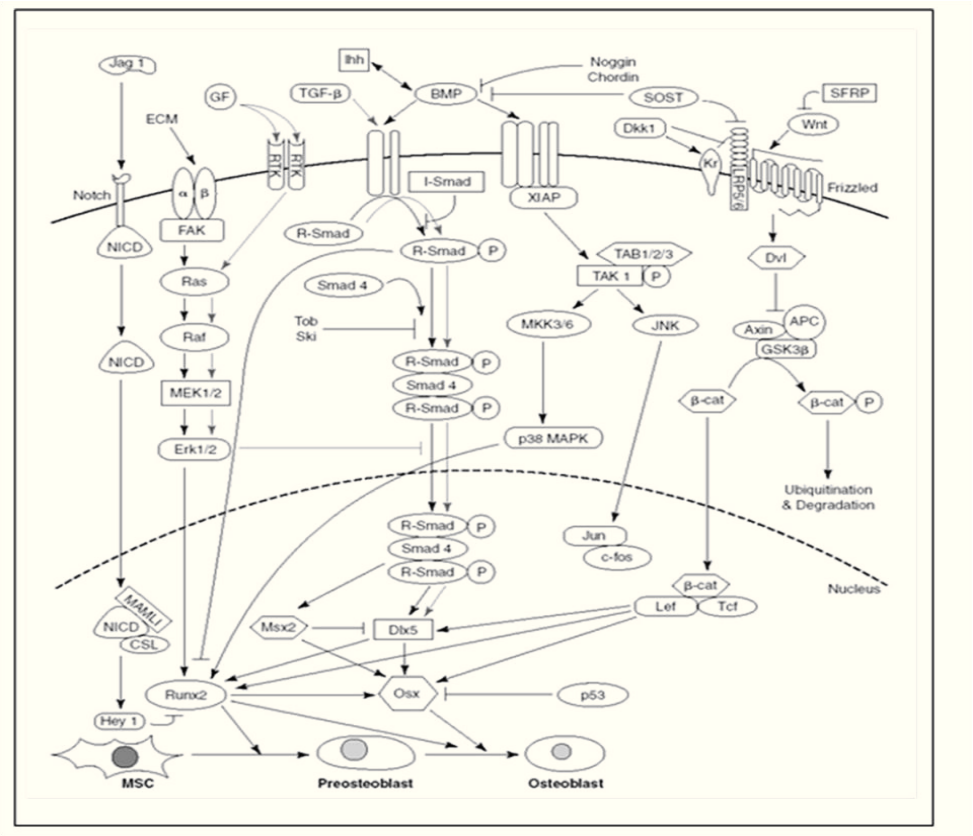

Fig.5: Signalling and transcription factors regulation in osteogenic differentiation.
BMP and Wnt pathways induce osteogenic differentiation through the up-regulation of some osteo-specific transcription factors such as Runx2, Osterix, Dlx5 and Msx2.

Recently a number of automated procedures for cell culture and manipulation have been developed (high-throughput screenings, HTS) making it possible to conduct a large number of tests with reduced manpower and more affordable costs. These screenings allow the identification of genes involved in a number of biological processes or compounds able to alter them. Recently, RNA interference-based approaches have become particularly popular for their ability to silence specific genes and, therefore, study the effect of the absence of a single gene product in a particular biological phenomenon. In addition HTS can be used to screen compounds libraries to directly identify chemical compounds able to induce or block a biological process in order to discover potential drugs.

1.6 – RNA Interference

RNA interference (RNAi) is a form of post-transcriptional gene silencing mediated by little double- strand molecules of RNA able to block the translation of mRNA targets. RNAi is a natural process preserved during evolution and it is involved in several mechanisms such as the defense against viral infections, gene expression regulation, protection against genome instability and developmental regulation. RNAi can be activated by a double strand of RNA brought into the cell (small interfering RNA, siRNA) that leads to the degradation of mRNA target, or by micro RNA (miRNAs), small non codifying transcripts synthesized within the cell; in this case not always the mRNA target is degraded through cleavage.

miRNAs are small conserved single-strand RNA molecules of about 20-22 nucleotides which negatively modulate gene expression primarily through base paring to the 3' untranslated region (UTR) of target mRNAs; this leads to mRNA cleavage and/or translation repression. miRNAs are involved in regulation of a variety of biological processes, such as cell proliferation, apoptosis and stress responses. Furthermore, miRNAs have been implicated in cancer, where they can act as tumor suppressors or oncogenes. Their biogenesis starts in the nucleus: miRNAs are first synthesized from their corresponding genes as longer precursors called primary miRNA (pri-miRNAs). Pri-miRNAs are processed by Drosha RNA polymerase III that generates molecules of 70-80 nucleotides with a stem and loop structure, known as precursor miRNAs (pre-miRNAs). Pre-miRNAs are translocated from nucleus to cytoplasm by a complex of receptors on the nuclear membrane, such as exportin 5 (Lund et al. 2004), and processed in miRNAs by Dicer, a ribonucleasic enzyme of the RNA polymerase III family. Each miRNA binds the enzymatic complex RNA-interference silencing complex (RISC), forming a RNA-protein complex named miRISC. Small RNA molecules are then separated: the sense strand is degraded while the antisense strand is driven towards the mRNA target by a RISC complex subunit, Argonauta 2 (Ago2) (Liu J et al., 2004). If miRNA and mRNA target strands are highly complementary, mRNA is cleaved, if they are partly mismatched, RISC complex linked to mRNA does not allow the translation; in both cases no protein is made.

siRNAs are short molecules of double-strand RNA of 21-23 nucleotides with two phosphate groups at 5' and 2 nucleotides 3' protruding generated by Dicer. They can be introduced into the cells by both transfection and infection. The antisense strand binds the RISC complex forming the RNA-protein complex siRISC which recognizes the mRNA target and cleaves it.

shRNAs (short hairpin RNA) are small RNAs with a stem and loop structure: they mimic the pre-miRNA structure and therefore follow their same processing. shRNA are expressed by plasmids or viral vectors and for this reason they present the advantage to perform a stable silencing of their mRNA targets.

1.6.1 - Off-target effects

Off-target effects are defined as the consequences of not desired interactions between RNA interference molecules and cellular components or no target mRNAs and can be classified in sequence-independent and sequence-dependent effects**.**

Sequence-independent effects include the transfection conditions and the inhibition of the activity of endogenous miRNAs that may be caused by RNA-interference machinery saturation, for example the saturation of exportin 5 (Yi et al. 2005).

Among the sequence-dependent effects there are immune response stimulation and interaction with no mRNA targets. The immune response can be provoked by type I interferons when siRNAs are longer than 30 base pairs or by the recognition of single or double strand RNA molecules by Toll-like receptors (TLRs). It is possible to reduce the interferon-mediated response avoiding the presence of some nucleotids motifs, such as GU traits, in the RNA sequence. However, the main cause of sequence-dependent effects is the interaction between RNA interference effectors and no target mRNAs; in order to overcome this issue it is fundamental that the RNA-interference molecule has the minimal homology with mRNA sequences other than its target. In addition, it is recommended to perform redundancy or phenotype rescue experiments. In redundancy experiments different effectors having the same mRNA target are employed. In this way, the probability that at least two different effectors with distinct sequences share the same sequence-dependent off target effects is minor. In phenotype rescue experiments it is used a functional version of the target gene resistant to RNA interference effector.

2 – Aims of the study

The aim of my study was the identification and characterization of novel determinants of osteogenic differentiation. Indeed, a better understanding of the molecular process that drive the differentiation of MSCs towards the osteogenic lineage is essential to identify new molecular targets and develop novel and more effective therapeutic strategies for the treatment of bone-related pathologies, such as osteoporosis, bone fractures and osteosarcoma.

In particular, I focused my attention on the study of a novel potential transcription factor, that we named Osteoblasts Inducer (ObI)-1, necessary for MSC differentiation into osteoblasts in vitro. Therefore, we performed experiments aimed at the characterization of ObI-1 function in osteogenesis as well as at the identification of the molecular pathways in which it is involved.

3 – Materials and Methods

3.1 – Mouse shRNA library

shRNA library (Open Biosystems, Thermo Scientific, Waltham, MA, USA) consists in 64.000 bacterial stocks (PirPlus competent bacteria) containing plasmid DNA expressing shRNA constructs that cover the entire mouse transcriptome. Bacterial stocks are stored in single wells in 96 well plates in glycerol stock at -80° C.

The plasmid DNA is pShag Magic Version 2.0 (pSM2) retroviral vector (Open Biosystems). This plasmid contains the following features (Fig.6): 1) Murine Stem Cell Virus (MSCV) backbone with Retroviral Signaling Sequences; 2) U6 promoter; 3) RK6γ conditional origin of replication. It requires the expression of Pir1 gene within the bacterial host to propagate; 4) Kanamycine and Chloramphenicol resistance as bacterial selection markers; 5) Puromycine resistance for selection after transfection in mammalian cells; 6) Sequence encoding the shRNA construct.

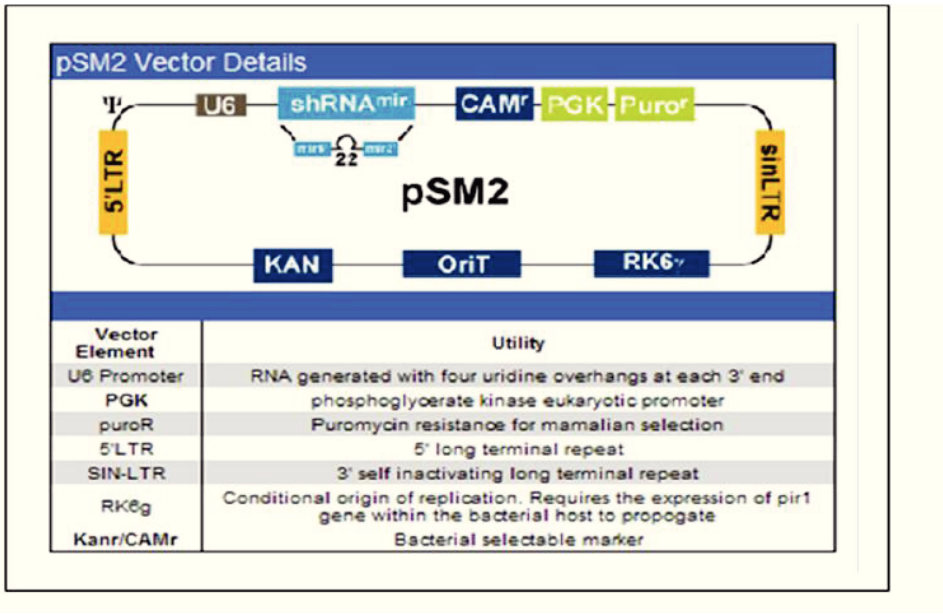

Fig.6 : pShag Magic Version 2.0 features.
Structure and functional elements of the DNA plasmid of the mouse shRNA library.

3.2 – Cells and culture conditions

W20-17 cell line was purchased from American Type Culture Collection (ATCC/LGC standards, Teddington, UK), primary murine MSCs (mMSCs) were isolated from C57Bl/6 mice's bone marrow in our laboratory (Esposito et al. 2009). Cells were cultured in Dulbecco's Modified Eagle's Medium (D-MEM, Euroclone, Pero, Italy) supplemented with 10% fetal bovine serum (FBS, HyClone, Thermo Scientific) and 2 mM L-glutamine (Gibco, Life Technologies, Carlsbad, CA, USA) in absence of antibiotics.

3.2.1 – Osteogenic differentiation

Cells were grown until they reached 70%-90% confluence and then cultured for 18 days (mMSCs) or 21 days (W20-17) in D-MEM supplemented with 10% FBS, 2 mM L-glutamine, 0.05 mM ascorbic acid 2-phosphate (Sigma-Aldrich, St. Louis, MO, USA), 10 mM glycerol 2-phosphate (Sigma-Aldrich), 1 μM dexamethasone (Sigma-Aldrich). Medium was replaced twice a week.

3.3 – ALP staining

Cells were washed with cold PBS and fixed with 10% cold Neutral formalin buffer (NFB) for 15 min. They were incubated with the staining solution for 45 min. in the dark and then washed 3-4 times using distilled water**.**

Staining solution:

a) 5 mg Naphtol AS MX-PO4 powder (Sigma-Aldrich) in 200 μl N,N-Dimethylformamide (Sigma-Aldrich).
b) 25 ml 0.2 M Tris-HCl, pH 8.3 + 25 ml distilled water.
c) 30 mg Red Violet LB salt (Sigma-Aldrich).

Note: Prepare (a) and (b) separately; add (a) + (b); add (c).

3.4 – Alizarin Red S Staining

Cells were washed with PBS and fixed in 10% formaldehyde for 1 hour. After rinsing with distilled water they were incubated with 2% Alizarin Red S (Sigma-Aldrich) solution with gentle agitation for 10 minutes and then washed 3 times with distillate water.

3.4.1 - Alizarin Red S staining quantification

Alizarin Red S solution bound to the calcium deposits of mineralized nodules was extracted through over-night incubation with 4M Guanidine-HCl (Sigma-Aldrich) at room temperature. Absorbance at 490 nm of the resulting supernatant was used for quantitative calcium determination.

3.5 - Lipofection

Cells were plated in the plastic support, allowed to grow until they reach the optimal confluence for transfection (80-90%) and then transfected with shRNA plasmids using Lipofectamine 2000 (Invitrogen, Life Technologies) according to manifacturer's instructions. Cotransfection with a plasmid for the expression of a reporter gene is performed to supervise transfection efficiency. Two days after transfection, the cells were culture in selective medium containing puromycin in order to enrich for cells that incorporated the plasmid DNA. Puromycin amount was established on the basis of kill-curve experiments (3 μg/ml for W2017, 2 μg/ml for primary mMSCs). The medium was replaced every 2 days. A plate of untrasfected cells was used as a control for the enrichment.

3.6 – RNA extraction

Total RNA was extracted from cells and tissues using TriReagent (Sigma-Aldrich) according to manifacturer's instructions.

3.7 – Mice experiments

C57Bl/6 mice were obtained from Jackson Laboratory (Bar Harbor, ME, USA). All experimental procedures were conducted in accordance with institutional guidelines for animal care and use. Food and water were provided ad libitum. Mice were euthanized with carbon dioxide vapors and organs and tissues were immediately collected in ice and homogenized in TriReagent.

3.8 – Real Time PCR

cDNAs were amplified from 2 μg of RNA using M-MuLV reverse transcriptase (New England Biolabs, Ipswich, MA, USA). RNA was incubated with dNTPs (Amersham Biosciences, GE Healthcare, Pittsburgh, PA, USA) and Random Examers (Promega, Fitchburg, WI, USA) at 70°C for 10 minutes and in ice for 1 minute; then, after the addition of M-MuLV and the specific buffer, the incubation was performed at 42°C for 1 hour followed by enzyme denaturation at 90°C for 10 minutes. Real time PCR was performed using the SYBR Green PCR master mixture in an Applied Biosystems 7900HT apparatus (Applied Biosystems, Foster City, CA, USA). Levels of target genes were quantified using specific oligonucleotide primers and normalized for glyceraldehyde-3-phosphate dehydrogenase (GAPDH) expression. Primers sequences are listed in Table 1.

Table 1: Primer sequences

Primer	Sequence (5'-3')
GAPDH Forward	GTATGACTCCACTCACGGCAAA
GAPDH Reverse	TTCCCATTCTCGGCCTTG
ObI-1 Forward	GGTGTGGCTGGGGCACTGTTT
ObI-1 Reverse	GCTTCTGCAACACCCCACGGT
Runx2 Forward	CCTGCCATCACTGACGTGC
Runx2 Reverse	GGCCAGAGGCAGAAGTCAGA
Osteopontin Forward	GCTGGTGCCTGACCCATCT
Osteopontin Reverse	CCTTTTCTTCAGAGGACACAGGCAT

3.9 - Construction of ObI-1 C-terminal Flag plasmid

RNA was extracted from mouse lungs and retro-transcribed in cDNA as previously indicated. The following primers were used to amplified the ObI-1 cDNA (2.043 Kb): Forward 5'-GGCCACGGGATCCAGCCATGGTGAGA AGACG-3' (BamHI restriction site-containing) and Reverse 5'-GGGCTCGCGGCCGCCAAATCCCAGA TAGGGTTTG-3' (NotI restriction site-containing). For PCR amplification with Phusion Taq polymerase (New

England Biolabs) the following protocol was performed: 98°C for 3 minutes, 15 cycles at 98°C for 1 minute, 49°C for 20 seconds and 72°C for 2 minutes, 5 cycles at 98°C for 1 minute, 60°C for 20 seconds and 72°C for 2 minutes, 15 cycles at 98°C for 1 minute and 72°C for 2 minutes and a final extension at 72°C for 10 minutes. The amplified product was resolved by agarose gel electrophoresis (1% agarose and 0.5 μg/ml ethidium bromide, Sigma-Aldrich) and the band was extracted using Wizard SV Gel and PCR Clean-up system (Promega). PCR product and pcDNA 3.1 vector (Invitrogen) were digested for 2 hours at 37°C with BamHI and NotI (New England Biolabs), resolved by agarose gel electrophoresis and extracted.
Vector dephosphorilation and ligation reactions were performed using the Rapid Dephosphorilation and Ligation kit (Roche) according to manifacturer's instructions. The ligation mixture was transformed into Calcium Chloride competent DH5α cells (Invitrogen, Life Technologies). Plasmids that after BamHI-NotI digestion showed the presence of a 2 Kb insert were validated by sequencing (Ceinge Sequencing Service).

3.10 – Western Blot assays

Total cell lysates were obtained by treatment with lysis buffer (1mM EDTA, 50 mM Tris-HCl, pH 7.5, 70 mM NaCl, 1% Triton X-100), protease inhibitors (Complete Protease Inhibitor Cocktail, Roche, Basel, Switzerland) and the phosphatase inhibitors 5mM sodium fluoride and 1mM sodium orthovanadate (Sigma-Aldrich).

Protein extracts were run on 10% SDS-PAGE gels, transferred on Immuno-Blot PVDF membranes (Bio-Rad Laboratories, Hercules, CA, USA) and analyzed using the following antibodies: Anti-Flag (Sigma-Aldrich, 1:500 dilution), Anti-GAPDH (Santa Cruz Biotechonology, Santa Cruz, CA, USA, 1:1000 dilution) and secondary HRP-conjugated antibody (Amsterdam Bioscience, Uppsala, Sweden, 1:5,000 dilution). Proteins were detected by chemiluminescence (ECL plus, GE Healthcare).

3.11 – Immunofluorescence

mMSCs were transfected with either pcDNA 3.1 expressing ObI-1-Flag or empty vector using Lipofectamine 2000. After 24 hours, cells were fixed in 4% paraformaldheyde, permeabilized with 0.2% TX-100 and blocked in 10% bovine serum albumin (BSA) in PBS for 30 minutes at room temperature. The samples were then incubated with primary murine anti-Flag antibody (1:250 dilution) and then with an anti-mouse IgG conjugated with Alexa Fluor 488 (Molecular Probes, Life technologies, 1/500 dilution). Both antibodies were diluted in 3% BSA/PBS. Cells nuclei were counterstained with 4',6-diamidino-2-phenylindole (DAPI) diluted 1/5,000 in PBS. Images were captured using a LSM 510 Meta confocal microscope (Carl Zeiss, Oberkochen, Germany).

4 – Results and Discussion

4.1 – Identification of genes involved in osteoblast differentiation with a shRNA-based approach

In order to identify novel genes that regulate MSCs differentiation towards the osteogenic lineage, we performed a screening based on an RNAi approach using the murine library described in materials and methods.

W20-17 cells were plated in 96 well-plates and after one day were transfected with shRNA-encoding plasmids. The cells were cultured 2-3 days in puromycin, in order to enrich the cell population that had incorporated the plasmid, and then treated with osteogenic medium. After 21 days the cells were stained with Alizarin Red S in order to detect mineralized deposits (Fig.7).

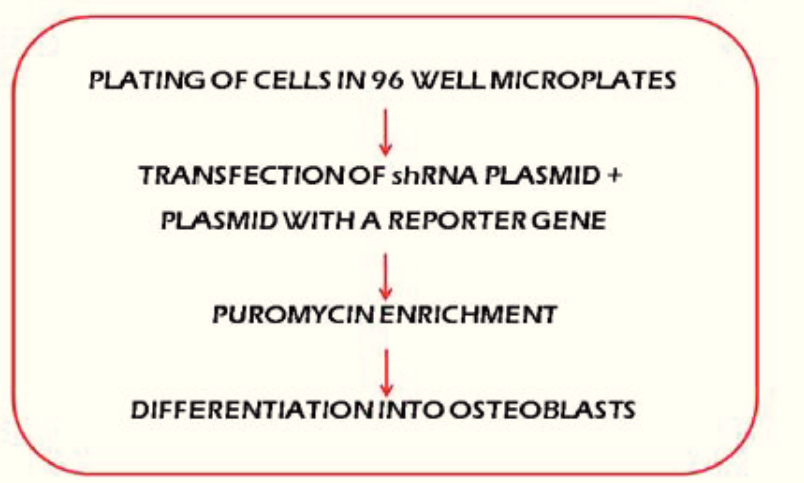

Fig.7: Experimental approach to perform screening.
Cells are plated in 96 well-plates and the day after transfected with shRNA plasmids. Cotransfection with a plasmid for the expression of a reporter gene is performed to supervise transfection efficiency. Cells are cultured for 2-3 days in presence of puromycin and then treated with osteogenic medium for 21 days in order to induce osteoblast differentiation.

In order to validate our experimental approach, we used several controls including controls of differentiation, represented by untransfected cells grown in osteogenic and normal medium, and a scrambled control for the RNA interference technique, represented by cells transfected with an shRNA that does not recognize any known murine transcript, shRNA Non Silencing (shRNA-NS). In addition, as controls for the efficiency of RNAi-mediated block of differentiation, we included cells in which we silenced genes known to be involved in osteogenic differentiation, such as BMP1 and SMAD5. The results of Alizarin Red staining and its quantification are reported in Fig.8.

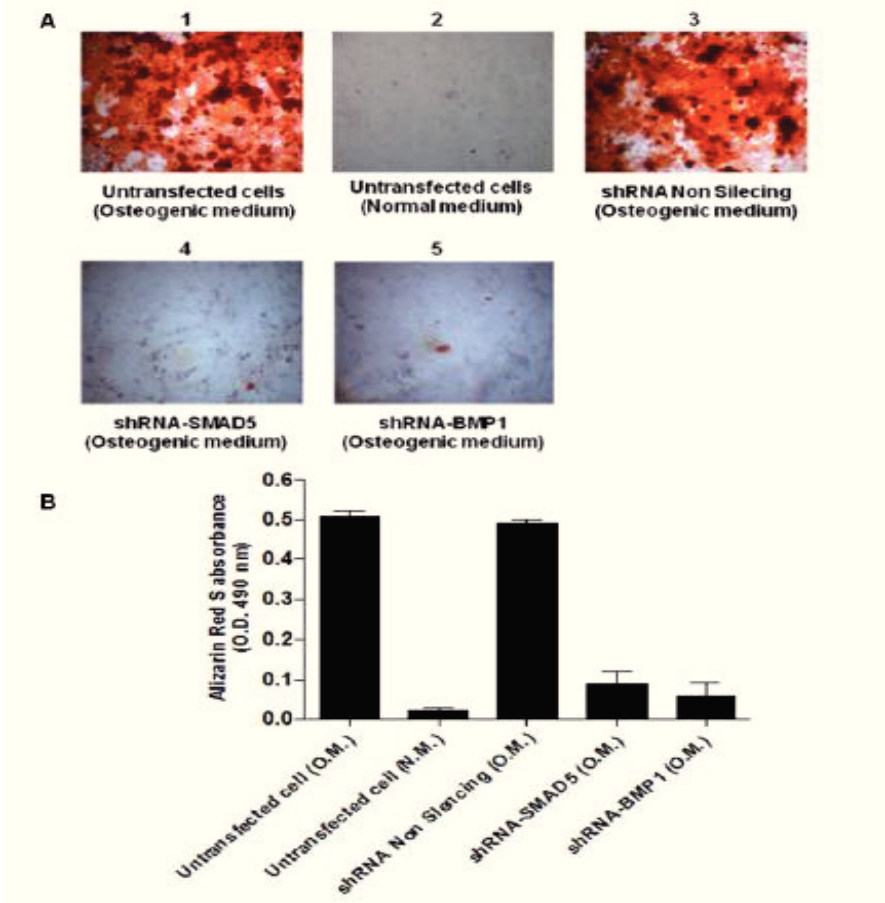

Fig.8: Experimental approach validation.
Alizarin Red S staining after 21 day of: 1) untransfected W20-17 cells cultured in osteogenic differentiation; 2) untransfected cells cultured in normal medium; 3) cells transfected with shRNA Non Silencing and cultured in osteogenic medium; 4) cells transfected with shRNA SMAD5 and cultured in osteogenic medium; 5) cells transfected with a shRNA for BMP1 and cultured in osteogenic medium (A). Calcium deposition was quantified using 4M Guanidine HCl and reading the adsorbance at 490nm.

So far, we have transfected about 10,000 constructs of the library in single wells and we collected the relative results. Genes whose silencing impaired the ability of W20-17 to produce a mineralized matrix were considered putative candidate genes (Fig.9). Up to now, we have identified 650 candidate genes, corresponding to 6.5% of the total number of screened genes.

4.2 – In silico characterization of candidate genes

We performed an in silico analysis of our results using bioinformatic tools to obtain a Gene Ontology classification of the candidate genes (Carmona-Saez et al. 2007). We found candidate genes involved in signal transduction, transcription, transport within and between the cells, apoptosis and developmental processes (Fig.10).

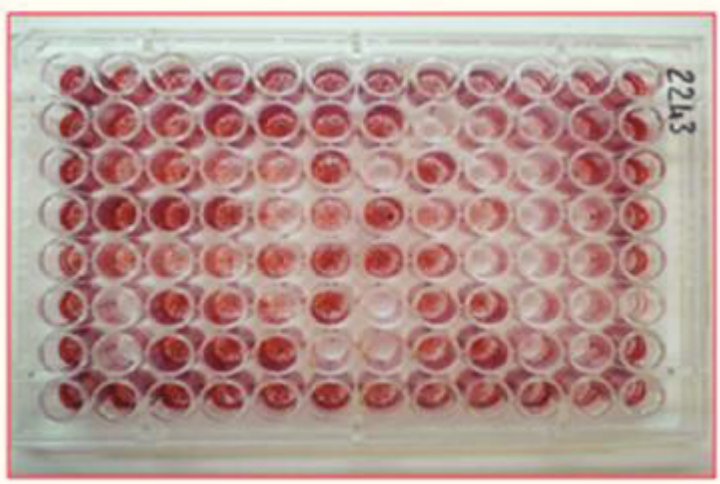

Fig.9: Representative image of a plate after Alizarin Red S staining.
Representative image of a plate as example of our screening results. Several wells do not show red staining: the corresponding silenced genes represent putative candidates of the screening.

A remarkable result of the Gene Ontology analysis was to find a consistent fraction of genes (30%) with unknown function at the time of the screening. These genes belong to the Riken collection. In particular, we focused our attention on a short number of them that we named Osteoblasts Inducer (ObI). These genes were chosen on the basis of their putative function: indeed, they are predicted to be transcription factors according bioinformatic analysis. In my thesis project I focused on one of these potential transcription regulators, named ObI-1.

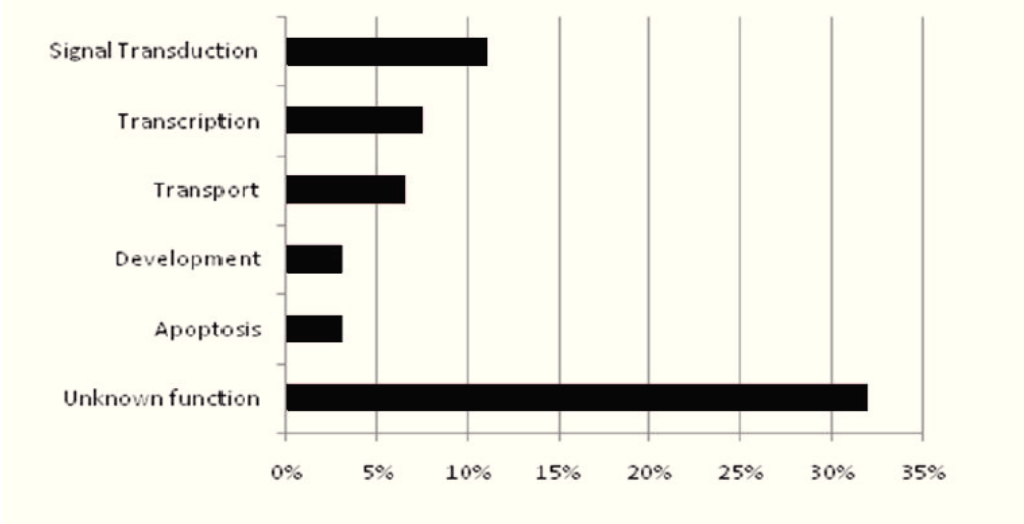

Fig.10: Gene Ontology classification of screening candidate genes.
Results of Gene Ontology classification of the candidate genes from the first part of our screening. Biological processes represented by more than 3% of our candidates are shown in the graphic.

4.3 – ObI-1 candidate gene

4.3.1 – ObI-1 silencing impairs formation of mineralized deposits

Among the candidate genes with unknown function, ObI-1 silencing with the corresponding shRNA construct of the library produced an almost total absence of Alizarin Red S staining compared to the positive control of differentiation. Furthermore, the effect seems to be specific for this shRNA since the transfection with the shRNA-NS produced the same effect of the positive control of differentiation (Fig.11).

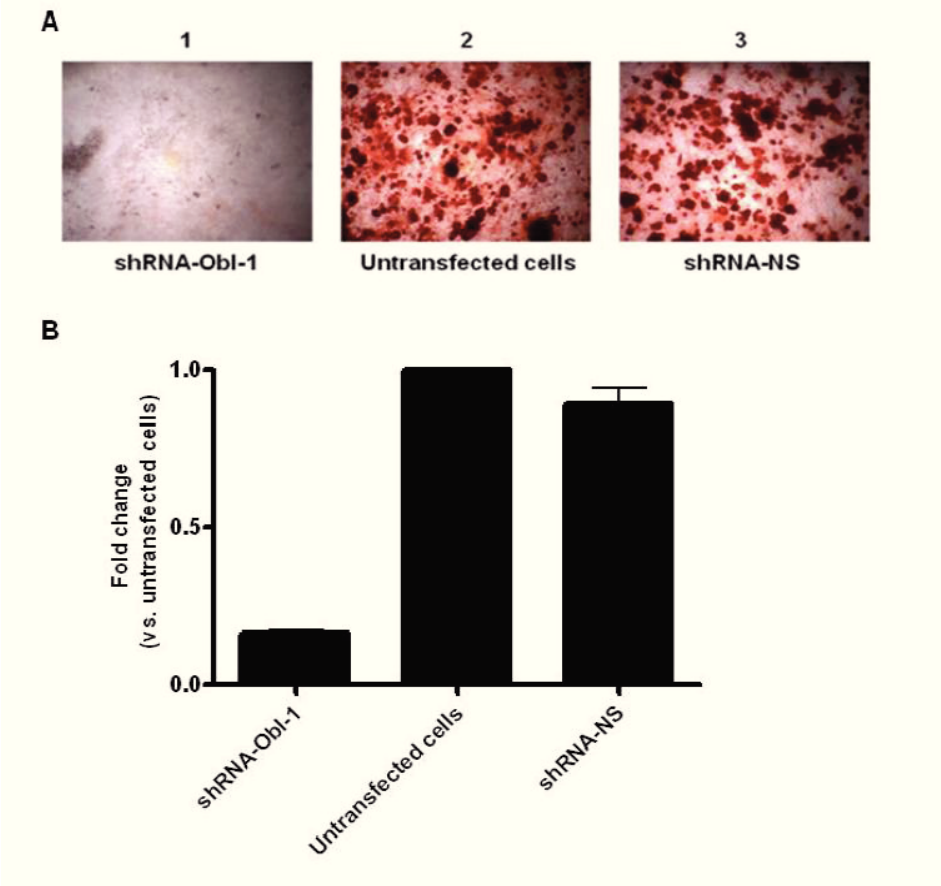

Fig.11: ObI-1 screening results.
Alizarin Red S staining after culture in osteogenic medium for 21 days of: 1) W20-17 cells transfected with shRNA-ObI-1; 2) untransfected cells; 3) cells transfected with shRNA Non Silencing (A). Calcium deposition quantitation using Guanidine HCl 4M and adsorbance reading at 490 nm (B). Data are means ± SD of 3 experiments.

In order to ensure the specificity of the data and to overcome off-target effects, we confirmed the screening results using two additional shRNA constructs interfering with ObI-1 gene available in the library; these shRNAs recognize different regions of ObI-1 mRNA, thereby minimizing the possibility of sequence-dependent off-target effects. Results obtained with all three constructs showed a significant reduction of Alizarin Red S staining (Fig.12 A-

B). To validate the efficiency of the silencing, transcript levels of ObI-1 gene were evaluated by Real-Time PCR analysis. In ObI-1 silenced cells, with all three constructs, the levels of transcript were extremely reduced compared to untransfected cells and Non-Silencing transfected cells, since full match with the target sequence resulted in all three cases in mRNA degradation (Fig.12 C). These results together confirmed that the observed impairment of osteogenic differentiation was specifically due to ObI-1 silencing.

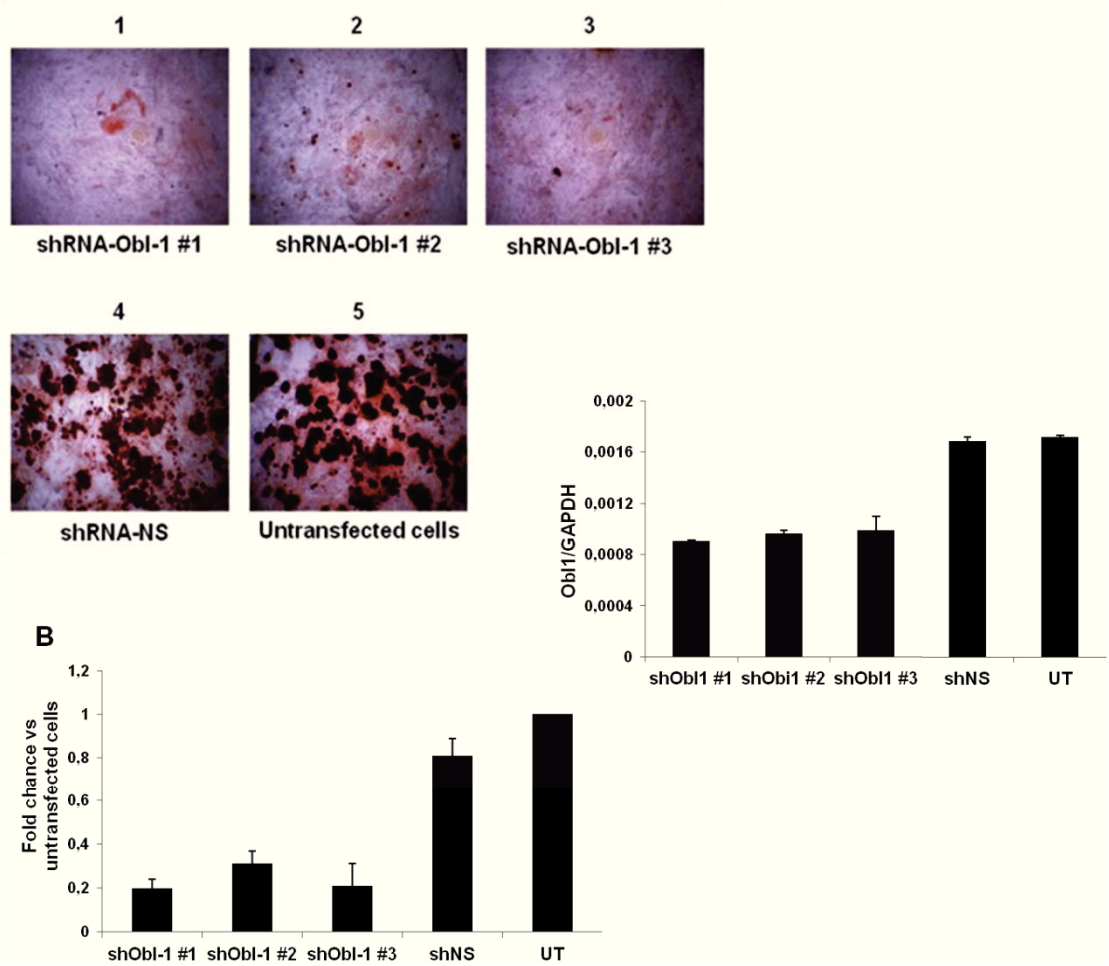

Fig.12: Confirmation of screening results.
Alizarin Red S staining after culture in osteogenic medium for 21 days of: 1) W20-17 cells transfected with shRNA-ObI-1#1 (shRNA construct used during the screening); 2-3) cells transfected with shRNA-ObI-1#2 and shRNA-ObI-1#3 (other two library constructs acting against ObI-1 gene); 4) cells transfected with shRNA-Non Silencing; 5) Untransfected (UT) cells (A). Calcium deposition quantitation using Guanidine HCl 4M and adsorbance reading at 490 nm (B). Real Time PCR analysis of ObI-1 transcript levels. Data are means ± SD of 3 experiments.

4.3.2 – In silico characterization of ObI-1 domains and phylogenesis

Prior to further experimental evaluations of the role of ObI-1, we proceeded with an in silico analysis to better understand its structure and function. Analysis on Ensembl database showed two predicted transcripts for ObI-1: a long form and a short form (Fig.13 A). Analysis of the protein domains revealed that ObI-1 could encode for a transcription factor; indeed, the long form presents an amino-terminal Kruppel-associated box (KRAB) domain, usually associated to transcriptional repression, and several zinc-finger domains (DNA binding domain) at the C-terminus (Fig.13 B). The short form instead contains only a KRAB domain (Fig.13 C).

The phylogenetic analysis of ObI-1 gene was also performed on Ensembl database in order to research orthologous genes in other species. We found orthologs in many species, such as Human (Homo Sapiens), Macaque (Macaca mulatta), Orangutan (Pongo abelii) and Rat (Rattus Norvegicus). In total, 25 orthologous genes were present in the latest Ensembl release (release 75, February 2014), including both known and predicted protein-coding genes; in this last Ensembl release the human ortholog, present in previous versions, is missing while non-human primates orthologs are still present. Therefore, orthologs research was also performed using Metaphors (http://orthology.phylomedb.org/), a public repository of phylogeny-based orthology and paralogy predictions computed using resources available in seven different homology prediction services, and we were able to confirmed the presence of an human ortholog, corresponding to the known protein coding gene ZNF717.

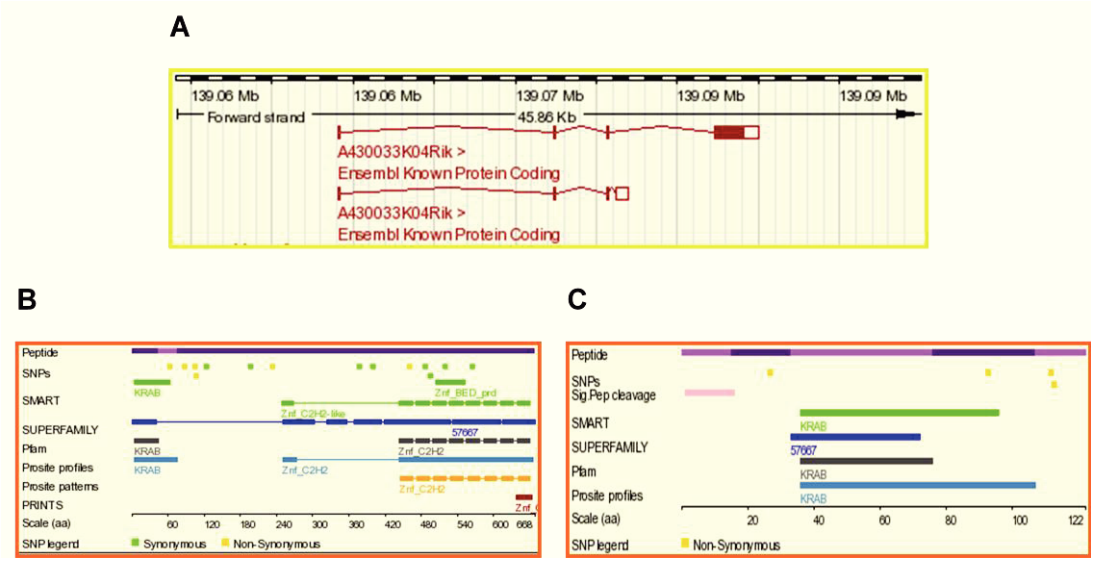

Fig.13: ObI-1 predicted transcripts and proteic domains.
Bioinformatic analysis (Ensembl) of ObI-1 transcripts (A). Bioinformatic analysis to evaluate the presence of functional domains in ObI-1 proteins: the long form presents a KRAB domain and several Zinc finger domains, short form presents only a KRAB domain (B).

4.3.3 – ObI-1 expression in mouse

We first performed an in silico analysis of ObI-1 expression in different tissues, consulting UniGene database of NCBI (National Centry of Biotechnology Information). The analysis of the expressed sequence tag (EST) profiles showed that ObI-1 is expressed in several murine adult tissues as well as during embryonic development (Fig.14).

Since EST profiles show approximate gene expression patterns and may not be accurate, we then performed a Real-Time PCR analysis to directly evaluate ObI-1expression in different mouse tissues and organs and we found that ObI-1 transcript is present in several tissues, including bone (Fig.15).

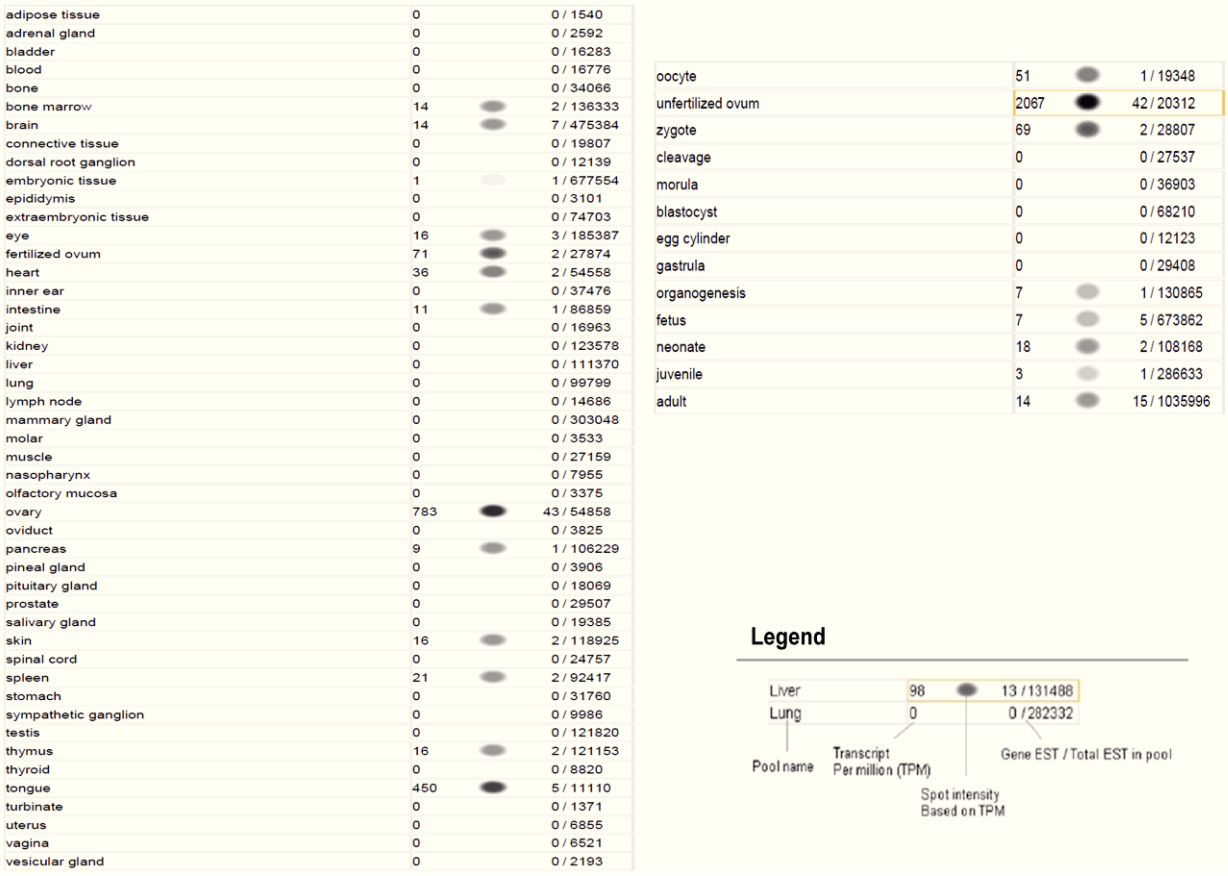

Fig.14: In silico analysis of ObI-1 expression.
EST profile of ObI-1 transcript in different mouse tissues and developmental stages. (http://www.ncbi.nlm.nih.gov/UniGene/ESTProfileViewer.cgi?uglist=Mm.36612).

4.3.4 – Expression analysis of ObI-1 during osteogenic differentiation

Expression analysis of ObI-1 gene in W20-17 cell line was performed to evaluate the presence of its transcripts during osteogenic differentiation. We analyzed by Real Time PCR the presence of both Obi-1 transcripts, at different time-points (T0, corresponding to the undifferentiated cells, and T4, T14 and T21). The levels of the long form of ObI-1 increase at day 4 of differentiation

and remain high during the whole process. The short form, instead, was almost undetectable, indicating that it might be either only thereotical or unrelevant in osteoblastic differentiation (Fig.16 A); therefore it was not further investigated.

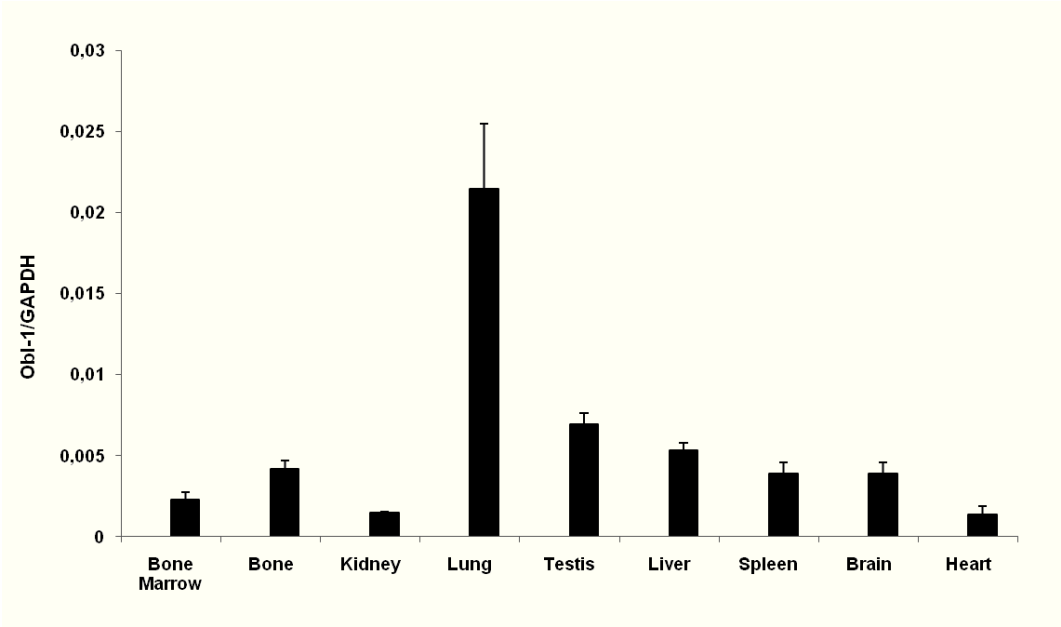

Fig.15: ObI-1 expression profile in tissues.
Real Time PCR analysis of ObI-1 expression in different mouse tissues and organs.

After analysis in W20-17 cell line, we also analyzed by Real Time PCR the expression of ObI-1 gene in primary murine mesenchymal stem cells (mMSC) isolated from bone marrow during osteogenic differentiation. In this case we evaluated only ObI-1 long transcript and we considered three different time points: T0, corresponding to undifferentiated cells, and T3 and T21. As previously reported for W20-17 cells, we detected an increase of ObI-1 transcript levels starting from the first days of osteogenic differentiation: indeed, ObI-1 expression rose at day 3 and further increased at day 21 (Fig.16 B).

4.3.5 – ObI-1 silencing affects osteogenic differentiation in primary mMSCs

To confirm the validity of our data, we analyzed the effects of ObI-1 silencing also in primary mMSCs. As previously observed for W20-17 cells, we were able to confirm that ObI-1 silencing significantly impaired the ability of cells to produce mineralized nodules, as assessed by Alizarin Red S staining after 18 days of osteogenic induction (Fig.17 A). We also confirmed the silencing efficiency by evaluating ObI-1 transcript levels by Real Time PCR. In ObI-1 silenced cells, with two distinct constructs targeting different regions of ObI-1 mRNA, the levels of transcript were extremely reduced compared to untransfected cells and Non-Silencing transfected cells (Fig.17 B).

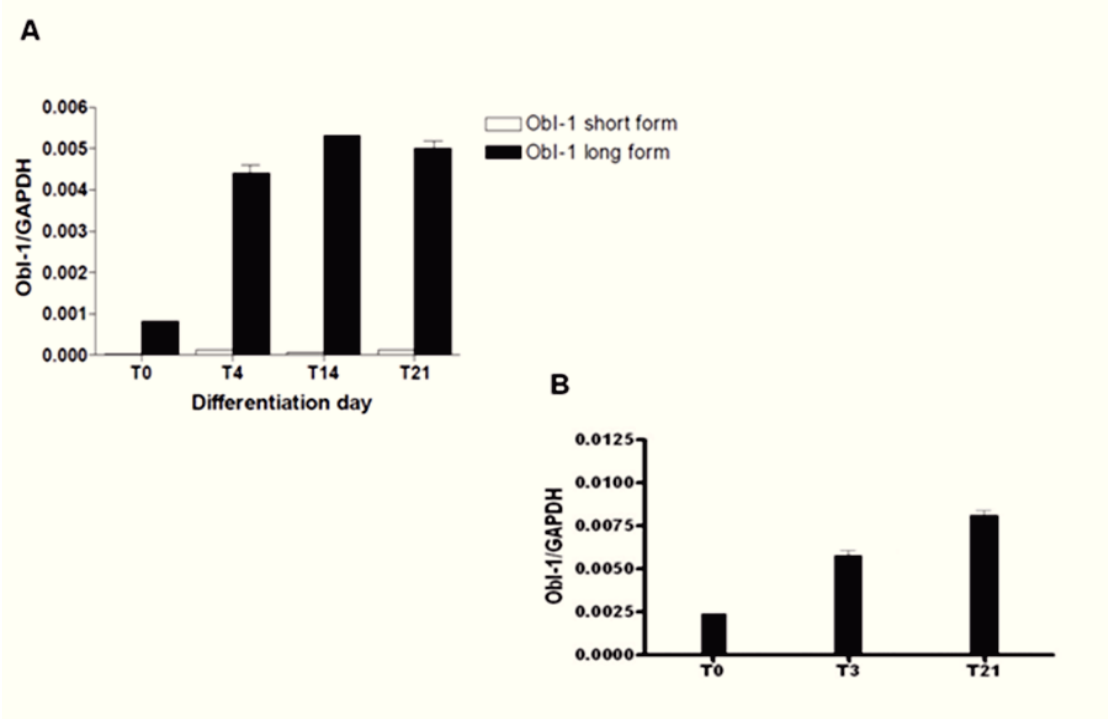

Fig.16: Expression analysis of ObI-1 during osteogenic differentiation.
Expression profile of ObI-1 transcripts during osteogenic differentiation of W20-17 cells at day 0, 4, 14 and 21 (A) and of mMSC cells at day 0, 3 and 21 (B). Data are means ± SD of 3 experiments.

Then, we evaluated whether the function of ObI-1 was required for the proper differentiation of mMSCs into osteoblasts. Indeed, by performing the Alizarin Red S staining, we investigated the end point of osteogenic differentiation, represented by the mineralized matrix production, but we were not able to discriminate if ObI-1 function is necessary during the first stages of the differentiation process, namely pre-osteoblast proliferation and subsequent differentiation; further experiments are required to determine whether ObI-1 silencing resulted in a reduced mineralization as a consequence of impaired osteoblasts differentiation and maturation or, rather, it is involved only in the latter mineralization phase. Therefore, we evaluated the expression of ALP, a marker expressed by mature osteoblasts, by performing an ALP staining, and we observed that ObI-1 silencing resulted in a reduced staining (Fig.18). This experiment showed that ObI-1 is not involved only in the mineralization phase, but osteoblasts differentiation and/or proliferation of osteogenic precursors may be dependent on the expression of this gene. Moreover, this result is in agreement with the previous observation that ObI-1 is expressed early during osteogenic differentiation of both W20-17 and primary cells.

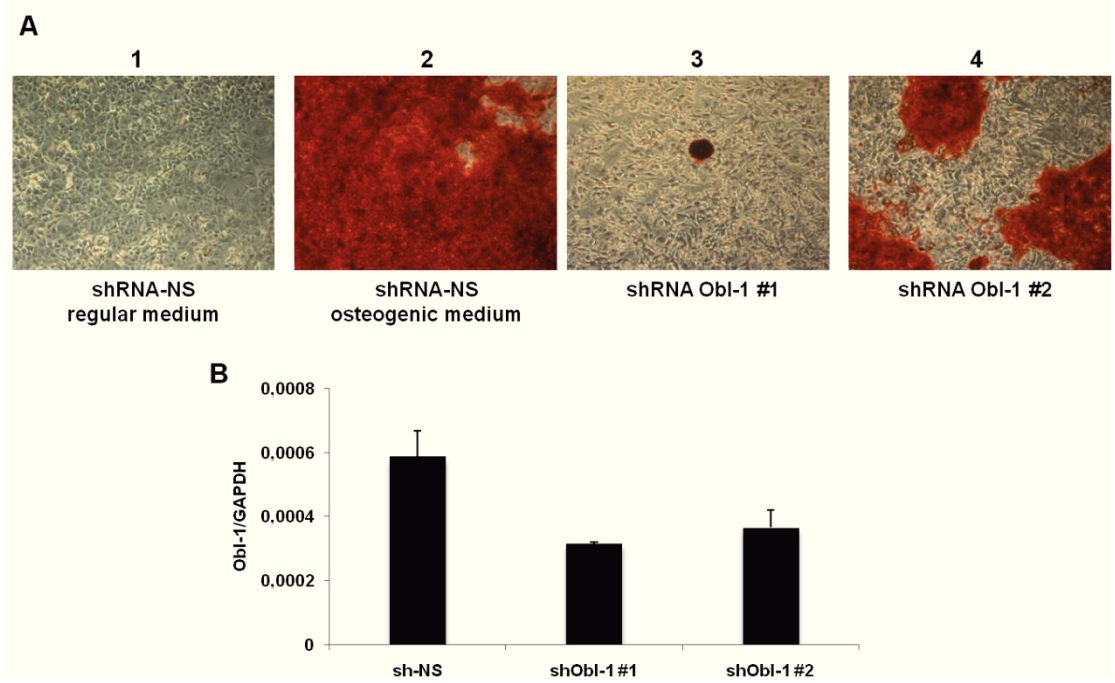

Fig.17: ObI-1 silencing effects in primary mMSCs.
Alizarin Red S staining of mMSCs after 18 days of culture. 1-2) mMSCs transfected with shRNA-NS cultured, respectively, in regular and osteogenic medium; 3-4) mMSCs cells transfected with shRNA-ObI-1#1 and shRNA-ObI-1#2 cultured in osteogenic medium (A). Real Time PCR analysis of ObI-1 transcript levels (B). Data are means ± SD of 3 experiments.

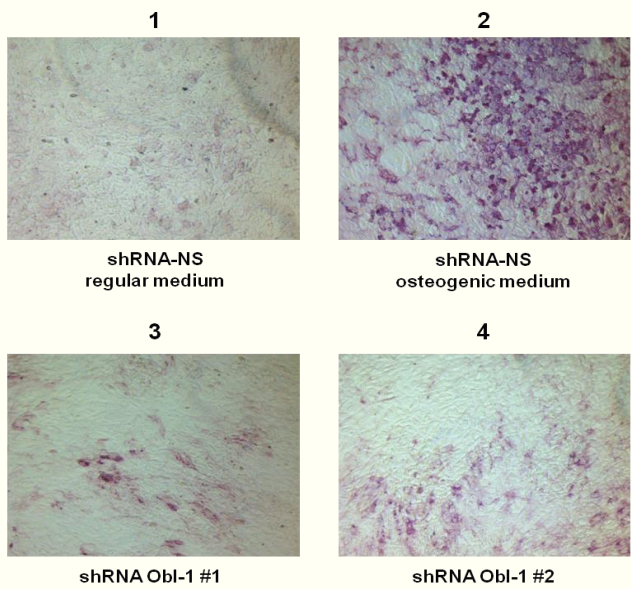

Fig.18: ObI-1 silencing effects on mMSCs differentiation into osteoblasts.
ALP staining of mMSCs after 12 days of culture. 1-2) mMSCs transfected with shRNA-NS cultured, respectively, in regular and osteogenic medium; 3-4) mMSCs cells transfected with shRNA-ObI-1#1 and shRNA-ObI-1#2 cultured in osteogenic medium.

4.3.6 - Expression profile of osteogenic differentiation markers in ObI-1 silenced cells

To better investigate the role of ObI-1 during osteogenic differentiation we evaluated, by Real Time PCR analysis, expression profile of some osteogenic differentiation markers in untransfected cells and in cells transfected with either shObI-1 or sh-NS. In particular, we analyzed the expression of two markers, Runx2 and osteopontin (OPN). The transcription factor Runx2 is considered the master gene of osteoblastogenesis; it is an early marker expressed during the first days of the differentiation process and it is absolutely required for the commitment of MSCs towards the osteogenic lineage as well as for the function of mature osteoblasts. OPN, on the other end, is a sialoprotein of the bone matrix and its levels increase steadily throughout the diffentiation process from the first days of differentiation, reaching a peak during the mineralization phase; therefore, OPN is considered also a late marker of osteoblastogenesis. We found that levels of both markers were significantly reduced in ObI-1 silenced cells while, in cells transfected with sh-NS, the expression levels were comparable to untransfected cells (Fig.19).

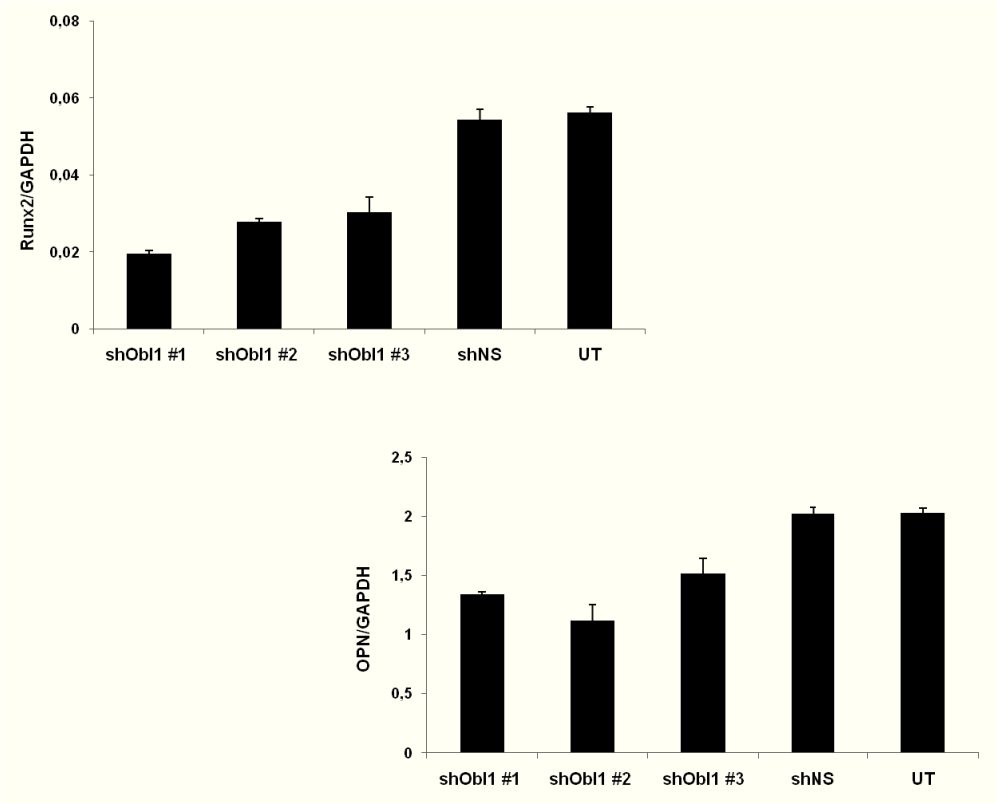

Fig.19: Effect of ObI-1 silencing on bone differentiation marker expression.
Expression profile of early differentiation markers in W20-17 ObI-1 silenced cells. Real Time PCR analysis was performed at day 4 of osteogenic differentiation and reveals a decreased expression of both Runx2 and osteopontin in ObI-1 silenced cells compared to untransfected (UT) cells and cells transfected with sh-NS.

4.3.7 – ObI-1 is a nuclear protein

We performed an immunofluorescence analysis in order to evaluate the sub-cellular localization of the protein product of ObI-1 gene. At this aim, we first cloned the cDNA of ObI-1 long form in pcDNA 3.1 plasmid with a carboxy-terminal Flag tag since specific antibodies against ObI-1 protein were not available at the moment. We collected protein lysates from mMSCs transfected with either the ObI-1 Flag-encoding plasmid or the empty vector 24 hours after transfection and we were able to confirm ObI-1 expression by Western Blot analysis (Fig.20 A). Subsequently, we performed an immunofluorescence analysis to assess ObI-1 protein cellular localization. Merge between the nuclear dye DAPI and the anti-Flag antibody indicated that ObI-1 localized only into the cell nucleus, thereby supporting the hypothesis that this gene encodes for a transcription factor; however ObI-1 seems to be excluded from the nucleoli (Fig.20 B).

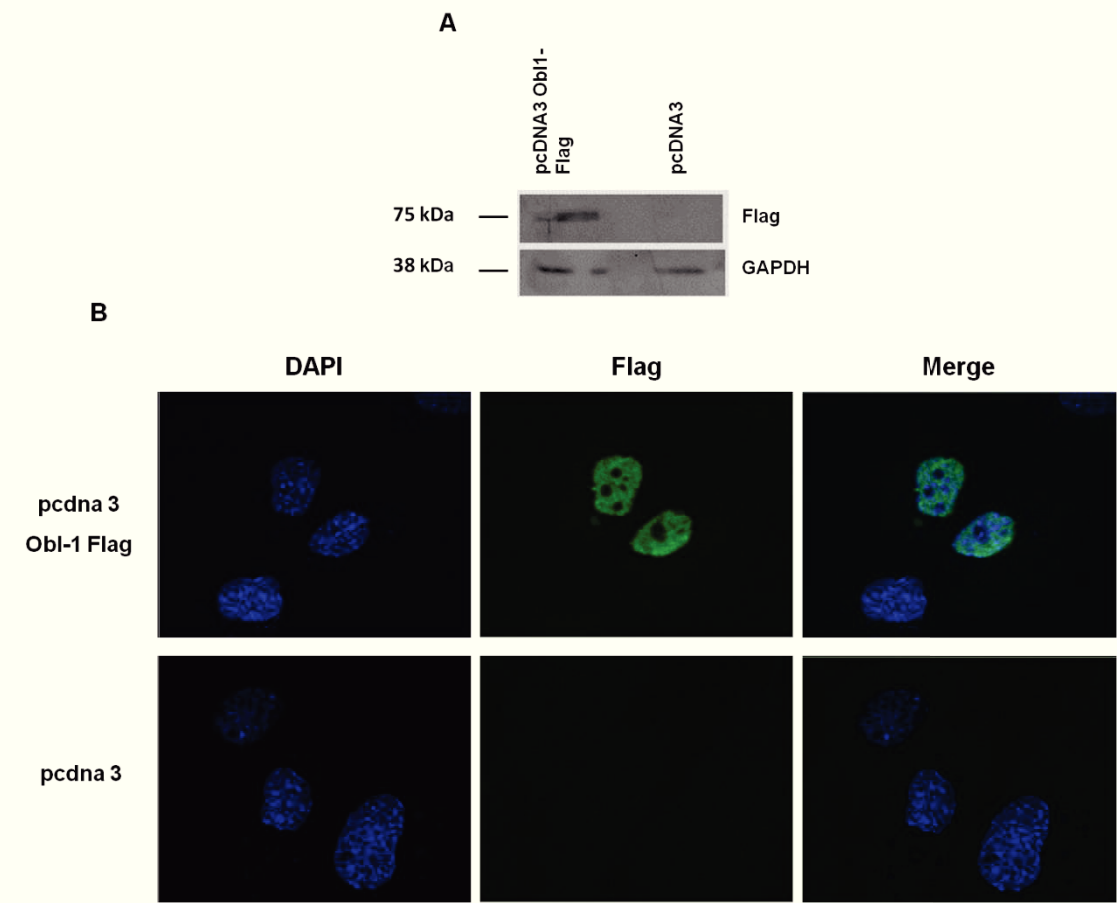

Fig.20: Analysis of ObI-1 sub-cellular localization.
Western Blot analysis to confirmed ObI-1 expression in mMSCs transfected with pcdna 3 ObI-1 Flag. Cells transfected with the empty vector were used as a negative control. GAPDH was used as control for protein loading (A). Immunofluorescence analysis indicating the nuclear localization of ObI-1 protein (B).

4.4 - Discussion

Osteoblastogenesis is a complex and still not yet completely elucidated biological process regulated by several hormones, signaling molecules and growth factors and characterized by the activation and inactivation of transcription factors and by the expression of bone-specific differentiation markers. Great efforts have been made to characterize the factors that drive MSCs commitment towards the osteogenic lineage and regulate osteoblasts maturation and bone synthesis; however, further studies are mandatory to identify the molecular mechanisms underlying cellular differentiation and all the pathways and the molecules involved. This is of paramount importance to identify new targets for the development of novel therapeutic options for the treatment of bone-related diseases as well as to optimize the differentiation process and to obtain the large amount of progenitor cells needed for tissue engineering applications.

To identify genes involved in this biological process, we performed a screening with an RNA interference-based approach and silenced a large number of genes during osteoblast differentiation of W20-17 cells, a murine MSC-derived cell line. The same library had been successfully used to identify genes involved in the maintenance of ESCs stemness (Parisi et al. 2008). With this procedures we were able to identify several genes potentially involved in osteogenesis since their silencing impaired the ability of cells to produced mineralized deposits, as assessed by Alizarin Red staining. We decided to performed Alizarin Red S staining to evaluate osteogenic differentiation for two principal reasons: the method is quite simple, largely described and used in literature and gives solid and reproducible results, and it allowed us to evaluate the end point of differentiation and, therefore, to identify genes involved in any stage of the process. We also validated our experimental approach as well as the functionality of the shRNAs of the library including several controls, such as untransfected cells in culture with normal and osteo-inductive medium, cells transfected with shRNA-NS and shRNAs that silenced known genes involved in osteogenesis regulation.

We then analyzed the Gene Ontology classification of candidate genes and we found a significant fraction (30%) of genes with unknown function at the time of the screening. Hence, we focused our attention on one of these genes, predicted to be a transcription factor, that we named Osteoblasts Inducer-1 (ObI-1). We found other constructs in the library that recognized ObI-1 gene and, therefore, we could perform silencing confirmation experiments with three different constructs; this represents a specificity control for the RNA interference technique. Indeed, in RNA-interference experiments, a molecule can cause off-target effects, independently by its activity on the putative mRNA target (Jackson and Linsley 2010). However, since we obtained the same results with different RNA molecules interfering with the same gene, we could exclude off-target effects.

We next proceeded with an in-silico analysis, particularly required for genes with unknown function. Ensembl analysis showed that ObI-1 encodes

for two potential transcripts, a long form and a short form. Interestingly, the long form encodes for a potential transcription factor as the protein contains several zinc-finger domains at C-terminus and an amino-terminal KRAB domain. Therefore, we hypothesized that ObI-1 could belong to the family of KRAB-containing zinc-finger transcription repressors. These transcription regulators represent the largest single family of transcription factors in mammals, they are present only in tetrapod vertebrates and have been involved in several biological processes, including cell proliferation and differentiation, apoptosis and neoplastic transformation (Urrutia 2003). Moreover, a recently identified KRAB-containing transcription factor have been involved in regulation of osteogenic differentiation (Jheon et al. 2001). To confirm this hypothesis we performed an immunofluorescence experiment aimed at the identification of ObI-1 sub-cellular localization and we were able to demonstrate the nuclear localization of the protein, reinforcing the idea that this gene may encode for a transcription factor.

Proceeding with the bioinformatic analysis on Ensembl, we demonstrated a possible conservation of this gene: in fact we found orthologues in several species. It was interesting to find homologous genes in Human with different levels of identity with the mouse gene (the better value was about 46% for one of them). However, in Ensembl last release 75 (February 2014) the human ortholog is no longer reported. Therefore, ortholog research was also performed using Metaphors (http://orthology.phylomedb.org/), a public repository of phylogeny-based orthology and paralogy predictions computed combining multiple prediction methods, and we confirmed the presence of an human ortholog. Ortholog prediction is a powerful comparative genomic tool, useful for gene function prediction and phylogenetic analysis, and a large variety of orthologs prediction methods have been developed in the last few years, including the Ensembl resource (EnsemblCompara; Vilella et al. 2009). However, the few comparative studies of the quality of the different algorithms currently available show that the predictions are not always accurate and reliable, that often different resources originate different results and that some methods perform better than others depending on the specific task (Chen et al. 2007; Altenhoff and Dessimoz 2009). Moreover, orthologs prediction is not a trivial issue, particularly for eukaryotic genomes because of their size, the complexity of protein domain architecture and extensive gene duplications (Doolittle 1995; Henikoff et al. 1997). Therefore, the results of such predictions should always be cautiously taken into account and, whether feaseble, complemented with experimental data.

Expression analysis of ObI-1 in tissues was investigated with both in silico analysis and Real-Time PCR experiments after RNA extraction from different mouse tissues. In-silico analysis was performed by EST profiles research on UniGene database of NCBI. ESTs derived from automated partial sequencing of a library of complementary DNA (cDNA) obtained from retro-transcription of longer mRNAs present in a specific tissue, cell types,

developmental stage or pathologic condition, used to construct the cDNA library. Therefore, an EST profile can give an approximate gene expression pattern of a specific gene. This analysis showed that ObI-1 is expressed in several tissues, including bone marrow, and during mouse development. Our analysis performed by Real-time PCR revealed a different distribution of ObI-1 gene in mouse tissues and organs. For example, we found that ObI-1 is expressed at high levels in lung, while no expression of the gene was found in this organ by EST profiles analysis. Also data regarding other organs were different, such as the expression of ObI-1 in bone. Concerning the inconsistencies between the two analyses, it is important to note that the EST profiles evaluation, although valuable, shows only approximate gene expression patterns and presents some limitations. In fact, EST sequences might contain errors and the accuracy of the predicted expression profiles is, especially for low-abundant transcripts, highly dependent on the cDNA library dimension and prone to misrepresentation (Alba et al. 2004).

Then, we evaluated by Real Time PCR the expression of ObI-1 in W20-17 cells. We analyzed the expression of both ObI-1 transcripts during osteogenic differentiation and we detected an increase in the levels of the long form only during the differentiation process; its levels increased from the first days of differentiation and remained high until the end, indicating that it could play a role in this process. The levels of the short form, instead, were very low, almost undetectable, during the all process and, therefore, it was no longer investigated. Indeed, this finding could indicate that either the short form is only theoretical or it is not involved in osteogenic regulation. Although the levels of ObI-1 long form significantly increased during osteogenic differention (5-fold increase from day 0 to day 4 of differentiation), they were generally quite low but seemingly sufficient to exert their effect.

In order to complete expression analysis in cells, we also performed a Real Time PCR analysis in primary mMSCs isolated from mouse in our laboratory (Esposito et al., 2009). Analysis in primary cells was very important since a cell line, such as W20-17, may not exactly reproduce a physiological cellular environment, although it presents several advantages, as a greater standardization and reproducibility of the experiments and the possibility to extensively expand the cells in an undifferentiated state. On the other hand, primary cells keep the distinctive features of the native organ or tissue and reflect better the biochemical activities of cells *in vivo* compared to a cell line. Expression of ObI-1 gene during osteogenic differentiation of mMSCs was comparable to the data obtained in W20-17 cells. This finding further confirmed a role of our candidate in osteogenic differentiation.

Therefore, we proceeded with the validation of ObI-1 silencing effects on osteogenic differentiation of primary mMSCs and, as previously reported for W20-17 cells, we observed a reduction in mineralized matrix synthesis, assessed by Alizarin Red S staining, in ObI-1 silenced cells compared to cells transfected with shRNA-NS. In addition, we also observed that ObI-1 silencing resulted in a reduced expression of ALP, a marker expressed by

mature osteoblasts. Thereby, we could conclude that ObI-1 plays a role not only in the latter mineralization stage, but its function is important also in an earlier phase of differentiation. This hypothesis was further corroborated by the observation that ObI-1 silencing caused a reduced expression, at day 4 of differentiation of W20-17 cells, of the osteogenic markers Runx-2 and OPN. Indeed, the transcription factor Runx-2 is an early marker of osteogenesis and it is required for the commitment of MSCs towards the osteogenic lineage; it is involved also in the later stages of differentiation but its role is still not clear. OPN, instead, is a bone sialoprotein expressed throughout osteogenic diffentiation, from the first days of the process.

5 – Conclusions

In conclusion, in this work we have described the identification, through an RNAi-based screening, and the characterization of ObI-1, a novel potential transcription factor involved in the regulation of osteogenic differentiation of mMSCs. Indeed, ObI-1 function seems to be important for the proper osteoblasts maturation and bone mineral matrix deposition.

Currently, we are investigating the potential role of ObI-1 as a transcription factor, its targets and the molecular pathways in which the gene is involved. Indeed, we are performing a microarray analysis to evaluate the differential gene expression in cells in which ObI-1 has been silenced compared to control cells. We have planned to performed also a chromatin immunoprecipitation assay followed by high-throughput DNA sequencing (ChIP-seq), in order to identify the specific DNA sequences bound by ObI-1 and, therefore, its direct targets. These assessments, indeed, could be useful to better understand the role played by ObI-1 during osteogenesis as well as to elucidate the biological pathways in which it is involved.

We are interested also in the better evaluation and identification of ObI-1 human ortholog, by combining the in silico analysis with different bioinformatic tools and experimental data. To accomplish this goal, for instance, we could take advantage of microarray and ChIP-seq data; indeed, the identification of ObI-1 targets and molecular pathways could be useful to identify the human protein that plays an analogous role.

We are also planning to analyze the expression profile of additional osteogenic markers in ObI-1 silenced cells as well as to investigate the potential involvement of this gene in regulating other differentiation processes.

Finally, we would like to examine ObI-1 function *in- vivo*, using a knock-out or a conditional knock-out mouse model. In this way, we could better understand not only the role of our candidate gene in osteogenesis but also its involvement in other biological processes.

References

Alba R, Fei Z, Payton P, Liu Y, Moore SL, Debbie P, Cohn J, D'Ascenzo M, Gordon JS, Rose JK, Martin G, Tanksley SD, Bouzayen M, Jahn MM, Giovannoni J. ESTs, cDNA microarrays, and gene expression profiling: tools for dissecting plant physiology and development. Plant J 2004;39:697-714.

Altenhoff AM, Dessimoz C. Phylogenetic and functional assessment of orthologs inference projects and methods. PLoS Comput Biol. 2009;5:e1000262.

Barlow S, Brooke G, Chatterjee K, Price G, Pelekanos R, Rossetti T, Doody M, Venter D, Pain S, Gilshenan K, Atkinson K. Comparison of human placenta- and bone marrow-derived multipotent mesenchymal stem cells. Stem Cells Dev 2008;17:1095-1107.

Carmona-Saez P, Chagoyen M, Tirado F, Carazo JM, Pascual-Montano A. GENECODIS: a web-based tool for find significant concurrent annotations in gene lists". Genome Biol 2007;8(1):R3.

Chen F, Mackey AJ, Vermunt JK, Roos DS.Assessing performance of orthology detection strategies applied to eukaryotic genomes. PLoS One 2007;2:e383.

Chen Y, Whetstone HC, Youn A, Nadesan P, Chow EC, Lin AC, Alman BA. Beta-catenin signaling pathway is crucial for bone morphogenetic protein 2 to induce new bone formation. J Biol Chem. 2007;282:526-33.

Dodig M, Tadic T, Kronenberg MS, Dacic S, Liu YH, Maxson R, Rowe DW, Lichtler AC. Ectopic Msx2 overexpression inhibits and Msx2 antisense stimulates calvarial osteoblast differentiation. Dev Biol 1999;209:298-307.

Dominici M, Le Blanc K, Mueller I, Slaper-Cortenbach I, Marini F, Krause D, Deans R, Keating A, Prockop D, Horwitz E. Minimal criteria for defining multipotent mesenchymal stromal cells. The International Society for Cellular Therapy position statement. Cytotherapy 2006;8:315-317.

Doolittle RF. The multiplicity of domains in proteins. Annu Rev Biochem 1995;64:287-314.

Ducy P, Zhang R, Geoffroy V, Ridall AL, Karsenty G. Osf2/Cbfa1: A transcriptional activator of osteoblast differentiation. Cell 1997;89:747–754.

Erlebacher A, Filvaroff EH, Gitelman SE, Derynck R. Toward a molecular understanding of skeletal development. Cell 1995;80:371-8.

Esposito MT, Di Noto R, Mirabelli P, Gorrese M, Parisi S, Montanaro D, Del Vecchio L, Pastore L. Culture conditions allow selection of different mesenchymal progenitors from adult mouse bone marrow. Tissue Eng Part A 2009;15:2525-2536.

Friedenstein AJ, Piatetzky S, II, Petrakova KV. Osteogenesis in transplants of bone marrow cells. J Embryol Exp Morphol 1966;16:381-390.

Henikoff S, Greene EA, Pietrokovski S, Bork P, Attwood TK, Hood L. Gene families: the taxonomy of protein paralogs and chimeras. Science. 1997;278:609-14.

Huang LF, Fukai N, Selby PB, Olsen BR, Mundlos S. Mouse clavicular development: analysis of wild-type and cleidocranial dysplasia mutant mice. Dev Dyn 1997;210:33-40.

Iso Y, Spees JL, Serrano C, Bakondi B, Pochampally R, Song YH, Sobel BE, Delafontaine P, Prockop DJ. Multipotent human stromal cells improve cardiac function after myocardial infarction in mice without long-term engraftment. Biochem Biophys Res Commun 2007;354:700-706.

Jackson AL, Linsley PS. Recognizing and avoiding siRNA off-target effects for target identification and therapeutic application. Nature Reviews Drug Discovery 2010;9:57-67.

Jheon AH, Ganss B, Cheifetz S, Sodek J. Characterization of a novel KRAB/C2H2 zinc finger transcription factor involved in bone development. J Biol Chem 2001;276:18282-9.

Komori T, Yagi H, Nomura S, Yamaguchi A, Sasaki K, Deguchi K, Shimizu Y, Bronson RT, Gao YH, Inada M, Sato M, Okamoto R, Kitamura Y, Yoshiki S, Kishimoto T. Targeted disruption of Cbfa1 results in a complete lack of bone formation owing to maturational arrest of osteoblasts. Cell 1997;89:755–764.

Lee KS, Hong SH, Bae SC. Both the Smad and p38 MAPK pathways play a crucial role in Runx2 expression following induction by transforming growth factor-beta and bone morphogenetic protein. Oncogene 2002;21:7156-63.

Lee NK, Sowa H, Hinoi E, Ferron M, Ahn JD, Confavreux C, Dacquin R, Mee PJ, McKee MD, Jung DY, Zhang Z, Kim JK, Mauvais-Jarvis F, Ducy P,

Karsenty G. Endocrine regulation of energy metabolism by the skeleton. Cell 2007;130:456-69.

Liu J, Carmell MA, Rivas FV, Marsden CG, Thomson JM, Song JJ, Hammond SM, Joshua-Tor L, Hannon GJ. Argonaute2 is the catalytic engine of mammalian RNAi. Science 2004;305:1437-41

Liu W, Toyosawa S, Furuichi T, Kanatani N, Yoshida C, Liu Y, Himeno M, Narai S, Yamaguchi A, Komori T. Overexpression of Cbfa1 in osteoblasts inhibits osteoblast maturation and causes osteopenia with multiple fractures. J Cell Biol 2001;155:157-66.

Lund E, Güttinger S, Calado A, Dahlberg JE, Kutay U. Nuclear export of microRNA precursors. Science 2004;303:95-8.

Miyama K, Yamada G, Yamamoto TS, Takagi C, Miyado K, Sakai M, Ueno N, Shibuya H. A BMP-inducible gene, dlx5, regulates osteoblast differentiation and mesoderm induction. Dev Biol 1999;208:123-33.

Moriscot C, de Fraipont F, Richard MJ, Marchand M, Savatier P, Bosco D, Favrot M, Benhamou PY. Human bone marrow mesenchymal stem cells can express insulin and key transcription factors of the endocrine pancreas developmental pathway upon genetic and/or microenvironmental manipulation *in vitro*. Stem Cells 2005;23:594-603.

Nakashima K, Zhou X, Kunkel G, Zhang Z, Deng JM, Behringer RR, de Crombrugghe B. The novel zinc finger-containing transcription factor osterix is required for osteoblast differentiation and bone formation. Cell 2002;108:17-29.

Oswald J, Boxberger S, Jorgensen B, Feldmann S, Ehninger G, Bornhauser M, Werner C. Mesenchymal stem cells can be differentiated into endothelial cells *in vitro*. Stem Cells 2004;22:377-384.

Parisi S, Passaro F, Aloia L, Mannabe I, Nagari R, Pastore L, Russo T. Klf5 is involved in self-renewal of mouse embryonic stem cells. J Cell Sci 2008;121(Pt16):2629-34.

Phinney DG, Isakova I. Plasticity and therapeutic potential of mesenchymal stem cells in the nervous system. Curr Pharm Des 2005;11:1255-1265.

Prockop DJ. Marrow stromal cells as stem cells for nonhematopoietic tissues. Science 1997;276:71-74.

Ren G, Chen X, Dong F, Li W, Ren X, Zhang Y, Shi Y. Concise review: mesenchymal stem cells and translational medicine: emerging issues. Stem Cells Transl Med 2012;1:51-58.

Robledo RF, Rajan L, Li X, Lufkin T. The Dlx5 and Dlx6 homeobox genes are essential for craniofacial, axial, and appendicular skeletal development.Genes Dev 2002;16:1089-101.

Satokata I, Ma L, Ohshima H, Bei M, Woo I, Nishizawa K, Maeda T, Takano Y, Uchiyama M, Heaney S, Peters H, Tang Z, Maxson R, Maas R. Msx2 deficiency in mice causes pleiotropic defects in bone growth and ectodermal organ formation. Nat Genet 2000;24:391-5.

Savarino L, Baldini N, Greco M, Capitani O, Pinna S, Valentini S, Lombardo B, Esposito MT, Pastore L, Ambrosio L, Battista S, Causa F, Zeppetelli S, Guarino V, Netti PA. The performance of poly-epsilon-caprolactone scaffolds in a rabbit femur model with and without autologous stromal cells and BMP4. Biomaterials 2007;28:3101-3109.

Takahashi K, Yamanaka S. Induction of pluripotent stem cells from mouse embryonic and adult fibroblast cultures by defined factors. Cell 2006;126:663-76.

Urrutia R. KRAB-containing zinc-finger repressor proteins.Genome Biol 2003;4:231.

Vilella AJ, Severin J, Ureta-Vidal A, Heng L, Durbin R, Birney E. EnsemblCompara GeneTrees: Complete, duplication-aware phylogenetic trees in vertebrates. Genome Res 2009;19:327-35.

Wozney JM, Rosen V, Celeste AJ, Mitsock LM, Whitters MJ, Kriz RW, Hewick RM, Wang EA. Novel regulators of bone formation: molecular clones and activities. Science 1988;242:1528-34.

Yi R, Doehle BP, Qin Y, Macara IG, Cullen BR. Overexpression of exportin 5 enhances RNA interference mediated by short hairpin RNAs and microRNAs. RNA 2005;11:220-6.

Bone 60 (2014) 198–212

Contents lists available at ScienceDirect

Bone

journal homepage: www.elsevier.com/locate/bone

Original Full Length Article

Mutant p53 gain of function can be at the root of dedifferentiation of human osteosarcoma MG63 cells into 3AB-OS cancer stem cells

Riccardo Di Fiore [a], Michela Marcatti [a], Rosa Drago-Ferrante [a], Antonella D'Anneo [a], Michela Giuliano [a], Daniela Carlisi [b], Anna De Blasio [a], Francesca Querques [c,d], Lucio Pastore [c,d], Giovanni Tesoriere [e], Renza Vento [a,e,*]

[a] Laboratory of Biochemistry, Department of Biological, Chemical and Pharmaceutical Sciences and Technologies, University of Palermo, Polyclinic, Palermo, Italy
[b] Laboratory of Biochemistry, Department of Experimental Biomedicine and Clinical Neurosciences, University of Palermo, Polyclinic, Palermo, Italy
[c] Department of Molecular Medicine and Medical Biotechnology, University of Naples "Federico II," Naples, Italy
[d] CEINGE-Advanced Biotechnology s.c.a.r.l., Naples, Italy
[e] Institute for Cancer Research and Molecular Medicine and Center of Biotechnology, College of Science and Biotechnology, Temple University, Philadelphia, PA, USA

ARTICLE INFO

Article history:
Received 31 July 2013
Revised 25 November 2013
Accepted 17 December 2013
Available online 27 December 2013

Edited by: Michael Amling

Keywords:
Human osteosarcoma
Cancer stem cells
Mutant p53 gain of function
Cancer cell dedifferentiation
3AB-OS cells

ABSTRACT

Osteosarcoma is a highly metastatic tumor affecting adolescents, for which there is no second-line chemotherapy. As suggested for most tumors, its capability to overgrow is probably driven by cancer stem cells (CSCs), and finding new targets to kill CSCs may be critical for improving patient survival. TP53 is the most frequently mutated tumor suppressor gene in cancers and mutant p53 protein (mutp53) can acquire gain of function (GOF) strongly contributing to malignancy. Studies thus far have not shown p53-GOF in osteosarcoma. Here, we investigated TP53 gene status/role in 3AB-OS cells—a highly aggressive CSC line previously selected from human osteosarcoma MG63 cells—to evaluate its involvement in promoting proliferation, invasiveness, resistance to apoptosis and stemness. By RT-PCR, methylation-specific PCR, fluorescent in situ hybridization, DNA sequence, western blot and immunofluorescence analyses, we have shown that—in comparison with parental MG63 cells where TP53 gene is hypermethylated, rearranged and in single copy—in 3AB-OS cells, TP53 is unmethylated, rearranged and in multiple copies, and mutp53 (p53-R248W/P72R) is post-translationally modified and with nuclear localization. p53-R248W/P72R-knockdown by short-interfering RNA reduced the growth and replication rate of 3AB-OS cells, markedly increasing cell cycle inhibitor levels and sensitized 3AB-OS cells to TRAIL-induced apoptosis by DR5 up-regulation; moreover, it strongly decreased the levels of stemness and invasiveness genes. We have also found that the ectopic expression of p53-R248W/P72R in MG63 cells promoted cancer stem-like features, as high proliferation rate, sphere formation, clonogenic growth, high migration and invasive ability; furthermore, it strongly increased the levels of stemness proteins. Overall, the findings suggest the involvement of p53-R248W/P72R at the origin of the aberrant characters of the 3AB-OS cells with the hypothesis that its GOF can be at the root of the dedifferentiation of MG63 cells into CSCs.

Introduction

Osteosarcoma (OS), the most common malignant bone tumor in adolescents and young adults, is a highly aggressive tumor exhibiting clinical, histologic and molecular heterogeneity [1]. The current standard chemotherapy regimen, which includes cisplatin, doxorubicin and methotrexate, provides only 65–70% long-term disease-free survival for OS patients without metastasis [2], and there is no established second-line chemotherapy for relapsed OS; thus, the identification of new therapeutic strategies to improve the clinical outcome of these patients is urgent.

It is well known that most solid tumors contain a distinct subpopulation of cancer stem cells (CSCs), which represent the source for tissue renewal, hold malignant potential and can be responsible for therapy resistance [3–6], and it has been suggested that a successful cure of cancer should requires eradication of CSCs [7–9].

Previously, we have demonstrated that the short-term treatment of human OS MG63 cells with 3-aminobenzamide (3AB), a potent inhibitor of the chromatin remodelling enzyme poly(ADP-ribose)polymerase, induced morphological and biochemical features of osteocyte differentiation, accompanied by the down-regulation of gene products required for proliferation and the up-regulation of those implicated in osteoblast differentiation [10]. However, prolonged treatment (about 100 days) of MG63 cells with 3AB induced osteocyte death accompanied by progressive

Abbreviations: CSCs, Cancer stem cells; FISH, Fluorescent in situ hybridization; GOF, Gain of function; MMPs, Matrix metalloproteinases; Mutp53, Mutant p53; OS, Osteosarcoma.

* Corresponding author at: University of Palermo, Polyclinic, via del Vespro 129, 90127 Palermo, Italy.
E-mail address: renza.vento@unipa.it (R. Vento).

8756-3282/$ – see front matter © 2013 Elsevier Inc. All rights reserved.
http://dx.doi.org/10.1016/j.bone.2013.12.021

enrichment of a new heterogeneous and stable cell population termed 3AB-OS [11], which have properties (self-renewal and pluripotency in vitro, tumorigenicity in vivo) that indicated them as CSCs [12,13] and allowed their patenting. 3AB-OS cells have been characterized at genetic and molecular level: compared to parental MG63 cells, which have a hypotriploid karyotype with chromosome number ranging from 61 to 66, they are hypertriploid with chromosome number ranging from 71 to 82; they also exhibit 49 copy number variations (gains/losses) spanning almost all the chromosomes, 3,512 dysregulated genes and 189 differentially expressed miRNAs. Moreover, bioinformatic analyses selected 196 genes and 46 anticorrelated miRNAs involved in carcinogenesis and stemness [14]. Remarkably, the abnormalities evidenced in 3AB-OS cells appear to be strongly congruent with abnormalities described in a large number of pediatric and adult OS patients, where karyotype ranging from haploid to near hexaploid with chromosome number ranging from 15 to 120 were described; in addition, a great number of chromosomal regions with structural abnormalities among which 17p11.2–13 that contains TP53 gene were found [15–17].

It is known that TP53 mutations occur in almost every type of cancer and often mutant p53 proteins (mutp53) express gain of function (GOF), which can enhance the ability of cancer cells to invade and metastasize, confer resistance to chemotherapies, promote genomic instability and drive multinucleation [18–27]. Recently, evidence linking p53 loss to stem-like phenotype in cancer has been reported [28]; however, how p53 contributes to acquisition of "stemness" at the molecular level and whether stem-like cells confer survival advantages to propagate the tumor remains to be resolved. Here, we investigated TP53 gene status and role in 3AB-OS cells. We demonstrated that in 3AB-OS cells, p53 is mutated (p53-R248W/P72R) and displays GOF activity. Furthermore, we showed that the ectopic expression of p53-R248W/P72R promoted cancer stem-like properties in osteosarcoma MG63 parental cells. The results suggest p53-R248W/P72R as a key regulator at the origin of the aggressiveness, chemoresistance and stemness of human 3AB-OS CSCs.

Materials and methods

Cell cultures

Human osteosarcoma MG63 cells were acquired from Interlab Cell Line Collection (ICLC, Genova, Italy). The human 3AB-OS cancer stem cells have been produced in our laboratory [11] and patented (Pluripotent cancer stem cells: their preparation and use. Renza Vento and Riccardo Di Fiore, Patent Appln. No. FI2008A000238, December 11, 2008). Cell lines were cultured as monolayers in T-75 flask in Dulbecco's modified Eagle medium (DMEM), supplemented with 10% (v/v) heat-inactivated fetal bovine serum (FBS), 2 mM L-glutamine, 100 U/ml penicillin and 50 μg/ml streptomycin (Euroclone, Pero, Italy) in a humidified atmosphere of 5% CO_2 in air at 37 °C. When cells grew to approximately 80% confluence, they were subcultured or harvested using 0.025% trypsin–EDTA (Life Technologies Ltd, Monza, Italy).

Morphological observation

Cell morphology was evaluated using a Leica DM IRB inverted microscope (Leica Microsystems Srl, Milano, Italy). Images were photographed and captured by a computer-imaging system (Leica DC300F camera and Adobe Photoshop for image analysis).

RT-PCR analysis for p53

RNA was isolated using RNeasy mini kit (Qiagen, Milano, Italy). cDNA was amplified from 1 μg of RNA as previously reported [29] followed by polymerase chain reaction (PCR). The reactions omitting reverse transcriptase enzyme served as negative control. GAPDH was used as a housekeeping gene to demonstrate equal loading of RNA. The amplified products were resolved by agarose gel electrophoresis (1% agarose, 0.5 μg/ml ethidium bromide; Sigma-Aldrich), and the bands were visualized and photographed with Chemi Doc XRS (Bio-Rad Laboratories Srl, Segrate (MI), Italy). The primer sequences (Proligo USA, Milan, Italy) are as follows: TP53 (432 bp), forward 5′-GGGACAGC CAAGTCTGTG-3′ and reverse 5′-GGAGTCTTCCAGTGTGAT-3′; GAPDH (200 bp), forward 5′-TGACATCAAGAAGGTGA-3′ and reverse 5′-TCCA CCACCCTGTTGCTGTA-3′. For PCR analysis, the following protocol was performed: 95 °C for 5 min, 30 cycles at 95 °C for 1 min, 54 °C for 1 min, 72 °C for 1 min and a final extension at 72 °C for 10 min.

Cell genomic DNA extraction, sodium bisulfite genomic treatment and TP53 methylation-specific PCR (MS-PCR)

Genomic DNA was extracted from cultured cells using QIAamp DNA Mini Kit (Qiagen) following the manufacturer's instructions. Genomic DNA was bisulfite treated using an EpiTect Bisulfite Kit (Qiagen). The treatment of genomic DNA with sodium bisulfite converts unmethylated, but not methylated cytosines, into uracil, producing sequence differences between methylated and unmethylated DNA. Two micrograms of DNA were modified in 40 μl of water with sodium bisulfite following the manufacturer's instructions. After bisulfite modification, PCR on the CpG island of the TP53 promoter was performed with the unmethylation-specific primers (U): 5′-TTAGTATTTA TGGTATTAGGTTGGT-3′ and 5′-AACAAATAATCCACCTACCAA-3′, and methylation-specific primers (M): 5′-GTATTTACGGTATTAGGTCGGC-3′ and 5′-AAATAATCCGCCTACCGA-3′, using 5U of AmpliTaq polymerase (Applied Biosystems, Foster City, CA) and the following PCR conditions: 95 °C for 5 min, 35 cycles of 95 °C for 30 s, 51 °C for 45 s and 72 °C for 60 s and a final 8 min at 72 °C. A methylated and bisulfite converted human control DNA (EpiTect PCR control DNA; Qiagen) was used as a positive control. Each PCR product was analyzed by electrophoresis on 2% agarose gel. Gel images were visualized and photographed with Chemi Doc XRS (Bio-Rad Laboratories Srl, Segrate (MI), Italy).

TP53 fluorescent in situ hybridization (FISH) analysis

FISH analyses were performed on MG63 and 3AB-OS cells by Toma Advanced Biomedical Assays S.p.A. (Busto Arsizio (VA), Italy) with p53 (17p13)/SE 17 probe (Kreatech Diagnostics, Amsterdam, The Netherlands), containing the p53 tumor suppressor gene-specific region and the chromosome 17 Satellite control probe. These analyses were performed following the manufacturer's protocol and analyzing 50 nuclei and 10 metaphases (1000× magnification).

DNA sequence analysis of p53 exons 1–11

DNA sequence analyses were performed on MG63 and 3AB-OS cells by BioRep S.r.l. (Milano, Italy). Genomic DNA was extracted from cultured cells using QIAamp DNA Mini Kit (Qiagen) following the manufacturer's instructions. PCR reactions were carried out under standard conditions with primer sets specific for the coding exons 1–11 of the TP53 gene reported in Supplementary Table 1. PCR products were purified using ExoSAP (Amersham Biosciences Italia, Milano, Italy) treatment and sequenced with the DYE-namic ET Dye Terminator Cycle Sequencing Kit (Amersham Biosciences Italia). Sequencing reactions were purified using the Montage SEQ96 Cleanup Kit (Millipore S.p.a., Milano, Italy), and sequencing runs were performed on the MegaBACE 500 DNA Analysis System (Amersham Biosciences Italia).

Immunofluorescence Staining for p53

The cells were fixed with 3.7% formaldehyde for 10 min at room temperature and permeabilized with 0.1% Triton® X-100 (all from Sigma) in phosphate-buffered saline (PBS) for 5 min. After washing with PBS, cells were incubated with anti-p53 primary antibody (diluted

1:100 in PBS + 1% BSA + 0.05% NaN_3; Santa Cruz Biotechnology, Santa Cruz, CA, USA) at 4 °C, overnight. Cells were washed three times with PBS and incubated for 1 h at room temperature with Cy3- or Cy2-conjugated secondary antibody (diluted 1:100 in PBS + 1% BSA + 0.05% NaN_3; Jackson ImmunoResearch Laboratories, West Grove, PA, USA). Nuclei were counterstained with 2.5 μg/ml Hoechst 33342 (Sigma-Aldrich) for 10 min. After three washes, cells were examined on a Leica DM IRB inverted microscope equipped with fluorescence optics and suitable filters for DAPI, FITC and rhodamine detection; images were photographed and captured by a computer-imaging system (Leica DC300F camera and Adobe Photoshop for image analysis).

Transient down-regulation of p53 by short interfering RNA (siRNA)

Cells were plated in a six-well plate format and cultured in DMEM medium, supplemented with 10% FBS, for 24 h to reach approximately 60–80% confluence. Specific siRNAs directed against p53, obtained by St Cruz Biotechnology as a pool of double-stranded RNA oligonucleotides, were transfected for 5 h into the cells at a final concentration of 50 nM, in the presence of 5 μl Metafectene Pro (Biontex, Martinsried/Planegg, GmBH, Munich, Germany) in a final volume of 1 ml serum-free DMEM. At the end, the reaction was stopped replacing the culture medium with DMEM + 10% FBS. Cells were examined for p53 down-regulation and other properties 24–72 h after transfection. siRNA, consisting in a scramble sequence, was used as a negative control.

Growth curve and cell viability assays

Total cell number and viability were evaluated by Trypan blue exclusion counting. Briefly, cells were harvested every 24 h and resuspended in PBS. Aliquots of cell suspensions were diluted with 0.4% trypan blue (Sigma-Aldrich Srl, Milano, Italy), pipetted onto a hemocytometer and counted under a microscope at 100× magnification. Live cells excluded the dye, whereas dead cells admitted the dye intensely staining with trypan blue. The number of viable cells for each experimental condition was counted and represented on a linear graph. Doubling time (DT) was estimated by the following equation: $DT = (t_2 - t_1)\ \ln 2 / \ln X_2 / X_1$, where X_2 and X_1 are the number of cells at t_2 and t_1.

EdU in corporation assay

For EdU (5-ethynyl-2′-deoxyuridine) incorporation experiments, cells were incubated with 10 μM EdU (Click-iT™ EdU Alexa Fluor High-Throughput Imaging Assay, Invitrogen, Life Technologies Ltd, Monza, Italy) for 2 h. Cells were then washed with PBS, fixed with 3.7% formaldehyde for 15 min at room temperature and permeabilized with 0.5% Triton X-100 (all from Sigma) in PBS for 20 min. After extensive washing with 3% bovine serum albumin (BSA) in PBS, incorporated EdU was detected by fluorescent-azide coupling reaction (Click-iT, Invitrogen). Briefly, cells were incubated for 30 min with azide-conjugated Alexa Fluor 488 dye in TBS supplemented with 4 mM $CuSO_4$. Cells were then washed three times with 3% BSA in PBS. Nuclei were counterstained with 2.5 μg/ml Hoechst 33342 (Sigma-Aldrich), for 10 min. After three washes, cells were examined by fluorescence microscopy using filters for DAPI and FITC. The percentage of EdU-positive nuclei was determined by counting five random high-powered fields (400×).

Cell death assays

Apoptotic morphology was studied in cells stained with Hoechst 33342 (Sigma-Aldrich). In particular, cells were stained with Hoechst 33342 (2.5 μg/ml medium) for 30 min at 37 °C, visualized by fluorescence microscopy using an appropriate filter for DAPI; images were photographed and captured. Cells were evaluated on the basis of their nuclear morphology, noting the presence of homogeneous chromatin, condensed chromatin, and fragmented nuclei.

Apoptosis was also studied by flow cytometry of either DNA content or annexin V labelling. For DNA staining, trypsinized cell suspensions were centrifuged, washed 3 times with PBS and resuspended at 1×10^6 cells/ml in PBS. Cells were mixed with cold absolute ethanol and stored for 1 h at 4 °C. After centrifugation, cells were rinsed 3 times in PBS, and the pellet was suspended in 1 ml of propidium iodide (PI) staining solution (3.8 mM sodium citrate, 25 μg/ml PI, 10 μg/ml RNase A; Sigma-Aldrich Srl, Milano, Italy) and kept in the dark at 4 °C for 3 h prior to flow cytometry analysis. The proportion of cells giving fluorescence in the sub-G0/G1 peak of cell cycle was taken as a measure of apoptosis.

For annexin V labelling, trypsinized cell suspensions were centrifuged, washed 3 times with PBS and resuspended in 1× annexin V binding buffer (BD Biosciences Pharmingen, San Diego, CA) at a concentration of 1×10^6 cells/ml. One hundred microliters of cell suspension was then incubated with 5 μL of annexin V-FITC (BD Biosciences) and 5 μL of PI for 15 min at a room temperature in the dark. Double labeled with annexin V and PI allows a distinction of early apoptotic (annexin V^+/PI^-) and late apoptotic/necrotic (annexin V^+/PI^+) cells. Flow cytometry analyses were performed by a COULTER EPICS XL flow cytometer (Beckman Coulter Srl, Cassina De Pecchi (MI), Italy) equipped with a single Argon ion laser (emission wavelength of 488 nm) and Expo 32 software. The green fluorescence was measured in the FL1 channel using a 515-nm BP filter, and the red fluorescence was measured in the FL3 channel using a 620-nm BP filter. At least 1×10^4 cells per sample were analyzed and data were stored in list mode files.

Measurement of mitochondrial transmembrane potential ($\Delta\psi m$)

Mitochondrial membrane potential was measured by the cationic lipophilic fluorochrome 3,3-dihexyloxacarbocyanine (DiOC6 Molecular Probes, Eugene, OR), which exclusively emits within the spectrum of green light. Loss in DiOC6 staining indicates disruption of the mitochondrial inner transmembrane potential ($\Delta\Psi m$). Cells were incubated with 40 nM DiOC6 for 20 min at 37°C, washed twice with PBS and analysed by flow cytometry. The green fluorescence was measured as above described.

In vitro matrigel invasion assay

Invasion assays were performed using 6-well invasion chamber system (BD Biosciences, Discovery Labware, Becton Dickinson, Buccinasco, Italy). Cells were trypsinized and counted with a hemocytometer using trypan blue, and viable cells were seeded in the upper chamber at 1×10^5 cells/well in serum-free DMEM. DMEM supplemented with 10% FBS (used as a chemoattractant) was placed in the bottom well. Incubation was carried out for 48 h at 37 °C in humidified air with 5% CO_2. Nonmigratory cells in the upper chamber were then removed with a cotton-tip applicator. Migrated cells on the lower surface were stained with Hoechst 33342 (2.5 μg/ml; Sigma-Aldrich) for 10 min and then visualized under an inverted microscope. The number of migrating cells was determined by counting five high-powered fields (200×) on each membrane. Four independent experiments were performed in triplicate.

Construction of expression vector expressing p53 mutation (p53-R248W/P72R) and stable transfection

RNA from 3AB-OS cell line was isolated using TRI Reagent (Sigma-Aldrich), according to manufacturer's instructions. cDNA was amplified from 2 μg of RNA using M-MuLV reverse transcriptase (New England Biolabs, Euroclone, Pero, Italy). The following protocol was performed: RNA was incubated with dNTPs (Amersham Biosciences) and Random Examers (Promega Italia Srl, Milano, Italy) at 70 °C for 10 min and in

ice for 1 min; then, after the addition of M-MuLV and the specific buffer, the incubation was performed at 42 °C for 1 h and at 90 °C for 10 min. The following primers were used to amplified TP53 (≈1.2 kb): forward (*Bam*HI restriction site-containing) 5′-CGTAGGATCCAGCCATGGAGGA GCCGCAG-3′ and reverse (*Xho*I restriction site-containig) 5′-CGGATC TCGAGCAATTCAGTCTGAGTCAGGCC-3′. For PCR amplification with Phusion Taq polymerase (New England Biolabs), the following protocol was performed: 98 °C for 2 min; 12 cycles at 98 °C for 10 s, 63 °C for 20 s and 72 °C for 30 s; 18 cycles at 98 °C for 10 s and 72 °C for 30 s; a final extension at 72 °C for 7 min. The amplified product was resolved by agarose gel electrophoresis (1% agarose and 0.5 μg/ml ethidium bromide; Sigma-Aldrich) and the band was extracted using Wizard SV Gel and PCR Clean-up system (Promega Italia Srl). PCR product and pcDNA 3.1 vector (Invitrogen) were digested for 2 h at 37 °C with *Bam*HI-HF and *Xho*I (New England Biolabs), resolved by agarose gel electrophoresis and extracted. Vector dephosphorylation and ligation reactions were performed using the Rapid Dephosphorylation and Ligation kit (Roche, Milano, Italy) according to manufacturer's instructions. The ligation mixture was transformed into calcium chloride-competent DH5α cells (Invitrogen). Plasmids after *Bam*HI–*Xho*I digestion that showed the presence of a 1.2-kb insert were validated by sequencing (Ceinge Sequencing Service, Ceinge, Napoli, Italy).

MG63 cells were plated in 6-well dishes until they reached 90% confluence and then transfected with p53-R248W/P72R-pcDNA 3.1 or empty vector, as a control, using Lipofectamine 2000 (Invitrogen) according to manufacturer's instructions. Two days after transfections, the cells were transferred in 100 mm dishes in selective medium containing 300 μg/ml G418 (Gibco, Life Technologies Ltd, Monza, Italy); the medium was replaced every 3–4 days. A plate of untrasfected cells was used as a control for the selection.

Sarcosphere formation assay

MG63 cells transfected with pcDNA3.1-p53-R248W/P72R or empty pcDNA3.1 vector were seeded in 6-well ultra-low attachment plates (Corning Costar, Euroclone) at a density of 500 cells/well with 3 ml stem cell medium consisting of DMEM/F12 (Gibco), B27 (1× Gibco), recombinant human epidermal growth factor (rhEGF, 20 ng/ml; Sigma-Aldrich) and basic fibroblast growth factor (bFGF, 20 ng/ml; Sigma-Aldrich). The stem cell medium was changed every 3 days, and cells were observed every day by microscopy. After the primary spheres reached approximately ≥50 μm in diameter (determined using the ImageJ software), they were collected by gentle centrifugation (800 rpm), enzymatically dissociated (10 min at 37 °C in 0.05% trypsin–EDTA; Life Technologies Ltd) to single cells and replanted into 6-well ultra-low attachment plates with 500 cells/well and cultured with stem cell medium to generate spheres of the next generation.

Colony formation assay

MG63 cells transfected with pcDNA3.1-p53-R248W/P72R or empty pcDNA3.1 vector were seeded in 6-well plates at a density of 100 cells/well with 3 ml culture medium and incubated for 10 days. The medium was changed every 3 days, and cells were observed every day by microscopy. On the tenth day, media was removed from the wells and washed once with ice-cold PBS. The colonies were fixed with 50% EtOH and stained with 1% methylene blue (Sigma-Aldrich) for 10 min. After three washes with PBS, the colonies consisting of >50 cells were counted using microscopy. Colony size was determined by measuring the area with the ImageJ software.

Scratch/wound-healing assay

To analyze cell migration by wound healing, confluent monolayers of MG63 cells transfected with pcDNA3.1-p53-R248W/P72R or empty pcDNA3.1 vector and cultured in 6-well plates were scratched with a 200-μl pipette tip to generate the wound. One hour before scratching, the medium was replaced with medium containing 0.1% FBS to minimize the cell proliferation. Phase-contrast photographs of the same region were taken with the same magnification (100×) at 0, 8 and 24 h post-wounding. The extent of wound closure was determined by measuring with the ImageJ software the area of cells that migrated into the wound and then dividing by the total area of wound.

Flow cytometry analysis of CD133, ABCG2 and p53 expression

Cells were detached using 0.025% trypsin–EDTA in PBS, counted and washed in 0.1% BSA in PBS at 4 °C. At least 500,000 cells (in 100 μl PBS/0.5% BSA) were incubated with fluorescent-labelled monoclonal antibodies or respective isotype controls (1/10 diluted 4 °C for 30 min in the dark). After washing steps, the labelled cells were analyzed by flow cytometry using COULTER EPICS XL (Beckman-Coulter Srl) and Expo 32 software. The antibodies used were mouse anti-human CD133/2 PE conjugated (Miltenyi Biotec S.r.l., Bologna, Italy), mouse anti-human ABCG2 nonconjugated (Santa Cruz Biotechnology) and mouse anti-human p53 nonconjugated (Santa Cruz Biotechnology). For indirect labelling, cells were incubated with a compatible secondary antibody FITC conjugated (Santa Cruz Biotechnology, Inc.). For intracellular staining of CD133, ABCG2 and p53, cells were processed using the Caltag Fix & Perm Kit (Invitrogen) following the manufacturer's guidelines. The green fluorescence was measured as described in the Cell death assays section, and the phycoerythrin fluorescence was measured in the FL2 channel using a 575-nm BP filter. At least 1×10^4 cells per sample were analyzed, and data were stored in list mode files. The expression of cell markers was determined by comparison with isotype control.

Cell cycle and proliferation analyses

Cell cycle phase distribution was studied by flow cytometry of DNA content. This method was described in the Cell death assays section. The proliferation index was calculated as the sum of cells in S and G2/M phases of cell cycle [30].

RNA extraction and real-time RT-PCR

RNA was extracted by Trizol reagent (Life Technologies Ltd, Monza, Italy); a DNase I treatment step was included. One microgram of total RNA was reverse transcribed in a final volume of 20 μl reverse transcription (RT) by using a Super-Script First-Strand Synthesis kit for RT-PCR (Life Technologies Ltd) according to the manufacturer's instructions. The resulting cDNAs were used for quantitative analysis by real-time PCR (qPCR) using the primers (Proligo, Milan, Italy) reported in Supplementary Table 2 and the Power SYBR Green PCR Master Mix (Applied Biosystem, Warrington, UK). Reactions were performed in 48-well plates according to manufacturer's instructions, using Applied Biosystems StepOneTM instrument. Each reaction mixture contained 2 μl of template cDNA, 12.5 μl of SYBR Green PCR Master Mix 2X, a final concentration of 300 nM of forward and reverse primers and RNase-free dH_2O to a final volume of 25 μl. qPCRs were performed in triplicate and repeated for confirmation. PCR cycling was performed as follows: 95 °C for 10 min, 95 °C for 30 s, 60 °C for 60 s, 72 °C for 30 s for 40 cycles and a final extension at 72 °C for 5 min. To determine primer specificity, three stages (95 °C for 15 s, 60 °C for 20 s and 95 °C for 15 s, with a ramping time of 20 min) were added at the end of the PCR to obtain dissociation curves for each gene. To verify that the RT-PCR signals derived from RNA rather than genomic DNA, for each gene tested a control identical to the test assay but omitting the RT reaction (no RT control) was included. qPCR data were analyzed by SDS 2.1 software. Relative transcript levels were determined using the $2^{-\Delta\Delta Ct}$ method and normalized to endogenous β-actin control.

Western blot analysis

Cells were washed in PBS and incubated on ice-cold lysis buffer (RIPA buffer 50 μl/10^6 cells) containing protease inhibitor cocktail (Sigma-Aldrich) for 30 min and sonicated three times for 10 s. Equivalent amounts of proteins (40 μg) were separated by SDS–polyacrylamide gel electrophoresis and transferred to a nitrocellulose membrane (Bio-Rad) for detection with primary antibodies and the appropriate horseradish peroxidase–conjugated secondary antibodies. Immunoreactive signals were detected using enhanced chemiluminescence (ECL) reagents (Bio-Rad). The correct protein loading was confirmed by stripping the immunoblot and reprobing with primary antibody for actin (diluted 1:500; Sigma). Bands were visualized and photographed with Chemi Doc XRS (Bio-Rad). Quantification was performed using Quantity One software, and the data (relative density normalized to actin) were expressed as mean ± SD of four experiments. The primary antibodies are provided in Supplementary Table 3.

Statistical Analysis

Data, represented as mean ± SD, were analyzed using the 2-tailed Student *t*-test using Microsoft Excel. Differences were considered significant when $P < 0.05$.

Results

p53 gene and protein status in MG63 and 3AB-OS cells

At first, we examined by RT-PCR analysis the expression of TP53 mRNA in both 3AB-OS and MG63 parental cells. We detected mRNA transcript for TP53 in 3AB-OS cells but not in MG63 cells (Fig. 1A). Because a low or unmeasurable level of TP53 gene expression may be correlated with promoter hypermethylation [31–34], we also evaluated the methylation status of the TP53 promoter by MSP in both cell lines. As it can be seen in Fig. 1B, in 3AB-OS cells, the promoter was found unmethylated, while MG63 cells showed an aberrant TP53 promoter methylation status.

To determine the chromosome 17 (chr17) and TP53 copy numbers, MG63 and 3AB-OS cells were hybridized using a dual-color direct labelled probe specific for chr17 α-satellite and for TP53 gene region. We have analyzed interphase (INT) and metaphase (MET) nuclei showing (Fig. 1C) that both cell lines exhibit alterations of chr17 and TP53 gene; MG63 cells show chr17 trisomy and one TP53 signal which did not colocalize with chr17, whereas 3AB-OS cells show chr17 tetrasomy with three and four TP53 signals, some of which colocalizing with chr17.

We also sequenced the coding exons 1–11 of TP53 gene in both 3AB-OS and MG63 cells. As shown in Fig. 1D, 3AB-OS cells evidenced alterations in the exons 4 and 7. More precisely, codon 72 CCC was altered into CGC in the sequence orientation (p53Ex4s), and from GGG into

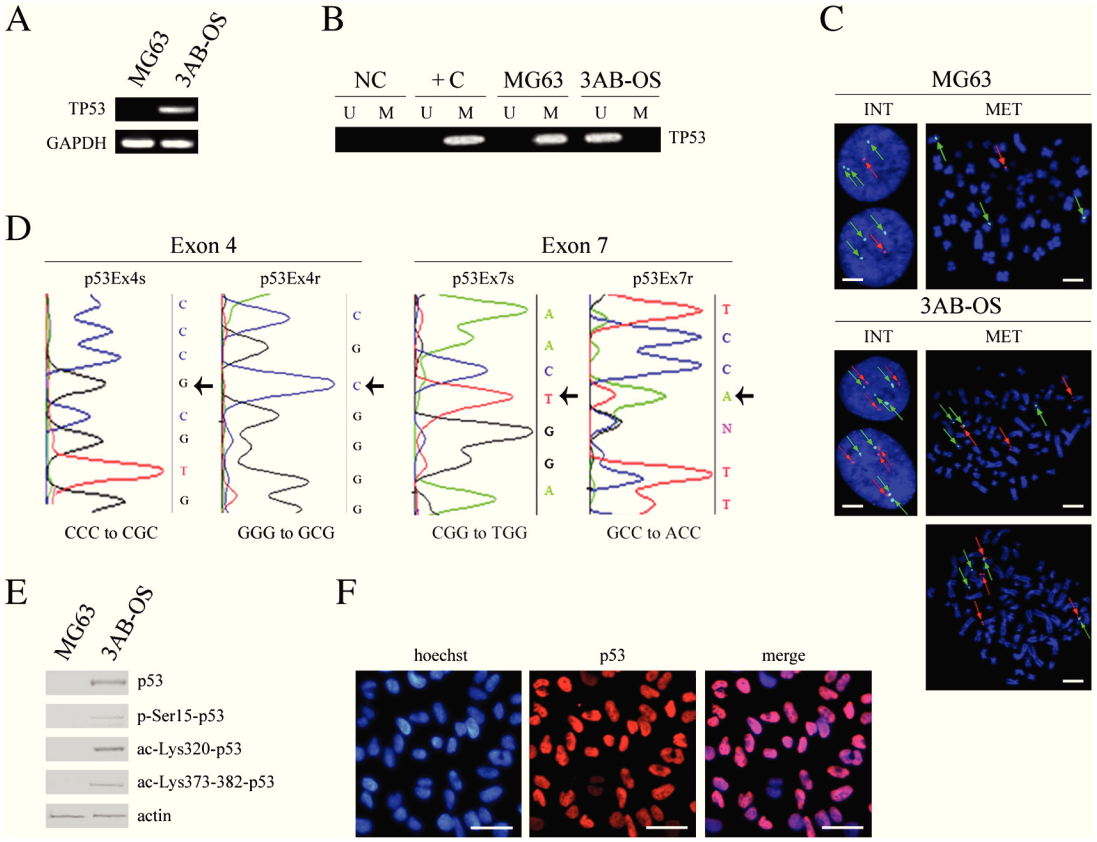

Fig. 1. Analysis of p53 gene and protein in MG63 and 3AB-OS cells. (A) Expression of TP53 mRNA detected by reverse transcriptase polymerase chain reaction (RT-PCR). GAPDH was amplified to confirm the quality and quantity of mRNA from each cell line. (B) Methylation-specific PCR of TP53. Primer sets used for amplification are designated as unmethylated (U) and methylated (M). A sample containing DNA-free water and mastermix solution was used as negative control (NC); a methylated and bisulfite converted human control DNA, designed as +C, was used as a positive control. (C) FISH analyses of the TP53 gene (17p13) performed using a p53-specific DNA probe (red fluorescent signals), simultaneously hybridized with a chromosome 17-centromeric probe (green fluorescent signals). Analyses were performed on interphase (INT) and metaphase (MET) nuclei. The scale bar represents 5 μm (D) DNA sequence analysis of the TP53 exons 4 and 7 in 3AB-OS cells. (E) Western blot analysis of both p53 and its phosphorylated (p) and acetylated (ac) forms. Actin was used as the internal control. Images are representative of four independent experiments. (F) Immunofluorescence analysis of p53 in 3AB-OS cells, by double staining cells with both Hoechst 33342 dye (blue, left panel) to localize the nucleus, and anti-p53 antibody and Cy3-conjugated secondary antibody (red, middle panel) to localize p53. In the right panel, the merge of the two dyes is shown. The scale bar represents 25 μm. Images are representative of four independent experiments.

GCG on the reverse strand (p53Ex4r). This transversion produced an amino acid substitution of arginine for proline (P72R), a common polymorphism of TP53 gene. Fig. 1D also shows that codon 248 CGG was altered into TGG in the sequence orientation (p53Ex7s), and from GCC into ACC on the reverse strand (p53Ex7r). This transition produced an amino acid substitution of tryptophan for arginine (R248W) that affects p53 DNA binding ability. Since sequencing reactions of both strands confirmed the presence of only the altered nucleotide, we noticed that the mutations were indeed homozygously present in 3AB-OS cells. No alterations were detectable in the exons of MG63 cells (data not shown).

Given the results obtained above, we have examined the expression of mutp53 (p53-R248W/P72R) by western blot analysis. As shown in Fig. 1E, the protein was detected in 3AB-OS cells while it was not found in MG63 cells. We have also analyzed the post-translational phosphorylation and acetylation status of the protein. As shown in Fig. 1E, the p53-R248W/P72R protein resulted phosphorylated at Ser15 and acetylated at Lys320 and Lys373-382; furthermore, immunofluorescence analysis (Fig. 1F) evidenced that in 3AB-OS cells, it exhibited a nuclear localization. Overall, these results demonstrated that in 3AB-OS cells, TP53 gene is mutated and that p53-R248W/P72R is stabilized and has nuclear localization.

Study of gain of function of p53-R248W/P72R in 3AB-OS cells

Aimed at evaluating whether, in 3AB-OS cells, p53-R248W/P72R has acquired GOF activities (enhanced cell proliferation, invasiveness and resistance to apoptosis), we have depleted the protein by small-interfering RNA (siRNA). To this purpose, 3AB-OS cells were transfected with p53-siRNA or a scrambled siRNA (Scr-siRNA). Then, first, we checked the effects of the p53-targeting siRNA on the level of endogenous protein. At 24–72 h after transfection, the content of the protein was assessed by western blot (Fig. 2A) and immunofluorescence (Fig. 2B) analyses. Both the analyses showed that after 24–72 h of p53-siRNA transfection, p53-R248W/P72R level potently lowered. The effects were observed at 24 h after transfection and peaked at 48 h when more than 70% reduction in the content of the protein was observed. Thereafter, p53-R248W/P72R levels markedly went up, so that at 72 h after transfection, we only observed a 22% reduction in its level. This suggested that, at that time, the transient silencing was in rapid recovery. Overall, the results suggested that the optimal silencing efficiency was reached at 48 h after transfection. The knockdown of the protein was specific as no protein reduction was observed in cells transfected with Scr-siRNA.

p53-R248W/P72R-knockdown inhibits 3AB-OS cell proliferation

To evaluate whether p53-R248W/P72R-knockdown modified the growth of 3AB-OS cells, untransfected cells and cells transfected with Scr-siRNA or with p53 siRNA were microscopically observed and analysed (0–72 h) for cell number, percentage of cells in the S-phase of cell cycle (EdU incorporation) and percentage of viability. In Fig. 3A, the image obtained by phase contrast microscopy shows that upon knockdown of p53-R248W/P72R, in comparison to untransfected or Scr-siRNA-transfected cells, cell number lowered. The results were in accordance with the trend of the p53-R248W/P72R protein level observed after p53siRNA transfection. Fig. 3B also shows that p53-R248W/P72R depletion reduced the growth rate and the replication rate of 3AB-OS cells, whereas it did not induce loss of cell viability. Also, the speed of cell growth and replication reflected the trend of p53-R248W/P72R-knockdown. There was no statistically significant difference between untransfected cells and cells transfected with Scr-siRNA. These results well agreed with microscopy analysis. Next, we examined the expression of a number of cell cycle-related proteins and genes at 48 h post-transfection. In Fig. 3C, western blot and real-time PCR analyses showed that the p53-R248W/P72R-knockdown markedly increased the levels of pRb, p130, p107, E2F1, E2F4, GADD45, p21 and p27, whereas it potently decreased CDK4 levels. No alteration in the expression of cyclins and other CDKs was observed (data not shown).

p53-R248W/P72R-knockdown reduces resistance to TRAIL-induced apoptosis and regulates Bcl-2 family members and mitochondrial membrane potential

We have previously demonstrated that 3AB-OS cells express low levels of the death receptors FAS and DR4 [14] and show strong resistance to TRAIL (TNF-related apoptosis inducing ligand) (effects evaluated using TRAIL concentrations up to 100 ng/ml, unpublished data). Here, we evaluated whether the p53-R248W/P72R-knockdown modifies the expression levels of DR4 (TRAIL-R1), KILLER/DR5 (TRAIL-R2) and FAS/CD95 at 48 h post-transfection. In Fig. 4A, western blot analyses show that p53-R248W/P72R depletion significantly increased protein expression levels of DR4 and DR5, whereas it did not change FAS level. Thus, to evaluate TRAIL sensitivity, untransfected cells and cells transfected for 24 h with Scr-siRNA or p53-siRNA were treated with TRAIL (40 ng/ml) for 36 h. In Fig. 4B, phase contrast microscopy shows that TRAIL markedly reduced cell number also inducing apoptosis in p53-silenced cells, as suggested by the presence of round-shaped cells floating in the medium, membrane blebbing and apoptotic body formation. As chromatin condensation and nuclear fragmentation remain the hallmarks of apoptotic cells, apoptosis was assessed by staining nucleic acid with Hoechst 33342. As shown Fig. 4B, in p53-siRNA-transfected cells, TRAIL induced typical apoptotic nuclei, exhibiting highly fluorescent condensed and fragmented chromatin. Apoptosis was also studied by flow cytometry of either DNA content or annexin V labelling. Fig. 4C shows that treatment with TRAIL resulted in 29% of cells accumulation in sub-G0–G1 phase with a 20% of early apoptotic cells (annexin V^+/PI^-) in p53-siRNA-transfected cells. The effects of TRAIL were also evidenced in both untransfected and Scr-siRNA-transfected cells, but these effects were much less pronounced than in p53-siRNA-transfected cells. Collectively, these results demonstrate that p53-R248W/P72R-knockdown sensitizes 3AB-OS cells to TRAIL-induced apoptosis. We also investigated by cytofluorimetric analysis if p53-R248W/P72R can attenuate mitochondrial apoptosis signalling pathways. $DiOC_6$ staining revealed that the p53-R248W/P72R-knockdown induced a significant decrease in fluorochrome uptake, indicating a loss of $\Delta\psi m$ (Fig. 4D). To further dissect the molecules involved in the mechanism, we investigated whether the p53-R248W/P72R-knockdown modifies the expression levels of both anti-apoptotic (Bcl-2 and Bcl-XL) and pro-apoptotic (Bax and Puma) factors. In Figs. 4E and 4F, real-time PCR and western blot analyses showed that the p53-R248W/P72R-knockdown significantly decreased Bcl-2 and Bcl-XL levels while it increased Bax and Puma levels. These results well agreed with those obtained by cytofluorimetric analysis.

p53-R248W/P72R shows the gain-of-function properties involved in promotion of cell invasiveness

To evaluate whether p53-R248W/P72R-knockdown influences 3AB-OS cells invasiveness, we performed Matrigel invasion transwell assays. As shown in Fig. 5A, p53-siRNA transfection potently decreased (−80%) the invasive capability of 3AB-OS cells, whereas no statistically significant difference was observed in untransfected and Scr-siRNA-transfected cells. We also examined the expression of a number of cell invasion-related genes and proteins at 48 h post-transfection. In Figs. 5B and 5C, real-time PCR and western blot analyses showed that p53-R248W/P72R-knockdown significantly decreased the levels of the invasive proteins matrix metalloproteinases 2 and 9 (MMP2 and MMP9), integrin alfa5 (ITGα5) and integrin alfaV (ITGαV) while it increased the levels of the cell adhesion protein E-Cadherin, without altering the expression of proteins involved in mesenchymal phenotype (N-cadherin, β-catenin and vimentin).

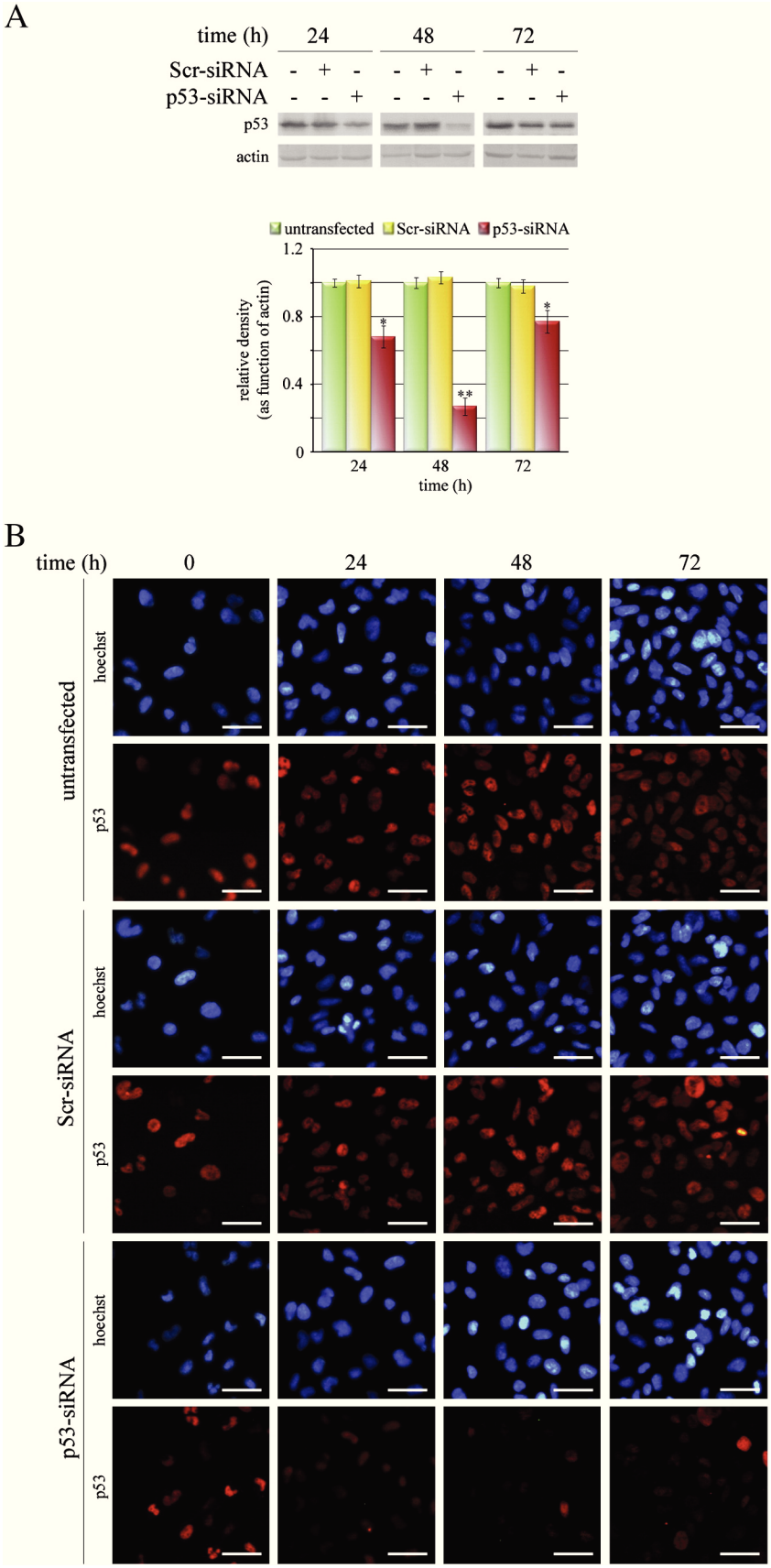

Fig. 2. Evaluation of knockdown efficiency of p53-R248W/P72R. 3AB-OS cells were transfected with scrambled siRNA (Scr-siRNA) or p53-siRNA and analyzed at 24–72 h after transfection. (A) Western blot analysis of p53-R248W/P72R and densitometric analysis of protein bands. Data (relative density normalized to actin) represent the mean with standard deviation ($n = 4$); $^{*}P < 0.05$ and $^{**}P < 0.01$ as compared to Scr-siRNA-transfected cells. (B) Immunofluorescence analysis by double staining cells with both Hoechst33342 dye (blue) to localize the nucleus and anti-p53 antibody and Cy3-conjugated secondary antibody (red) to localize p53. The scale bar represents 25 μm. Images are representative of four independent experiments.

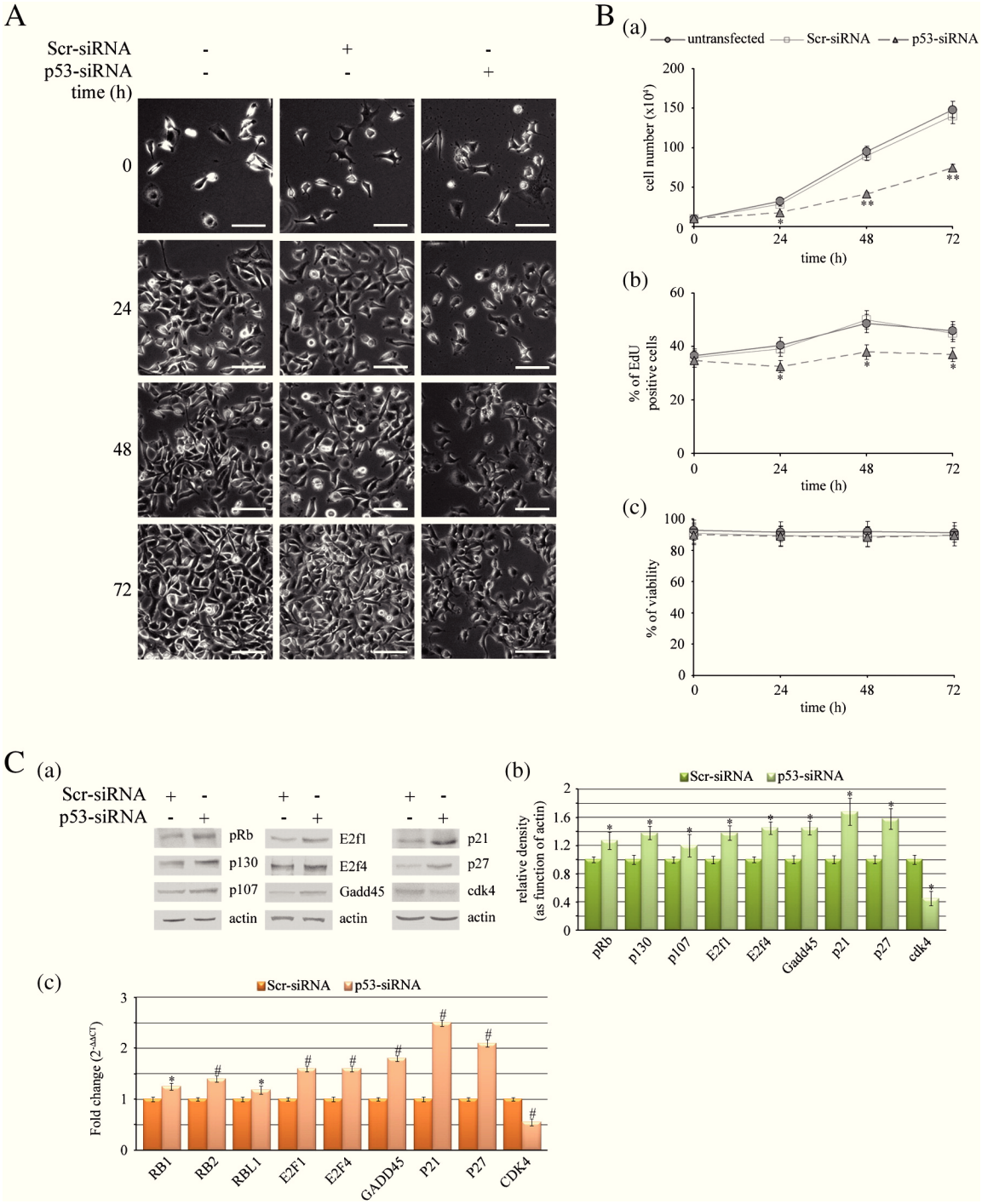

Fig. 3. Effect of p53-R248W/P72R-knockdown on growth advantage of 3AB-OS cells. (A) Inverted phase contrast microscopy at 0–72 h after transfection. The scale bar represents 100 μm. Images are representative of four independent experiments. (B) Analysis of total cell number (a), percentage of cells in the S-phase of cell cycle (b) by EdU incorporation and percentage of cell viability (c). The data represent the mean with standard deviation ($n = 4$); $^{*}P < 0.05$ and $^{**}P < 0.01$ as compared to Scr-siRNA-transfected cells. (C) Analyses of cell-cycle regulators at 48 h after silencing. Western blot analysis (a) and quantification of protein bands by densitometric analysis (b) and real-time PCR (c). Data (relative density normalized to actin) represent the mean with standard deviation ($n = 4$); $^{*}P < 0.05$ as compared to Scr-siRNA-transfected cells. Data represent the mean with standard deviation ($n = 4$); $^{*}P < 0.05$ and $^{\#}P < 0.005$ as compared to Scr-siRNA-transfected cells.

p53-R248W/P72R-knockdown affects the expression of stem-cell markers

Previously, we have shown that 3AB-OS cells express a large number of genes required for maintaining stemness [11] and that they morphologically and functionally transdifferentiate *in vitro* into cells of all three primary germ layers (ectoderm, endoderm and mesoderm) [12]. We also demonstrated that stemness markers were profoundly downregulated in differentiated cells. Here we have shown (Fig. 6A) that undifferentiated 3AB-OS cells strongly expressed p53-R248W/P72R while it profoundly lowered in derived cell lineages. We also investigated whether p53-R248W/P72R-knockdown affected the expression of the most important stemness markers (Oct3/4, Nanog, Sox2, nucleostemin (NS) and CD133) that exhibited very high levels in untransfected 3AB-OS cells. In Figs. 6B and 6C, western blot and real-time PCR analyses showed that p53-R248W/P72R-knockdown potently decreased the levels of all the analysed pluripotency markers.

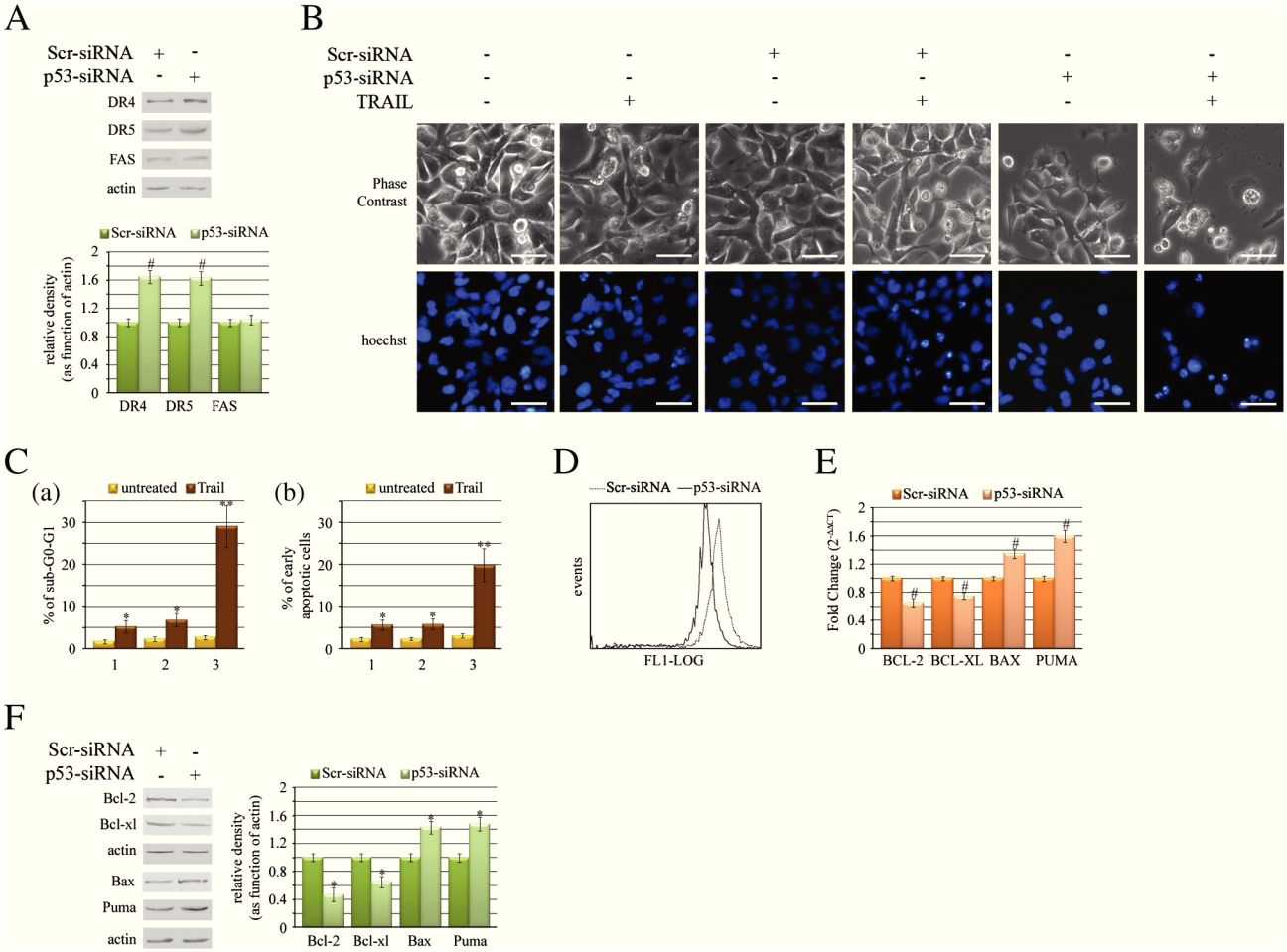

Fig. 4. Effect of p53-R248W/P72R-knockdown on: DR4, DR5 and FAS receptors, TRAIL-induced apoptosis, mitochondrial membrane potential and Bcl-2 family members. (A) Western blot analysis of DR4, DR5 and FAS receptors at 48 h after transfection and quantification of protein bands by densitometric analysis. Data (relative density normalized to actin) represent the mean with standard deviation ($n = 4$); $^{\#}P < 0.005$ as compared to Scr-siRNA-transfected cells. (B) Analysis of TRAIL-induced apoptosis by inverted phase contrast microscopy (upper panels) and fluorescence microscopy (Hoechst 33342 staining, bottom panels). The scale bar represents 25 μm. Images are representative of four independent experiments. (C) Percentages of cells in sub-G0–G1 phase (a) evaluated by flow cytometric analysis of propidium iodide DNA staining, and percentages of early apoptotic cells (b) measured by flow cytometric analysis of annexin V labelling after TRAIL treatment (1, untransfected cells; 2, cells transfected with Scr-siRNA; 3, cells transfected with p53-siRNA). The data represent the mean with standard deviation ($n = 4$). $^{*}P < 0.05$ and $^{**}P < 0.01$ as compared to untreated cells. (D) Citofluorimetric analysis by DiOC6 staining of mitochondrial membrane potential ($\Delta\psi m$). The decrease of fluorescence intensity indicates loss of $\Delta\psi m$. (E) Real-time PCR analysis of Bcl-2 family mRNAs at 48 h after transfection. Data represent the mean with standard deviation ($n = 4$); $^{\#}P < 0.005$ as compared to Scr-siRNA-transfected cells. (F) Western blot analysis of Bcl-2 family proteins at 48 h after transfection and quantification of protein bands by densitometric analysis. Data (relative density normalized to actin) represent the mean with standard deviation ($n = 4$); $^{*}P < 0.05$ as compared to Scr-siRNA-transfected cells.

Ectopic expression of p53-R248W/P72R promotes cancer stem-like properties in osteosarcoma MG63 cells

The above-described findings suggest that the GOF property of p53-R248W/P72R could be at the root of 3AB-OS stemness. To evaluate such a hypothesis, first—as reported in materials and methods—we produced a pcDNA3.1-vector containing p53-R248W/P72R; then, we stably transfected MG63 cells with either empty pcDNA3.1 vector or pcDNA3.1-p53-R248W/P72R. MG63 cells transfected with pcDNA3.1-p53-R248W/P72R were designated R248W/P72R cells, while MG63 cells transfected with empty pcDNA3.1 vector were designated vector cells. Selected cells were then used to evaluate p53-R248W/P72R protein expression and localization. Western blot analysis (Fig. 7A) shows that, as expected, p53 protein was not detectable in vector cells, while it was expressed in R248W/P72R cells; in addition, flow cytometry analysis (Fig. 7B) shows a strong positivity for p53 (>75%) in R248W/P72R cells. Immunofluorescence analysis shows the nuclear localization of p53 protein in R248W/P72R cells (Fig. 7C).

Thereafter, we evaluated *in vitro* whether p53-R248W/P72R expression in MG63 cells promotes cancer stem-like features, as high proliferation rate, sphere formation, clonogenic growth, high migration and invasive ability [35]. Initially, we compared the growth curves of R248W/P72R cells and vector cells. As shown in Fig. 7D, with respect to vector cells, R248W/P72R cells possess a higher proliferative output, exhibiting a doubling time of approximately 25 h, whereas vector cells show a doubling time of 33 h. This was confirmed by DNA content profiles—revealed by flow cytometry analysis of propidium iodide stained cells—showing that R248W/P72R cells were mostly in the S-G2\M phase, while vector cells were predominantly in G0\G1 (Fig. 7E).

It has been reported that cancer stem-like cells can be cultured in suspension to generate floating spheroid-like bodies under serum-free medium with bFGF and EGF [36]. Thus, we tested sarcosphere-forming ability of R248W/P72R cells compared to vector cells. Fig. 7F shows that both vector and R248W/P72R cells were capable of forming sarcospheres. In particular, after 5 days in culture, vector cells formed sarcospheres having a mean diameter of 60.2 ± 5.7 μm, at a frequency of approximately 1/54 (9.3 ± 1.5 spheres/500 cells), while R248W/P72R cells formed larger sarcospheres (mean diameter of 68.7 ± 7.6 μm) at a frequency of approximately 1/42 (12 ± 2.0 spheres/500 cells). After 10 days, R248W/P72R sarcospheres increased in size and number, having a mean diameter of 110 ± 23 μm and containing about 576 cells/sphere. Even vector sarcospheres increased in size and number,

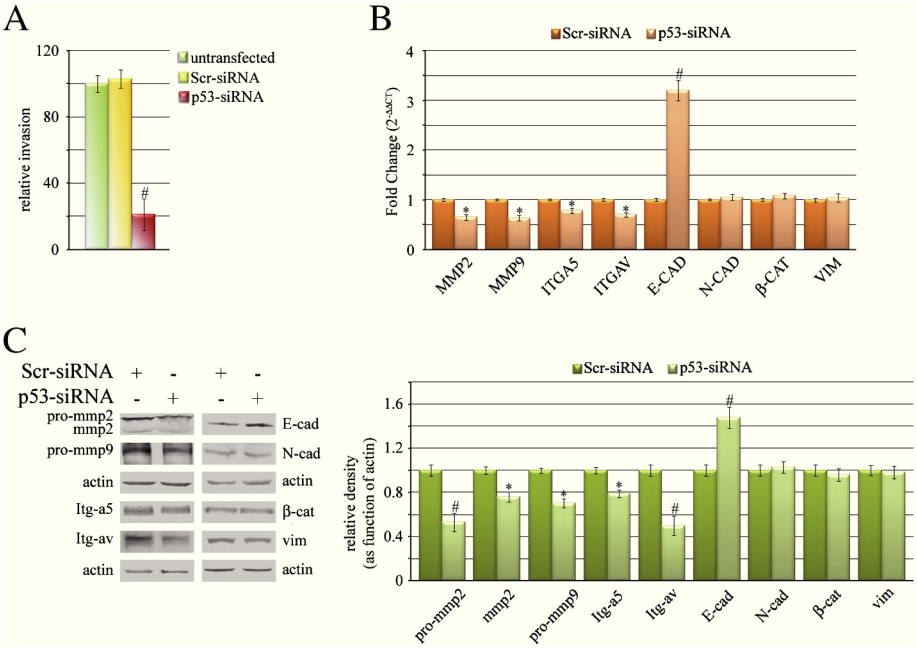

Fig. 5. Effect of p53-R248W/P72R-knockdown on invasive properties of 3AB-OS cells. (A) *In vitro* invasive capacity of untransfected cells and cells transfected with Scr-siRNA or p53-siRNA through the Matrigel-transwell membranes after 48 h of incubation. Data represent the mean of the percentage of the number of cells relative to untransfected cells with standard deviation ($n = 4$; $^{*}P < 0.05$). (B) Real-time PCR analysis of both cell invasion and epithelial-mesenchymal-transition-related genes at 48 h after transfection. Data are the mean with standard deviation ($n = 4$); $^{*}P < 0.05$ and $^{\#}P < 0.005$ as compared to Scr-siRNA-transfected cells. (C) Western blot analysis of both cell invasion and epithelial-mesenchymal-transition-related proteins at 48 h after transfection; quantification of protein bands by densitometric analysis. Data (relative density normalized to actin) represent the mean with standard deviation ($n = 4$); $^{*}P < 0.05$ and $^{\#}P < 0.005$ as compared to Scr-siRNA-transfected cells.

but they were fewer in number and much smaller (mean diameter of 74.9 ± 18.2 μm, containing about 214 cells/sphere). On analyzing sarcosphere-forming ability through subsequent passages (2° and 3° spheres), we found (Fig. 7G) that the number of sarcospheres generated from vector and R248W/P72R cells in each passage remained consistent; however, R248W/P72R cells formed ~2-fold sarcospheres than vector cells, demonstrating their higher *in vitro* self-renewing potential. In addition, in a colony-forming assay that correlates with self renewal [37], R248W/P72R cells formed more numerous and larger colonies than vector cells (Fig. 7H).

We also examined the motility and invasivity of the cells in scratch/wound healing and in Matrigel transwell invasion assays, respectively. Compared with vector cells, R248W/P72R cells showed higher migratory (Figs. 8A and 8B) and invasive (Figs. 8C and 8D) activity. These data suggest that p53-R248W/P72R expression can significantly promote the migratory and invasive function of MG63 cells.

To further determine whether R248W/P72R cells could express putative cancer stem cell markers, we chose to analyze by flow cytometry the expression profile of two representative stem cell surface markers of OS, CD133 and ABCG2 [11,35]. As shown in Fig. 8E, the cell surface expression of CD133 and ABCG2 was very low in both vector (0.7% and 1.5%, respectively) and R248W/P72R (0.9% and 4.3%, respectively) cells. However, when we analyzed the CD133 and ABCG2 intracellular staining, we found a much higher intracellular positivity in both vector and R248W/P72R cells. In particular, as shown in Fig. 8F, R248W/P72R cells express a much higher percentage of CD133-ABCG2-positivity (24.5% and 88.3%, respectively) than vector cells (8.3% and 63.1%, respectively). In addition, western blot analyses for CD133 and ABCG2 show an up-regulation of both markers in R248W/P72R cells, with an increase of 1.38-fold for CD133 and of 1.25-fold for ABCG2 with respect to vector cells (Fig. 8G). Furthermore, we investigated, by western blot analyses, the proteins regulating and maintaining the stem cell phenotype, as Nanog, OCT3/4, nucleostemin (NS) and Sox2. Interestingly, with respect to vector cells, Nanog, OCT3/4 and NS were found to significantly increase in R248W/P72R cells, with an increase of 1.56-fold, 1.22-fold and 1.37-fold for Nanog, OCT3/4 and NS, respectively (Fig. 8G). No significant change was observed in Sox2 level.

In the reported experiments, statistically significant difference was not observed in untransfected and vector cells.

Discussion

TP53 mutations occur in almost every type of cancer at rates varying between 10% in hematopoietic malignancies [38] and 98% in high-grade serous carcinoma of the ovary [39]. Unlike the majority of tumor suppressor genes, which are inactivated by deletions or truncated mutations, TP53 mostly undergoes missense mutations [40]. These alterations produce a full-length mutp53 with a single amino acid substitution that loses its ability to bind DNA [41], induce apoptosis, inhibit growth and suppress transformation [42]. Mutp53 is stable, its accumulation is regarded as a hallmark of cancer [43], and in most cases it not only loses its tumor-suppressive activities but also gains oncogenic functions [44]. In OS patients, alterations of TP53 occurs in 50%–60% of cases and consist of point mutations (20%–30%, mostly missense mutations), gross gene rearrangements (10%–20%) and allelic loss (75%–80%) [1], with its mutation status serving as a valuable indicator for predicting chemoresistance [45]. Accordingly, patients with Li-Fraumeni syndrome, a disorder characterized by a germline mutation at the p53 locus, have a significantly higher risk of developing OS [46].

In this study, we investigated the TP53 gene status/role of human 3AB-OS CSCs compared with parental MG63 cells. We demonstrated that in MG63 cells, where TP53 is not expressed and in single copy [47], the gene does not colocalize on chromosome 17 and is endowed with a methylated promoter. Instead, 3AB-OS cells strongly express a p53 protein (p53-R248W/P72R) whose TP53 gene is rearranged and in multiple copies characterized by P72R polymorphism and hot spot mutation R248W. It has been reported that TP53 mutations strongly predominate in exons 4–9 most of which fall within 6 “hotspot” residues (R175, G245, R248, R249, R273 and R282) in almost all types of

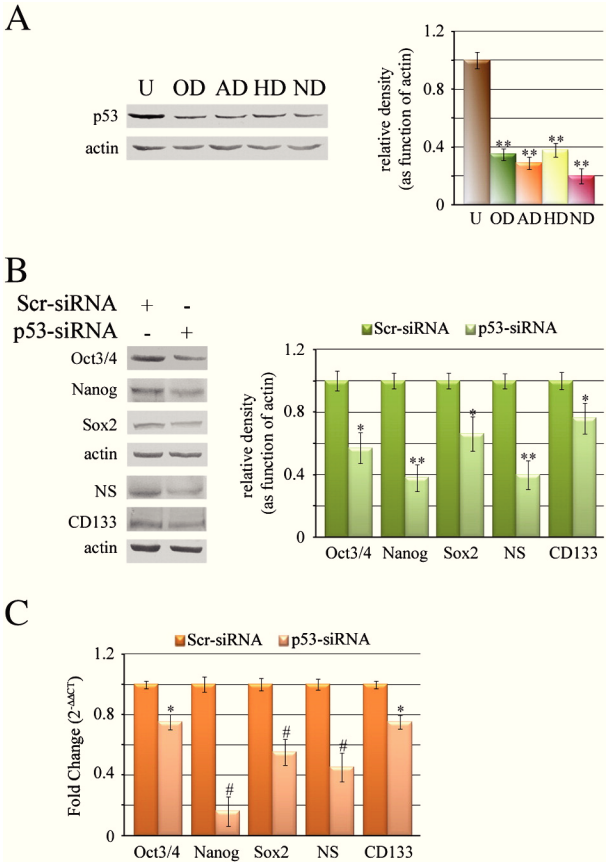

Fig. 6. Effect of p53-R248W/P72R-knockdown on various stem-cell markers in 3AB-OS cells. (A) Western blot analysis of p53-R248W/P72R in undifferentiated (U) and differentiated 3AB-OS cells (see below the abbreviations for derived cell lineages) and quantification of protein bands by densitometric analysis. Data (relative density normalized to actin) represent the mean with standard deviation ($n = 4$); $^{**}P < 0.01$ as compared to undifferentiated cells. Abbreviations: OD, osteogenic differentiation; AD, adipogenic differentiation; HD, hepatogenic differentiation; ND, neurogenic differentiation. (B) Western blot analysis of stemness proteins at 48 h after transfection and quantification of protein bands by densitometric analysis. The data (relative density normalized to actin) represent the mean with standard deviation ($n = 4$); $^{*}P < 0.05$ and $^{**}P < 0.01$ as compared to Scr-siRNA-transfected cells. (C) Real-time PCR analysis of stemness genes at 48 h after transfection. Data represent the mean with standard deviation ($n = 4$); $^{*}P < 0.05$ and $^{\#}P < 0.005$ as compared to Scr-siRNA-transfected cells.

cancer [48]. Intriguingly, OS patients carrying TP53 hot spot mutations (most regarding codon 248) were found to have a significantly increased death risk [49].

It is well known that wild-type p53 is regulated by post-translational modifications as phosphorylation at Ser15 (required for its stabilization [50] and interaction with transcriptional co-activators) and acetylation at Lys320, 373 and 382 (required for both its transcriptional activity and its transcription-independent proapoptotic function [51,52]). Although it has been observed that in UV-induced mouse skin tumors mutp53 is phosphorylated at Ser15 and accumulated exclusively to the nucleus [53], up to now little is known about post-translational modifications of mutp53 in human OS cell lines or patients. Herein, we show that in 3AB-OS cells p53-R248W/P72R is constitutively modified by both phosphorylation at Ser15 and acetylation at Lys320, 373 and 382, and it is localized to the nucleus.

Our results also demonstrated that p53-R248W/P72R-knockdown strongly reduces the growth and replication rate of 3AB-OS cells and concomitantly increases the expression of genes, inhibiting cell cycle progression (pRb, p130, p107, E2F4, GADD45, p21 and p27) while lowering CDK4, the activator of the cell cycle progression through G1/S phase. The findings are in accordance with alteration of genes involved in cell cycle seen in up to 80% of pediatric/adult OS patients [54–56], which demonstrate that genetic lesions deregulating G1/S cell cycle checkpoint may be a constant feature in the pathogenesis of OS.

Another distinctive feature of mutp53 is its ability to confer on cells an elevated resistance to a variety of apoptotic signals [44]. Studies designed to investigate the prognostic significance of bax and bcl-2 expression in surgically treated OS patients demonstrate that a high bax(+)/bcl-2(−) protein expression ratio is associated with an unfavourable outcome in patients with primary OS, with this coexpression pattern probably counterbalancing the accelerated proliferation status of the malignant cells and indirectly characterizing a more aggressive tumor [57]. Moreover, analyses of death receptors in OS samples and in OS cell lines—among which MG63 cells—demonstrated alterations only within the DR4 gene, suggesting that these genetic alterations may be implicated in OS formation [58]. We have previously shown that 3AB-OS cells highly express a great number of genes required for inhibiting apoptosis [11] and much lower levels of FAS and DR4 receptors than parental MG63 cells [14]. Here we show that in 3AB-OS cells p53-R248W/P72R-knockdown potently increases the expression of DR4 and DR5 receptors and sensitivity to TRAIL-induced apoptosis. Since, as above reported, DR4 receptor is mutated in parental MG63 cells, we maintain that 3AB-OS cells can carry such a mutation and suggest that sensitivity to TRAIL-induced apoptosis in p53-R248W/P72R-knockdown cells could arise from DR5 receptor up-regulation. Overall, this finding, together with the observation that p53-R248W/P72R-knockdown markedly increased the levels of the proapoptotic factors Bax and Puma while decreased those of the antiapoptotic factors Bcl-2 and Bcl-XL, suggests that in 3AB-OS cells p53-R248W/P72R could hinder cell response to TRAIL-treatment.

Stemness acquisition is a key event in cancer development as it may induce progression, invasion, dissemination and metastasis. OS is a highly metastatic tumor with metastases being the major cause of death, and in patients with high-grade OS, increased MMP expression was identified as prognostic marker for poor outcome [59,60]. Herein, we show that p53-R248W/P72R-knockdown causes a striking reduction of *in vitro* invasive capacity of 3AB-OS cells with a decrease of the invasion-related gene and protein (MMP2, MMP9, ITGα5 and ITGαV) levels and a concomitant marked increase in E-cadherin. This suggests that the oncogenic properties of p53-R248W/P72R could also enable 3AB-OS cells to promote invasion.

Recently Sarig et al. [61] reported a novel GOF property for mutp53, which markedly enhanced the efficiency of the reprogramming process compared with p53 deficiency. This novel activity of mutp53 induced alterations in the characteristics of the reprogrammed cells. Indeed, although p53-knockout cells reprogrammed with Oct4 and Sox2 maintained their pluripotent capacity *in vivo*, reprogrammed cells expressing mutp53 lost this capacity and gave rise to malignant tumors.

Since osteosarcomas contain highly proliferative malignant cells that are largely arrested in their differentiation, OS is proposed to be a "differentiation-flawed disease," resulting from genetic and epigenetic disruption of the osteoblast differentiation pathway [1]. Moreover, the presence of OS stem-like cells has been reported in patient tumors [62] as well as in established human OS cell lines [63]. We have previously shown [11,13,14] that 3AB-OS cells highly express a large panel of stemness-related genes/proteins and that efficiently transdifferentiate *in vitro* into cells of all the three primary germ layers [12], whereas when 3AB-OS cells were engrafted in nude mice, they potently induced malignant tumors, although preserving multilineage commitment [13]. Here, we show that, after *in vitro* 3AB-OS differentiation, in each derived cell lineage, p53-R248W/P72R was profoundly down-regulated and after p53-R248W/P72R-knockdown the expression of pluripotent markers (Oct3/4, Nanog, Sox2, nucleostemin and CD133) markedly lowered, suggesting that p53-R248W/P72R might be responsible for 3AB-OS cells pluripotency and self-renewal.

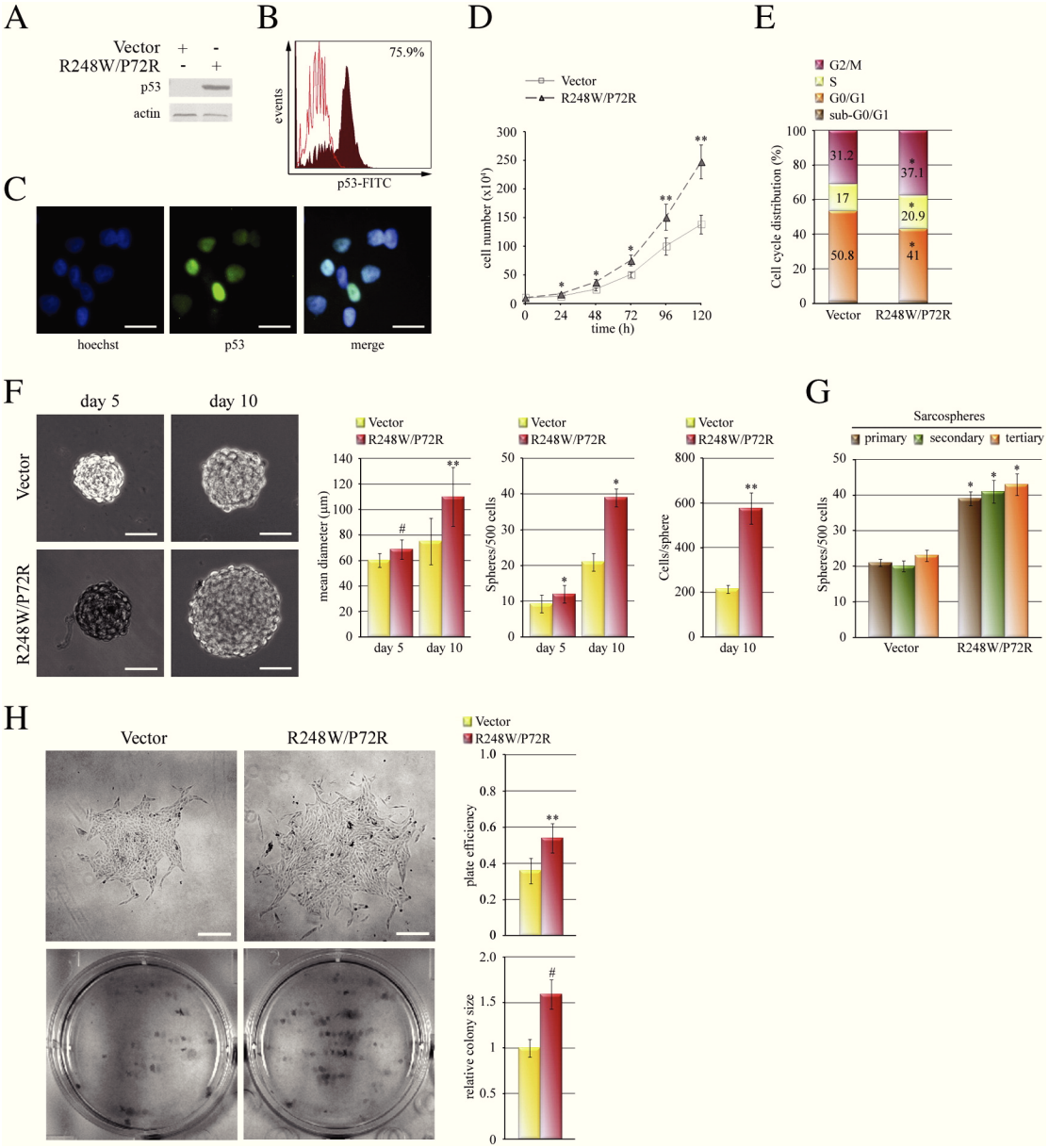

Fig. 7. Ectopic expression of p53-R248W/P72R in osteosarcoma MG63 cells and its effect on cell proliferation and sarcosphere- and colony-forming ability. (A) Western blot analysis of p53 in MG63 cells transfected with either pcDNA3.1-p53-R248W/P72R (R248W/P72R) or empty pcDNA3.1 vector (vector). Actin was used as the internal control. Images are representative of four independent experiments. (B) Cytometric analysis for p53 in R248W/P72R cells. The open histogram indicates isotype control, filled histogram, indicates the expression of p53. Images are representative of four independent experiments. (C) Immunofluorescence analysis of p53 in R248W/P72R cells, by double staining cells with both Hoechst 33342 dye (blue, left panel) to localize the nucleus and anti-p53 antibody and Cy2-conjugated secondary antibody (green, middle panel) to localize p53. In the right panel the merge of the two dyes is shown. The scale bar represents 25 μm. Images are representative of four independent experiments. (D) Growth curves of vector and R248W/P72R cells. The data represent the mean with standard deviation ($n = 4$); $^{*}P < 0.05$ and $^{**}P < 0.01$ as compared to vector cells. (E) Cell cycle distributions in vector and R248W/P72R cells determined using flow cytometry. Results are indicated as relative percentage of total cell cycle ($^{*}P < 0.05$, as compared to vector cells). (F) Phase contrast images of primary sarcospheres formed from vector and R248W/P72R cells after 5 and 10 days of culturing. The scale bar represents 50 μm. Graphs summarizing size and number of sarcospheres from 500 cells (on days 5 and 10) and number of cells/sphere on day 10. The data represent the mean with standard deviation ($n = 4$); $^{*}P < 0.05$, $^{**}P < 0.01$ and $^{\#}P < 0.005$ as compared to vector cells. (G) Graph summarizing numbers of 1°, 2° (generated from dissociated 1° spheres) and 3° (generated from dissociated 2° spheres) sarcospheres on day 10 from 500 cells. The data represent the mean with standard deviation ($n = 4$); $^{*}P < 0.05$ as compared to vector cells. (H) Clonogenic growth of vector and R248W/P72R cells after 10 days of culturing. Phase contrast images (top; the scale bar represents 200 μm) and a photograph (bottom) of 6-well plate after staining with methylene blue are shown. Graphs summarizing plate efficiency (colonies/100 cells) and relative colony size (mean area relative to vector cells). The data represent the mean with standard deviation ($n = 4$); $^{**}P < 0.01$ and $^{\#}P < 0.005$ as compared to vector cells.

Here, we also show that the ectopic expression of p53-R248W/P72R promotes cancer stem-like properties in osteosarcoma MG63 parental cells. Indeed, when MG63 cells were transfected with pcDNA3.1-p53-R248W/P72R, R248W/P72R cells showed strong positivity for p53 and its nuclear localization. Moreover, R248W/P72R cells, with respect to vector cells, showed a higher proliferative output, were capable of forming 2-fold sarcospheres, formed more numerous and larger colonies and showed higher migratory and invasive activity. In addition, R248W/P72R cells showed significant increase in the expression of stemness markers.

In conclusion, the findings that in 3AB-OS cells p53-R248W/P72R-knockdown profoundly changed the expression of genes/proteins correlated to stemness, proliferation, apoptosis and invasiveness, and that in MG63 parental cells, the ectopic expression of p53-R248W/

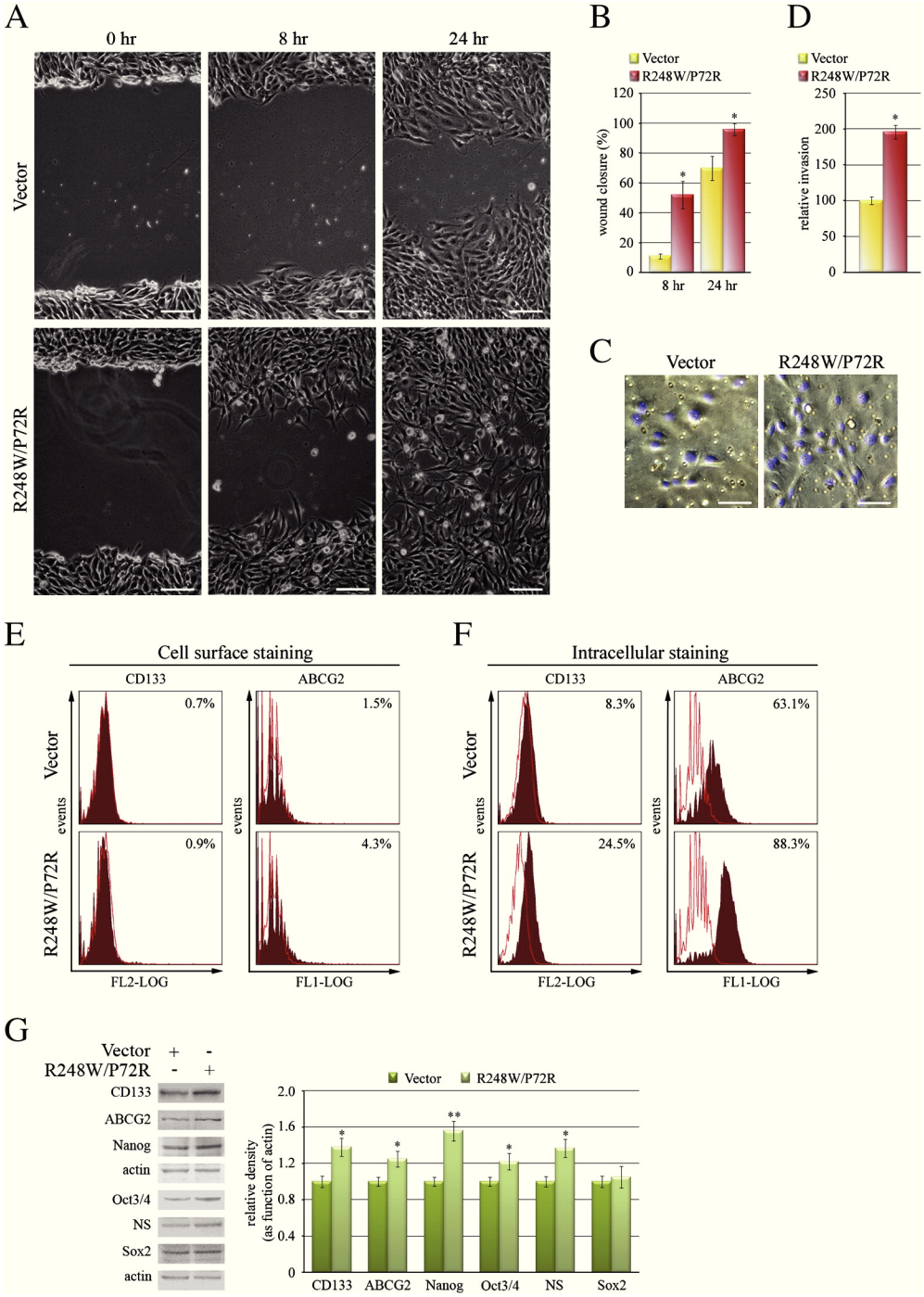

Fig. 8. Effects of ectopic expression of p53-R248W/P72R on cell migration, invasion and expression of stemness markers in MG63 cells. (A) Representative images from the scratch wound-healing assay in MG63 cells transfected with either pcDNA3.1-p53-R248W/P72R (R248W/P72R) or empty pcDNA3.1 vector (Vector). Cells were scratched and wound margins were imaged 0, 8 and 24 h later. The scale bar represents 100 μm. (B) Quantification of the scratch wound-healing assay is shown. The extent of wound closure was quantified by measuring the wound area compared to the initial wound area. The data represent the mean with standard deviation ($n = 4$); $^{*}P < 0.05$ as compared to vector cells. (C) Representative images from the transwell invasion assays in vector and R248W/P72R cells. After 48 h of incubation, cells migrated to the underside of the insert were stained with Hoechst 33342. The scale bar represents 50 μm. (D) Data are the mean of the percentage of the number of cells relative to vector cells with standard deviation ($n = 4$; $^{*}P < 0.05$). (E) Cytometric analyses showing cell surface expression of CD133 (left panels) and ABCG2 (right panels) in vector and R248W/P72R cells. The open histograms indicate isotype control; filled histograms indicate the expression of CD133 and ABCG2. (F) Cytometric analyses showing intracellular expression of CD133 (left panels) and ABCG2 (right panels) in vector and R248W/P72R cells. The open histograms indicate isotype control; filled histograms indicate the expression of CD133 and ABCG2. (G) Western blot analysis of stemness proteins and quantification of protein bands by densitometric analysis. The data (relative density normalized to actin) represent the mean with standard deviation ($n = 4$); $^{*}P < 0.05$ and $^{**}P < 0.01$ as compared to vector cells.

P72R promoted cancer stem-like properties, suggest that the GOF property of p53-R248W/P72R can be at the root of the dedifferentiation of MG63 cells into 3AB-OS CSCs. We believe that 3AB-OS cells could provide a best-fit to understand p53-R248W/P72R properties and its potential involvement in osteosarcomagenesis.

Acknowledgments

We thank Dr. Francesca Malvestiti (Research and Development Area–Toma Advanced Biomedical Assays S.p.A., Busto Arsizio, VA, Italy) for her helpful technical discussion on FISH analysis. We also

thank Dr. Giulia Malferrari laboratory Responsible at BioRep S.r.l. (Milano, Italy) for her technical help on DNA sequence analysis.

This work was partially funded by the European Regional Development Fund, European Territorial Cooperation 2007–2013, CCI 2007 CB 163 PO 037, OP Italia-Malta 2007–2013; the Italian Ministry of Education, University and Research (MIUR) ex-60%, 2013; and the MIUR-PRIN, contract number 2008P8BLNF (2008). R. Di Fiore was a recipient of a fellowship granted by MIUR (contract number 867/06/07/2011); D. Carlisi was a recipient of a fellowship granted by MIUR (contract number 2223/12/19/2011); R. Drago-Ferrante was a recipient of a fellowship granted by MIUR-PRIN (contract number 144/01/26/2012); M. Marcatti and F. Querques are PhD students supported by Italian Ministry of Education, University and Research (MIUR).

The authors declare no conflict of interest.

Appendix A. Supplementary data

Supplementary data to this article can be found online at http://dx.doi.org/10.1016/j.bone.2013.12.021.

References

[1] Tang N, Song WX, Luo J, Haydon RC, He TC. Osteosarcoma development and stem cell differentiation. Clin Orthop Relat Res 2008;8:2114–30.
[2] Chou AJ, Gorlick R. Chemotherapy resistance in osteosarcoma: current challenges and future directions. Expert Rev Anticancer Ther 2006;6:1075–85.
[3] Clevers H. The cancer stem cell: premises, promises and challenges. Nat Med 2011;17:313–9.
[4] Li L, Neaves WB. Normal stem cells and cancer stem cells: the niche matters. Cancer Res 2006;66:4553–7.
[5] Maitland NJ, Collins AT. Prostate cancer stem cells: a new target for therapy. J Clin Oncol 2008;26:2862–70.
[6] Bapat SA. Evolution of cancer stem cells. Semin Cancer Biol 2007;17:204–13.
[7] Frank NY, Schatton T, Frank MH. The therapeutic promise of the cancer stem cell concept. J Clin Invest 2010;120:41–50.
[8] Morrison R, Schleicher SM, Sun Y, Niermann KJ, Kim S, Spratt DE, et al. Targeting the mechanisms of resistance to chemotherapy and radiotherapy with the cancer stem cell hypothesis. J Oncol 2011;2011:941876.
[9] Prud'homme GJ. Cancer stem cells and novel targets for antitumor strategies. Curr Pharm Des 2012;18:2838–49.
[10] De Blasio A, Messina C, Santulli A, Mangano V, Di Leonardo E, D'Anneo A, et al. Differentiative pathway activated by 3-aminobenzamide, an inhibitor of PARP, in human osteosarcoma MG63 cells. FEBS Lett 2005;579:615–20.
[11] Di Fiore R, Santulli A, Drago-Ferrante R, Giuliano M, De Blasio A, Messina C, et al. Identification and expansion of human osteosarcoma-cancer-stem cells by long-term 3-aminobenzamide treatment. J Cell Physiol 2009;219:301–13.
[12] Di Fiore R, Drago-Ferrante R, D'Anneo A, De Blasio A, Santulli A, Messina C, et al. Differentiation of human osteosarcoma 3AB-OS stem-like cells in derivatives of the three primary germ layers as an useful in vitro model to develop several purposes. Stem Cell Discov 2013;3:188–201.
[13] Di Fiore R, Guercio A, Puleio R, Di Marco P, Drago-Ferrante R, D'Anneo A, et al. Modeling human osteosarcoma in mice through 3AB-OS cancer stem cell xenografts. J Cell Biochem 2012;113:3380–92.
[14] Di Fiore R, Fanale D, Drago-Ferrante R, Chiaradonna F, Giuliano M, De Blasio A, et al. Genetic and molecular characterization of the human osteosarcoma 3AB-OS cancer stem cell line: a possible model for studying osteosarcoma origin and stemness. J Cell Physiol 2013;228:1189–201.
[15] Bridge JA, Nelson M, McComb E, McGuire MH, Rosenthal H, Vergara G, et al. Cytogenetic findings in 73 osteosarcoma specimens and a review of the literature. Cancer Genet Cytogenet 1997;95:74–87.
[16] Batanian JR, Cavalli LR, Aldosari NM, Ma E, Sotelo-Avila C, Ramos MB, et al. Evaluation of paediatric osteosarcomas by classic cytogenetic and CGH analyses. Mol Pathol 2002;55:389–93.
[17] Niini T, Lahti L, Michelacci F, Ninomiya S, Hattinger CM, Guled M, et al. Array comparative genomic hybridization reveals frequent alterations of G1/S checkpoint genes in undifferentiated pleomorphic sarcoma of bone. Genes Chromosomes Cancer 2011;50:291–306.
[18] Adorno M, Cordenonsi M, Montagner M, Dupont S, Wong C, Hann B, et al. A mutant-p53/Smad complex opposes p63 to empower TGF^2-induced metastasis. Cell 2009;137:87–98.
[19] Muller PA, Caswell PT, Doyle B, Iwanicki MP, Tan EH, Karim S, et al. Mutant p53 drives invasion by promoting integrin recycling. Cell 2009;139:1327–41.
[20] Bossi G, Lapi E, Strano S, Rinaldo C, Blandino G, Sacchi A. Mutant p53 gain of function: reduction of tumor malignancy of human cancer cell lines through abrogation of mutant p53 expression. Oncogene 2006;25:304–9.
[21] Dittmer D, Pati S, Zambetti G, Chu S, Teresky AK, Moore M, et al. Gain of function mutations in p53. Nat Genet 1993;4:42–6.
[22] Sigal A, Rotter V. Oncogenic mutations of the p53 tumor suppressor: the demons of the guardian of the genome. Cancer Res 2000;60:6788–93.
[23] Scian MJ, Stagliano KE, Anderson MA, Hassan S, Bowman M, Miles MF, et al. Tumor-derived p53 mutants induce NF-kappaB2 gene expression. Mol Cell Biol 2005;25:10097–110.
[24] Blandino G, Levine AJ, Oren M. Mutant p53 gain of function: differential effects of different p53 mutants on resistance of cultured cells to chemotherapy. Oncogene 1999;18:477–85.
[25] Song H, Hollstein M, Xu Y. p53 gain-of-function cancer mutants induce genetic instability by inactivating ATM. Nat Cell Biol 2007;9:573–80.
[26] Xu Y. Induction of genetic instability by gain-of-function p53 cancer mutants. Oncogene 2008;27:3501–7.
[27] Noll JE, Jeffery J, Al-Ejeh F, Kumar R, Khanna KK, Callen DF, et al. Mutant p53 drives multinucleation and invasion through a process that is suppressed by ANKRD11. Oncogene 2012;31:2836–48.
[28] Spike BT, Wahl GM. p53, stem cells, and reprogramming: tumor suppression beyond guarding the genome. Genes Cancer 2011;2:404–19.
[29] De Blasio A, Musmeci MT, Giuliano M, Lauricella M, Emanuele S, D'Anneo A, et al. The effect of 3-aminobenzamide, inhibitor of poly(ADP-ribose) polymerase, on human osteosarcoma cells. Int J Oncol 2003;23:1521–8.
[30] Gawrychowski J, Lackowska B, Gabriel A. Prognosis of the surgical treatment of patients with non-small cell lung cancer (NSCLC)—relation to DNA ploidy. Eur J Cardiothorac Surg 2003;23:870–7.
[31] Kang JH, Kim SJ, Noh DY, Park IA, Choe KJ, Yoo OJ, et al. Methylation in the p53 promoter is a supplementary route to breast carcinogenesis: correlation between CpG methylation in the p53 promoter and the mutation of the p53 gene in the progression from ductal carcinoma in situ to invasive ductal carcinoma. Lab Invest 2001;81:573–9.
[32] Amatya VJ, Naumann U, Weller M, Ohgaki H. TP53 promoter methylation in human gliomas. Acta Neuropathol 2005;110:178–84.
[33] Agirre X, Vizmanos JL, Calasanz MJ, García-Delgado M, Larráyoz MJ, Novo F. Methylation of CpG dinucleotides and/or CCWGG motifs at the promoter of TP53 correlates with decreased gene expression in a subset of acute lymphoblastic leukemia patients. Oncogene 2003;22:1070–2.
[34] Pogribny IP, James SJ. Reduction of p53 gene expression in human primary hepatocellular carcinoma is associated with promoter region methylation without coding region mutation. Cancer Lett 2002;176:169–74.
[35] Tirino V, Desiderio V, d'Aquino R, De Francesco F, Pirozzi G, Graziano A, et al. Detection and characterization of CD133 + cancer stem cells in human solid tumours. PLoS One 2008;3:e3469.
[36] Lee J, Kotliarova S, Kotliarov Y, Li A, Su Q, Donin NM, et al. Tumor stem cells derived from glioblastomas cultured in bFGF and EGF more closely mirror the phenotype and genotype of primary tumors than do serum-cultured cell lines. Cancer Cell 2006;9:391–403.
[37] Patrawala L, Calhoun T, Schneider-Broussard R, Zhou J, Claypool K, Tang DG. Side population is enriched in tumorigenic, stem-like cancer cells, whereas ABCG2 + and ABCG2- cancer cells are similarly tumorigenic. Cancer Res 2005;65:6207–19.
[38] Peller S, Rotter V. TP53 in hematological cancer: low incidence of mutations with significant clinical relevance. Hum Mutat 2003;21:277–84.
[39] Ahmed AA, Etemadmoghadam D, Temple J, Lynch AG, Riad M, Sharma R, et al. Driver mutations in TP53 are ubiquitous in high grade serous carcinoma of the ovary. J Pathol 2010;221:49–56.
[40] Hainaut P, Hollstein M. p53 and human cancer: the first ten thousand mutations. Adv Cancer Res 2000;77:81–137.
[41] Bullock AN, Fersht AR. Rescuing the function of mutant p53. Nat Rev Cancer 2001;1:68–76.
[42] Hollstein M, Sidransky D, Vogelstein B, Harris CC. p53 mutations in human cancers. Science 1991;253:49–53.
[43] Rivlin N, Brosh R, Oren M, Rotter V. Mutations in the p53 tumor suppressor gene: important milestones at the various steps of tumorigenesis. Genes Cancer 2011;2:466–74.
[44] Oren M, Rotter V. Mutant p53 gain-of-function in cancer. Cold Spring Harb Perspect Biol 2010;2:a001107.
[45] Petitjean A, Mathe E, Kato S, Ishioka C, Tavtigian SV, Hainaut P, et al. Impact of mutant p53 functional properties on TP53 mutation patterns and tumor phenotype: lessons from recent developments in the IARC TP53 database. Hum Mutat 2007;28:622–9.
[46] Malkin D, Jolly KW, Barbier N, Look AT, Friend SH, Gebhardt MC, et al. Germline mutations of the p53 tumor-suppressor gene in children and young adults with second malignant neoplasms. N Engl J Med 1992;326:1309–15.
[47] Masuda H, Miller C, Koeffler HP, Battifora H, Cline MJ. Rearrangement of the p53 gene in human osteogenic sarcomas. Proc Natl Acad Sci U S A 1987;84:7716–9.
[48] Cho Y, Gorina S, Jeffrey PD, Pavletich NP. Crystal structure of a p53 tumor suppressor-DNA complex: understanding tumorigenic mutations. Science 1994;265:346–55.
[49] Gokgoz N, Wunder JS, Mousses S, Eskandarian S, Bell RS, Andrulis IL. Comparison of p53 mutations in patients with localized osteosarcoma and metastatic osteosarcoma. Cancer 2001;92:2181–9.
[50] Shieh SY, Ikeda M, Taya Y, Prives C. DNA damage-induced phosphorylation of p53 alleviates inhibition by MDM2. Cell 1997;91:325–34.
[51] Luo J, Li M, Tang Y, Laszkowska M, Roeder RG, Gu W. Acetylation of p53 augments its site-specific DNA binding both in vitro and in vivo. Proc Natl Acad Sci U S A 2004;101:2259–64.
[52] Caelles C, Helmberg A, Karin M. p53-dependent apoptosis in the absence of transcriptional activation of p53-target genes. Nature 1994;370:220–323.
[53] Melnikova VO, Santamaria AB, Bolshakov SV, Ananthaswamy HN. Mutant p53 is constitutively phosphorylated at Serine 15 in UV-induced mouse skin tumors: involvement of ERK1/2 MAP kinase. Oncogene 2003;22:5958–66.

[54] Wei G, Lonardo F, Ueda T, Kim T, Huvos AG, Healey JH, et al. CDK4 gene amplification in osteosarcoma: reciprocal relationship with INK4A gene alterations and mapping of 12q13 amplicons. Int J Cancer 1999;80:199–204.
[55] Lonardo F, Ueda T, Huvos AG, Healey J, Ladanyi M. p53 and MDM2 alterations in osteosarcomas: correlation with clinicopathologic features and proliferative rate. Cancer 1997;79:1541–7.
[56] Nielsen GP, Burns KL, Rosenberg AE, Louis DN. CDKN2A gene deletions and loss of p16 expression occur in osteosarcomas that lack RB alterations. Am J Pathol 1998;153:159–63.
[57] Kaseta MK, Khaldi L, Gomatos IP, Tzagarakis GP, Alevizos L, Leandros E, et al. Prognostic value of bax, bcl-2, and p53 staining in primary osteosarcoma. J Surg Oncol 2008;97:259–66.
[58] Dechant MJ, Fellenberg J, Scheuerpflug CG, Ewerbeck V, Debatin KM. Mutation analysis of the apoptotic "death-receptors" and the adaptors TRADD and FADD/MORT-1 in osteosarcoma tumor samples and osteosarcoma cell lines. Int J Cancer 2004;109:661–7.
[59] Bjørnland K, Flatmark K, Pettersen S, Aaasen AO, Fodstad O, Maelandsmo GM. Matrix metalloproteinases participate in osteosarcoma invasion. J Surg Res 2005;127:151–6.
[60] Ferrari C, Benassi S, Ponticelli F, Gamberi G, Ragazzini P, Pazzaglia L, et al. Role of MMP-9 and its tissue inhibitor TIMP-1 in human osteosarcoma: findings in 42 patients followed for 1–16 years. Acta Orthop Scand 2004;75:487–91.
[61] Sarig R, Rivlin N, Brosh R, Bornstein C, Kamer I, Ezra O, et al. Mutant p53 facilitates somatic cell reprogramming and augments the malignant potential of reprogrammed cells. J Exp Med 2010;207:2127–40.
[62] Tirino V, Desiderio V, Paino F, De Rosa A, Papaccio F, Fazioli F, et al. Human primary bone sarcomas contain CD133+ cancer stem cells displaying high tumorigenicity in vivo. FASEB J 2011;25:2022–30.
[63] Wang L, Park P, Lin CY. Characterization of stem cell attributes in human osteosarcoma cell lines. Cancer Biol Ther 2009;8:543–52.